

The radiation of Sound from Surfaces at Grazing Angles of
Incidence

Vladimir Pavasovic

Master of Applied Science

RMIT

The radiation of Sound from Surfaces at Grazing Angles of Incidence

A thesis submitted in fulfilment of the requirements for the degree of Master of Applied Science

Vladimir Pavasovic

School of Applied Sciences
RMIT University
June 2006

Declaration

I declare that work presented in this thesis is that of my own, except where due acknowledgment has been made, and has not been submitted previously, in whole or part, to qualify for any other academic award.

The content of the thesis is the result of work which has been carried out since 15th March, 2003, this being the official date of commencement of this programme.

Signature:

Name: Vladimir Pavasovic

Date: June, 2006.

Acknowledgements

I would like to thank my wife, Marija, for her understanding, endless patience and encouragement when it was most required.

I would also like to extend my gratitude to my supervisor, Dr. John L. Davy, for his guidance and support throughout the process of this research.

Table of Contents

Declaration		iii
Acknowledgements		iv
Table of Contents		v
List of Figures		viii
List of Symbols		xvii
Abstract		xix
Chapter	1: Introduction	1
	1.1 Background	1
	1.2 Scope and Objective of the Research	1
	1.3 Rationale for the Research	2
	1.4 Summary	3
Chapter	2: Literature Review	5
Chapter	3: Methods	10
	3.1 Data Analysis	10
	3.2 Procedure	10
Chapter	4: Prediction of Radiation Efficiency of Finite Size Flat Panels	12
	4.1 Infinite Panels	12
	4.2 Line Sources	14
	4.2.1 Two Sources	14
	4.2.2 Multiple Sources	16

	4.3	Infinite Strips	18
	4.3.1	Argument 1	21
	4.3.2	Argument 2	22
	4.4	Finite size square panels	27
Chapter	5:	Relative Sound Level	35
	5.1	Analysis and comparison of the level of sound radiated as predicted by different models	39
	5.1.1	The equations used for calculation	39
	5.1.1.1	Why are openings and finite panels different?	45
	5.1.2	Roberts' experimental results and prediction model for finite openings	47
	5.1.3	Rindel's experimental results for finite openings and panels	57
	5.1.3.1	Opening	58
	5.1.3.2	A thin single panel	62
	5.1.3.3	Coincidence Region	64
	5.1.3.4	A Thick Single Panel	68
	5.1.4	Stead's experimental results for sound reduction through single isotropic glass panels of finite size	71
	5.1.5	Bies & Hansen's directivity prediction model for an un baffled duct opening	76
	5.1.6	B & K Microphone	83
	5.1.7	Levine & Schwinger's analytic calculations on the radiation from an unflanged circular pipe	87
	5.1.8	Environment Protection Authority experimental results on the directivity loss in a free field	89

	5.1.9	Sharland's prediction model for sound radiation in ventilating systems	93
	5.1.10	Woods' directivity prediction model for louvres and grilles	96
	5.1.11	Linear Interpolation	100
	5.1.11.1	Opening with width of 0.5 m	100
	5.1.11.2	Opening with width of 1.5 m	103
Chapter	6:	Conclusion	105
	6.1	Recommendation for further study	109
References			110

List of Figures

Figure	Page
4.1. Infinite plane sinusoidal sound wave incident on an infinite panel	12
4.2. Two sources separated by distance $2a$	15
4.3. The reflection and transmission at a finite size opening or thin panel of a plane wave incident at an angle of ϕ to the normal.	19
4.4. Approximation of $\frac{\sin^2 [ka(\theta - \phi) \cos \phi]}{[ka(\theta - \phi) \cos \phi]^2}$ with a rectangular function	22
4.5. Only half of the integral is included at $\theta = \frac{\pi}{2}$ as shown in this polar diagram of the integrand.	23
4.6. Calculated values of radiation efficiency. Square panel with incidence in x-z plane [4].	28
4.7. Radiation efficiency as a function of the angle of incidence and the values of ka shown in the legend.	31
5.1. Directivity pattern for a circular piston in a large baffle when ka is large [46].	35
5.2. 3-D directivity pattern field for a circular piston in a larger piston when ka is large [46].	36
5.3. Animation of sound field for a circular piston in a larger piston when ka is large [47].	36
5.4. The radiation function $\left(\frac{\sin x}{x}\right)^2$ for a single frequency [49].	37
5.5. Measured radiation pattern from a plane surface [50].	38
5.6. Definition of angles of incidence and reflection from a rectangular surface[49].	38

- 5.7. Comparison of Roberts experimental data with the theory of section 5.1.1 for the sound level at 90 degrees relative to the sound level at 0 degrees. The theory of section 5.1.1 is used with the weighting function using a weighting angle ϕ_w of 78 degrees. 48
- 5.8. Comparison of Roberts calculated data with the theory of section 5.1.1 for the sound level at 90 degrees relative to the sound level at 0 degrees. The theory of section 5.1.1 is used with the weighting function using a weighting angle ϕ_w of 78 degrees. A negative relative sound level constant of -1.5 dB was added to results of the theory of section 5.1.1. 49
- 5.9. Comparison of Roberts measured data with the theory of section 5.1.1 for the sound level at 90 degrees relative to the sound level at 0 degrees. The theory of section 5.1.1 is used with the weighting function using a weighting angle ϕ_w of 78 degrees. A negative relative sound level constant of -1.5 dB was added to results of the theory of section 5.1.1. 50
- 5.10. Comparison of Roberts measured data with the theory of section 5.1.1 for the sound level at 90 degrees relative to the sound level at 0 degrees. The theory of section 5.1.1 is used with the weighting function using a weighting angle ϕ_w of 90 degrees. A negative relative sound level constant of -1.5 dB was added to results of the theory of section 5.1.1. 51
- 5.11. Comparison of Roberts measured data with the theory of section 5.1.1 for the sound level at 90 degrees relative to the sound level at 0 degrees. The theory of section 5.1.1 is used with the weighting function using a weighting angle ϕ_w of 95 degrees. A negative relative sound level constant of -1.5 dB was added to results of the theory of section 5.1.1. 52

- 5.12. Comparison of Roberts measured data with the theory of section 5.1.1 for the sound level at 90 degrees relative to the sound level at 0 degrees. The theory of section 5.1.1 is used with the weighting function using a weighting angle ϕ_w of 100 degrees. A negative relative sound level constant of -1.5 dB was added to results of the theory of section 5.1.1. 53
- 5.13. Comparison of Roberts measured data with the theory of section 5.1.1 for the sound level at 90 degrees relative to the sound level at 0 degrees. The theory of section 5.1.1 is used with the weighting function using a weighting angle ϕ_w of 110 degrees. A negative relative sound level constant of -1.5 dB was added to results of the theory of section 5.1.1. 54
- 5.14. Comparison of Roberts measured data with the theory of section 5.1.1 for the sound level at 90 degrees relative to the sound level at 0 degrees. The theory of section 5.1.1 is used with the weighting function using a weighting angle ϕ_w of 120 degrees. A negative relative sound level constant of -1.5 dB was added to results of the theory of section 5.1.1. 55
- 5.15. Comparison of different data with the theory of section 5.1.1 for the sound level at 90 degrees relative to the sound level at 0 degrees. The theory of section 5.1.1 is used with the weighting function using a weighting angle ϕ_w of 100 degrees. A negative relative sound level constant of -1.5 dB was added to results of the theory of section 5.1.1. 56
- 5.16. Comparison of Rindel's measured data with the theory of section 5.1.1 for the sound level at 90 degrees relative to the sound level at 0 degrees. The theory of section 5.1.1 is used with the weighting function using a weighting angle ϕ_w of 200 degrees. 59

5.17.	Comparison of Rindel's measured data with the theory of section 5.1.1 for the sound level at 75 degrees relative to the sound level at 0 degrees. The theory of section 5.1.1 is used with the weighting function using a weighting angle ϕ_w of 200 degrees.	60
5.18.	Comparison of Rindel's measured data with the theory of section 5.1.1 for the sound level at 45 degrees relative to the sound level at 0 degrees. The theory of section 5.1.1 is used with the weighting function using a weighting angle ϕ_w of 200 degrees.	61
5.19.	Comparison of Rindel's measured data with the theory of section 5.1.1 for the sound level at 90 degrees relative to the sound level at 0 degrees. The theory of section 5.1.1 is used with the weighting function using a weighting angle ϕ_w of 120 degrees.	63
5.20.	Comparison of Rindel's measured data with the theory of section 5.1.1 for the sound level at 75 degrees relative to the sound level at 0 degrees. The theory of section 5.1.1 is used with the weighting function using a weighting angle ϕ_w of 120 degrees.	65
5.21.	Comparison of Rindel's measured data with the theory of section 5.1.1 for the sound level at 45 degrees relative to the sound level at 0 degrees. The theory of section 5.1.1 is used with the weighting function using a weighting angle ϕ_w of 120 degrees.	66
5.22.	Rindel vs. Stead.	67
5.23.	Comparison of Rindel's measured data with the theory of section 5.1.1 for the sound level at 90 degrees relative to the sound level at 0 degrees. The theory of section 5.1.1 is used with the weighting function using a weighting angle ϕ_w of 120 degrees.	68
5.24.	Comparison of Rindel's measured data with the theory of section 5.1.1 for the sound level at 75 degrees relative to the sound level at 0 degrees. The theory of section 5.1.1 is used with the weighting function using a weighting angle ϕ_w of 120 degrees.	69

5.25.	Comparison of Rindel's measured data with the theory of section 5.1.1 for the sound level at 45 degrees relative to the sound level at 0 degrees. The theory of section 5.1.1 is used with the weighting function using a weighting angle ϕ_w of 120 degrees.	70
5.26.	Typical TL as a function of frequency for a single panel.	71
5.27.	Comparison of Stead's measured data with the theory of section 5.1.1 for the sound level at 90 degrees relative to the sound level at 0 degrees. The theory of section 5.1.1 is used with the weighting function using a weighting angle ϕ_w of 83 degrees.	73
5.28.	Comparison of Stead's measured data with the theory of section 5.1.1 for the sound level at 75 degrees relative to the sound level at 0 degrees. The theory of section 5.1.1 is used with the weighting function using a weighting angle ϕ_w of 83 degrees.	74
5.29.	Comparison of Stead's measured data with the theory of section 5.1.1 for the sound level at 45 degrees relative to the sound level at 0 degrees. The theory of section 5.1.1 is used with the weighting function using a weighting angle ϕ_w of 83 degrees.	75
5.30.	Comparison of Bies & Hansen's data with the theory of section 5.1.1 for the sound level at 90 degrees relative to the sound level at 0 degrees. The theory of section 5.1.1 is used with the weighting function using a weighting angle ϕ_w of 78 degrees. A negative relative sound level constant of -1.5 dB was added to results of the theory of section 5.1.1.	77
5.31.	Comparison of Bies & Hansen's data with the theory of section 5.1.1 for the sound level at 90 degrees relative to the sound level at 0 degrees. The theory of section 5.1.1 is used with the weighting function using a weighting angle ϕ_w of 19 degrees. A negative relative sound level constant of -1.5 dB was added to results of the theory of section 5.1.1.	78

- 5.32. Comparison of Bies & Hansen's data with the theory of section 5.1.1 for the sound level at 90 degrees relative to the sound level at 0 degrees. The theory of section 5.1.1 is used with the weighting function using a weighting angle ϕ_w of 55 degrees. A negative relative sound level constant of -1.5 dB was added to results of the theory of section 5.1.1. 79
- 5.33. Comparison of Bies & Hansen's data with the theory of section 5.1.1 for the sound level at 60 degrees relative to the sound level at 0 degrees. The theory of section 5.1.1 is used with the weighting function using a weighting angle ϕ_w of 55 degrees. A negative relative sound level constant of -1.5 dB was added to results of the theory of section 5.1.1. 80
- 5.34. Comparison of Bies & Hansen's data with the theory of section 5.1.1 for the sound level at 45 degrees relative to the sound level at 0 degrees. The theory of section 5.1.1 is used with the weighting function using a weighting angle ϕ_w of 55 degrees. A negative relative sound level constant of -1.5 dB was added to results of the theory of section 5.1.1. 81
- 5.35. Comparison of Bies & Hansen's data with the theory of section 5.1.1 for the sound level at 30 degrees relative to the sound level at 0 degrees. The theory of section 5.1.1 is used with the weighting function using a weighting angle ϕ_w of 55 degrees. A negative relative sound level constant of -1.5 dB was added to results of the theory of section 5.1.1. 82
- 5.36. Free-Field Correction Curves. 83
- 5.37. Comparison of Bruel & Kjaer microphone data with the theory of section 5.1.1 for the sound level at 90 degrees relative to the sound level at 0 degrees. The theory of section 5.1.1 is used with the weighting function using a weighting angle ϕ_w of 50 degrees. 84

- 5.38. Comparison of Bruel & Kjaer microphone data with the theory of section 5.1.1 for the sound level at 60 degrees relative to the sound level at 0 degrees. The theory of section 5.1.1 is used with the weighting function using a weighting angle ϕ_w of 50 degrees. 85
- 5.39. Comparison of Bruel & Kjaer microphone data with the theory of section 5.1.1 for the sound level at 30 degrees relative to the sound level at 0 degrees. The theory of section 5.1.1 is used with the weighting function using a weighting angle ϕ_w of 50 degrees. 86
- 5.40. Comparison of Levine & Schwinger's data with the theory of section 5.1.1 for the sound level at 90 degrees relative to the sound level at 0 degrees. The theory of section 5.1.1 is used with the weighting function using a weighting angle ϕ_w of 1 degree. 87
- 5.41. Comparison of Levine & Schwinger's data with the theory of section 5.1.1 for the sound level at 60 degrees relative to the sound level at 0 degrees. The theory of section 5.1.1 is used with the weighting function using a weighting angle ϕ_w of 1 degree. 88
- 5.42. Comparison of Levine & Schwinger's data with the theory of section 5.1.1 for the sound level at 30 degrees relative to the sound level at 0 degrees. The theory of section 5.1.1 is used with the weighting function using a weighting angle ϕ_w of 1 degree. 89
- 5.43. Comparison of Environmental Protection Authority data with the theory of section 5.1.1 for the sound level at 90 degrees relative to the sound level at 0 degrees. The theory of section 5.1.1 is used with the weighting function using a weighting angle ϕ_w of 200 degrees. A negative relative sound level constant of -1.5 dB was added to results of the theory of section 5.1.1. 90

- 5.44. Comparison of Environmental Protection Authority data with the theory of section 5.1.1 for the sound level at 45 degrees relative to the sound level at 0 degrees. The theory of section 5.1.1 is used with the weighting function using a weighting angle ϕ_w of 200 degrees. A negative relative sound level constant of -1.5 dB was added to results of the theory of section 5.1.1. 92
- 5.45. Comparison of Sharland's calculated data with the theory of section 5.1.1 for the sound level at 90 degrees relative to the sound level at 0 degrees. The theory of section 5.1.1 is used with the weighting function using a weighting angle ϕ_w of 87 and 25 degrees. 93
- 5.46. Comparison of Sharland's calculated data with the theory of section 5.1.1 for the sound level at 60 degrees relative to the sound level at 0 degrees. The theory of section 5.1.1 is used with the weighting function using a weighting angle ϕ_w of 87 degrees. 94
- 5.47. Comparison of Sharland's calculated data with the theory of section 5.1.1 for the sound level at 30 degrees relative to the sound level at 0 degrees. The theory of section 5.1.1 is used with the weighting function using a weighting angle ϕ_w of 87 degrees. 95
- 5.48. Comparison of Woods' calculated data with the theory of section 5.1.1 for the sound level at 90 degrees relative to the sound level at 0 degrees. The theory of section 5.1.1 is used with the weighting function using a weighting angle ϕ_w of 85 and 160 degrees. 97
- 5.49. Comparison of Woods' calculated data with the theory of section 5.1.1 for the sound level at 60 degrees relative to the sound level at 0 degrees. The theory of section 5.1.1 is used with the weighting function using a weighting angle ϕ_w of 160 degrees. 98
- 5.50. Comparison of Woods' calculated data with the theory of section 5.1.1 for the sound level at 30 degrees relative to the sound level at 0 degrees. The theory of section 5.1.1 is used with the weighting function using a weighting angle ϕ_w of 160 degrees. 99

5.51.	Comparison of the relative sound level at 90 degrees for different prediction models for the opening with a width of 0.5 m.	101
5.52.	Comparison of the relative sound level at 45 degrees for different prediction models for the opening with a width of 0.5 m.	102
5.53.	Comparison of the relative sound level at 90 degrees for different prediction models for the opening with a width of 1.5 m.	103
5.54.	Comparison of the relative sound level at 45 degrees for different prediction models for the opening with a width of 1.5 m.	104

List of Symbols

a	Half length of the panel in the direction of the source
c	Speed of sound in fluid
g	Cosine of angle of incidence
g_l	Cosine of limiting angle of incidence
I	Radiated sound intensity on one side
I_0	Reference radiated intensity on one side
I_Q	Intensity in direction (θ, ϕ)
k	Wave number of the sound
k_b	Wave number in panel
k_s	Wave number of incident sinusoidal sound wave
m	Constant or mass per unit area
L	Relative sound pressure level
N	Number of sound sources
p	Sound pressure in air
p_{rms}	Transmitted root mean square pressure
q	Inverse of low frequency radiation efficiency
r	Radius of sphere or hemisphere
t	Time
S	Surface area of the panel
u	Particle velocity in air
u_n	Normal component of particle velocity
u_{iz}	Incident velocity in the z-axis direction
u_{rz}	Reflected velocity in the z-axis direction
u_{tz}	Transmitted velocity in the z-axis direction
v	Normal velocity of panel
v_{rms}	Root mean square normal velocity of panel
w	Weighting function
x	Variable
y	Complement of angle of incidence

- $Z_e(\varphi)$ Effective impedance of a finite panel in an infinite baffle
- $Z_{wfi}(\varphi)$ The wave impedance of the fluid as experienced by the finite panel in an infinite baffle, whose vibration is due a plane sound wave incident at an angle of φ to the normal to the panel, on the side from which the plane sound wave is incident (this is the fluid loading on the incident side),
- $Z_{wft}(\varphi)$ The wave impedance of the fluid as experienced by the finite panel in an infinite baffle, whose vibration is due a plane sound wave incident at an angle of φ to the normal to the panel, on the side opposite to which the sound is incident (this is the fluid loading on the non-incident or transmitted side)
- $Z_{wp}(\varphi)$ The wave impedance of the finite panel in an infinite baffle to a plane sound wave incident at an angle of φ to the normal to the panel, ignoring fluid loading
- Z_c Characteristic impedance of air
- α Angle of transmitted sound relative to x-axis
- α_0 Angle of incident sound relative to x-axis
- β Angle of transmitted sound relative to y-axis
- β_0 Angle of incident sound relative to y-axis
- δ Half total phase change at observer
- ϕ Angle of incidence relative to normal
- ϕ_b, ϕ_m Limiting angles of incidence relative to normal
- η Damping loss factor of panel
- λ Wavelength in air
- λ_b Wavelength in panel
- θ Angle of radiation relative to normal
- ρ Density of fluid
- σ Radiation efficiency into the fluid of one side of the finite panel in an infinite baffle, whose vibration is due a plane sound wave incident at an angle of φ to the normal to the panel.
- ψ Phase difference
- ω Angular frequency
- ω_c Critical angular frequency of panel

Abstract

It is difficult to predict the sound radiation from large flat factory roofs. This is because sound insulation is measured as the average over all angles of sound incidence. With large flat factory roofs one needs to know the sound transmission at grazing angles with directional sound fields. The research in this thesis examined what will be the best method for effectively modelling sound radiation from factory roofs.

The existing infinite panel theories of sound insulation are not sufficient when the sound radiates at grazing angles. It has been shown that the reason for the collapse of the theory is the well known result for the radiation efficiency. The radiation efficiency of an infinite flat panel, which is radiating an infinite plane wave into an infinite half space, can be shown to be equal to the inverse of the cosine of the angle between the direction of propagation of the plane wave and the normal to the panel. The fact that this radiation efficiency tends to infinity as the angle tends to 90° causes problems with simple theories of sound insulation. Sato has calculated numerical values of radiation efficiency for a finite size rectangular panel. This research will present a simple analytic strip theory, which agrees reasonably well with Sato's numerical calculations for a rectangular panel. Simple analytic strip theory has led to the conclusion that it is mainly the length of the panel in the direction of radiation, rather than its width that is important in determining its radiation efficiency.

The findings of the current research also indicated that apart from the effect due to coincidence, a panel was non-directional compared to an opening. Rindel's results in the case of an anechoic chamber confirmed that apart from the coincidence angle for particular frequency, radiation of panel was not very directional.

CHAPTER 1

1. Introduction

1.1 *Background*

Several acoustic consultants have stated that it is difficult to predict the sound radiation from large flat factory roofs because of the uncertainties of sound energy radiated to listening positions at angles other than directly above. It is contended that this is because laboratory sound insulation of roofing materials is measured as the average over all angles of sound transmission. With large flat factory roofs one needs to know the sound radiation at grazing angles due to excitation by interior sound fields. The sound radiation at grazing angles cannot be predicted with existing infinite panel theories of sound insulation. Better understanding of sound insulation at grazing incidence will also enable better theories of diffuse field sound insulation to be developed. Most of the directivity information in the literature is for openings so they will also be considered.

1.2 *Scope and Objective of the Research*

The aim of this research was to develop a method for predicting the level of sound radiated from a finite flat panel or finite opening in any particular direction relative to the level of sound radiated in the direction normal to the finite flat panel or finite opening.

This research has attempted to answer the following questions:

- What is the best method for effectively modeling sound radiation at grazing angles relative to that in the normal direction?
- What are the contributing factors to the amount of sound propagated to the far-field?

- What is the sound radiation when the angle of incidence is close to 90° ?

It is hoped that this research will provide a deeper understanding of how sound radiates from factory roofs and from finite plates in general. The understanding gained from this project will assist and provide information to professionals who predict noise emission out of factory buildings and recommend noise control treatments to reduce noise to overcome noise related complaints from nearby residences. The research report can also be used as a tool or basis for further research, where sound radiation to the surroundings from structural vibrations excited by incident sound is predicted.

1.3 *Rationale for the Research*

In previous studies, in order to obtain an analytical solution for practical applications, the plate was normally assumed infinite in size [1, 2]. For radiation from a plate there are two different cases. The first case is when the wavelength of the plate vibrations is greater than the wavelength of sound in the surrounding medium. In this case the plate will radiate a plane wave into the medium at an angle that is determined by the ratio of the wavelength of the plate vibration to the wavelength of the sound in the surrounding medium. The sound pressure in the near region of the plate will be in the phase with the plate velocity [1, 3]. The other case will be when the wavelength of the plate vibrations is smaller than the wavelength of sound in the surrounding medium. In this second case the near-field that occurs, decays exponentially with distance from the surface of the plate. Here the sound pressure will be 90° out of the phase with the plate velocity, and no sound will be radiated to the far field [1, 3].

For bending wavelengths greater than the acoustic wavelengths in the surrounding medium, which occurs for free bending waves above the critical frequency, the radiation efficiency is always greater than unity. For free bending waves below the critical frequency there is no radiation if the plate is of infinite extent [1].

Bending waves in a plate which are forced by incident sound waves always have longer wavelengths than the incident sound waves. From a previous study [1] it can be concluded

that the radiation results for free bending waves obtained for the infinite plate can apply to finite plates only for frequencies that are considerably above the critical frequency. Below the critical frequency the finite dimensions and the boundary conditions affect the radiation efficiency considerably.

This thesis will only consider the radiation of sound from a finite panel or opening whose vibration is forced by sound incident from the opposite side. In this case the wavelength of the forced vibration is always longer than the wavelength of sound in the surrounding medium. Sato [4] has calculated numerical values of the radiation efficiency for a finite size square panel whose vibration is forced by incident sound. This research project will present a simple analytical strip theory which will agree reasonably well with Sato's numerical calculations for a square panel. An infinite strip of width $2a$ that is cut from an infinite plate will be considered. It will be of interest how much power per unit length it radiates from one side when excited by an infinite plane sinusoidal wave incident on the other side at an angle of ϕ to the normal to the strip. In order to extend the results to values of ka less than one, a finite size square panel with sides of length $2a$ will be assumed. Since only the power that is radiated to the far field is of interest, the real part of the normalized fluid wave impedance z_{wf} will be considered. For sources whose size is small compared to the wavelength of sound, it will be expected that their sound radiation will depend only on their volume velocities.

1.4 *Summary*

This thesis will only consider the radiation of sound from a finite panel or opening whose vibration is forced by sound incident from the opposite side. In this case the wavelength of the forced vibration is always longer than the wavelength of sound in the surrounding medium. The thesis will be particularly concerned with radiation from finite flat panels at grazing angles because this case can be used for the prediction of sound radiation from factory roofs to the surrounding community. The thesis will also include finite openings to emphasize the difference between the directivity of finite openings and finite flat panels.

The two dimensional analytic approximation of the strip model derived in this research project will give reasonable agreement with the two dimensional numerical calculations of

Ljunggren [5] and with the three dimensional numerical calculations of Sato [4] and Novak [6]. It will also agree with the experimental measurements of Roberts [7] which show that the directivity of a rectangle depends mainly on its length in the direction of measurement, rather than its width at right angles to the direction of measurement.

CHAPTER 2

2. Literature Review

This literature review is restricted to sound radiation by forced transmission through finite panels and openings. Substantial research has addressed the important problem of sound radiation from finite panels. Early work by Alfredson [8], Beranek [9], Cremer [1], Holmer and Vér [10] was concerned with sound radiation from the structures. Maidanik [11] predicted the radiation from the free vibration rather than the forced vibration of panels. Maidanik investigated the response of ribbed panels to reverberant acoustic fields. He discussed a statistical method for estimating the response of ribbed panels to acoustic excitation. Maidanik's analysis predicted that ribbing increases the radiation resistance of the panel and hence its coupling to the acoustic field. Wallace predicted the radiation from individual panel modes for both baffled beams [12] and rectangular panels [13]. A common task using the theory of sound radiation from the structures is the prediction of sound transmission and noise reduction through structures.

Concerning transmission loss, a large database of test data (at least from 100 to 5000 Hz), verified transmission loss theory, and practical equations for relatively simple constructions are all readily available. The theory of sound transmission for solid materials has been studied for over 85 years. As reported by Heckl [14] almost all of the basic equations can be found in the book by Lord Rayleigh [15]. Theoretical methods for the prediction of transmission loss have been summarised by Bies and Hansen [16], Beranek [2], Beranek and Ver [17], Davy [18], Heckl [14], Rindel [19] and Takahashi [20]. Rindel [19] considered these prediction methods in his work on the transmission of traffic noise through windows. Rindel compared the external or outdoor noise level to the internal room level [19]. He made 1:4 scale model measurements on the sound insulation of windows installed in one wall of a box in an anechoic room. The sound was incident from outside the box at an angle normal to the window. Stead [21] considered these prediction methods in his work on sound radiation through single isotropic glass panels of finite size. Stead measured the sound insulation of a 6 millimeters glass window installed in one wall of a room. The sound was incident from

outside the room at an angle normal to the window. The window was part of the external wall acting as a baffle.

The characteristic regions of the transmission loss spectrum are the stiffness controlled region, the mass law region, the coincidence region and the damping controlled region. Panel mass and angle of sound incidence are primary influences in the mass law region. The coincidence or critical frequency is determined by material properties and the angle of sound incidence and the dip minimum value is determined by the amount of damping in the panel. Panel damping also influences transmission loss above the coincidence region which is a damping controlled region. Bies and Hansen [16] have reported experimental model investigations of the directivity of exhaust ducts. Their model is based on data for both rectangular and circular ducts and is presented in terms of Strouhal number based on frequency and the geometric mean diameter of the duct, and the angle measured from the centerline of the duct.

Several researchers addressed the problem of stack directivity. Wells & Crocker [22], Waters, Labate and Beranek [23], Joseph and Morley [24], Sutton [25], Croft [26], Dewhurst [27] studied various aspects of this subject. One of the aims of Dewhurst's project was to verify the results published by Croft and Sutton relating to the directivity of a rectangular exhaust stack. It is important to note that a copy of the Croft results was only sourced at the last moment without a copy of the actual report. In a report on exhaust stack directivity, Dewhurst has demonstrated that it could prove useful to utilize a rectangular cross-section rather than the more common square cross-section. This is due to the fact that larger amounts of attenuation can be obtained for the short side of the rectangular stack than can be obtained for a square stack.

In analyses for predicting the sound insulation of a partition, infinitely extended panels have been used as a sound transmission model, because there are many difficulties in analyzing, the finite system. In practice, the panel is obviously finite. The frequency response of finite-system derived from the rigorous solution generally appears to be complex, having violent peaks and dips due to resonance involving modal behavior and fluid-structure coupling Sewell [28]. Some more detailed discussions and rigorous analytical procedures concerning this matter are given by Fahy [29].

In evaluating the sound insulation performance of finite systems, the use of different methods and analysis becomes practically important. Crocker and Price [30, 31] considered different aspects of sound transmission, depending on whether the frequency under consideration is above or below the critical frequency of coincidence. In their studies they applied statistical energy analysis. Above the critical frequency, transmission is dominated by resonance modes (resonance transmission). The effect of resonance becomes smaller below the critical frequency, and this frequency region is called forced or non-resonance transmission region. The mass-law is generally used in the non-resonant region, and is derived from the infinite theory.

Using a modal expansion method, Sewell [28] analyzed the transmission through a rectangular panel in a rigid baffle. This method is mathematically rigorous, and has been commonly used for panels of finite width and finite length mounted in a rigid baffle. Using some assumptions and approximations he developed a simple expression for predicting the forced transmission below coincidence. This forced transmission, together with the contribution of the resonance factor which is considered to be affected by the edge conditions, gives the total transmission through the finite panel.

Several researchers studied the forced transmission of finite sized panels. Gösele [3] derived the radiation efficiency for a finite panel where he also included panel wavelengths which are less than the wavelength of the sound in air, for which the infinite model predicts zero radiation efficiency. Gösele gave approximate formulae for certain ranges of parameters and graphed results of numerical calculations for three different sizes of panels.

Sato [4] calculated the radiation factor of a square portion of an infinite vibrating surface, and discussed the sound insulation performance of a finite panel. He provided extensive numerical calculations for the forced wave case where the panel wavelength is longer than the wavelength in air. Sato also numerically calculated the radiation efficiency averaged over all possible directions of sound incidence. On the basis of this result Novak [32] calculated the sound insulation of finite double walls using the impedance method developed by Beranek and Work [33], and presented results in good agreement with measurements at low frequencies.

Rindel [16] used Sato's [4] numerical results for radiation efficiency in his theory of sound insulation as a function of angle of incidence. According to Novak [32], Lindblad [34] provided an approximate formula for the radiation efficiency at high frequencies based on Gösele's [3] results. Lindblad [35] provided a simpler approximation which could be integrated over all angles of incidence where he extended the integrated formula to low frequencies. Rindel presented a slightly more complicated version of Lindblad's formula with constants which were selected to provide good agreement with Sato's radiation efficiencies.

Ljunggren [5] considered the situation where a finite single wall is excited over only part of its surface. He repeated Sato's [4] calculations using a two dimensional model and obtained agreement to within 0.5 dB for both as a function of angle of incidence and averaged over all angles of incidence. Novak [6] has performed even more extensive three dimensional calculations than Sato.

The studies of White and Powell [36], Cummings and Mulholland [37] and Mulholland and Lyon [38] deal with sound transmission through finite sized panels.

Noise reduction from space to space as a function of radiation patterns from partitions and building elements are rarely found in the literature or acoustical texts. A large variety of noise reduction situations arise in practice. Roberts [7], Rindel [19], Stead [21], Sharland [39] and Woods [40] studied various aspects of this subject.

Roberts [7] made measurements on the sound radiation from a room via a sliding window which was open and varied the width of the window opening. He compared the sound radiated at grazing angles to that radiated normal to the window. He also developed a theory to predict his results.

Levine and Schwinger [41] studied the radiation of sound from the end of an unflanged circular pipe below the cut off frequency of the first cross mode. In this situation only plane waves propagate. To describe the radiation characteristics of the pipe, Levine and Schwinger calculated the power-function, which compares the intensity of radiation in a given direction with that of an isotropically radiating point source of equal power output.

In a report on a specific case, Sharland [39] investigated and calculated the amount of noise radiated in a ventilating system particularly through an atmospheric louver fixed in a wall. For example, schools or residential premises could have a noise problem which is due to fan noise generated in ventilation ducting and then radiated to an adjacent property. Additional work by Woods and the Environmental Protection Authority (EPA) [42] deals with the directivity of the source.

CHAPTER 3

3. Method

3.1 *Data Analysis*

Data calculations were extensive and mostly programmed in Microsoft Excel 2000. Visual Basic for Applications (VBA) codes were also generated to assist in more complex calculations that could not have been programmed in Microsoft Excel.

All AutoCad LT 2000i drawings used in some of the figures are in Microsoft Word 2000 format.

3.2 *Procedure*

In this research, numerical analyses of the airborne sound produced by structural vibrations have been performed using Microsoft Excel. The simulations of the sound radiation have been performed firstly for simple configurations such as spherical sources and infinite plates, and then for more complex structures such as finite plates. The directionality of the radiated sound was important as well as determination of the radiated power, which is of primary interest for noise control [1].

The initial analysis involved sound radiation for a spherical source that consisted of a sphere whose volume varies with time. It was simplest to consider because it radiates sound uniformly in all directions [2]. Such a sound source is rarely encountered in practice, but is of great importance because complicated sound sources can often be considered as made up of a large number of spherical or hemispherical sources.

The next step was to analyze the combination of simple sources. Basically, the problem was to add, in phase space, at the desired point in space, the sound pressures arriving at that point

from all the simple sources [2]. For this particular situation, it was assumed that the distance from the two point sources to some point in space at which the pressure p is being measured was large compared with the separation between the two sources. When the separation between the two sources was very small compared with a wavelength and the sources were in phase, the two sources united and the pressure at a distance at any angle was double that of one source acting alone. As the separation between the sources became larger, the pressures arriving from the two sources were different in phase and the directivity pattern was not a circle. In other words, the sources radiated sound in some directions better than in others [2].

The greater the separation between the two sources, the sharper the principal lobe and the greater the number of side lobes [2]. In order to observe these findings, the simulations of a linear array of simple sources were produced. During these simulations the number of sources, as well as the length over which the simple in phase sources were evenly spaced, was varied in order to produce the idea of principal difference among directivity patterns. The principle difference among directivity patterns for a given ratio of array length to wavelength was in the suppression of the 'side lobes' [2]. Sound was radiated well in directions where angles are equal to 0 and 180 degrees. As the array became longer and the number of elements became greater, the radiation became less in other directions than at those angles mentioned previously.

This project has focused on sound radiation from finite plates such as factory roofs. The best approach was to deal with a strip of width $2a$ that was cut from an infinite plate. Plane waves propagating across that strip were considered. This was a two-dimensional problem where we wanted to find the radiation into the half-space due to a given velocity distribution across the strip. The forced sound radiation from plates below the critical frequency has also been investigated.

Finally, this research has attempted to develop the best method for effectively modeling the level of sound radiated from a finite flat panel or finite opening in any particular direction relative to the level of sound radiated in the direction normal to the finite flat panel or finite opening.

CHAPTER 4

4. Prediction of Radiation Efficiency of Finite Size Flat Panels

4.1 *Infinite Panels*

The classical theory of sound transmission is based on an infinite panel model [1]. The initial analysis involved the radiation efficiency of an infinite flat panel, which was radiating an infinite plane wave into an infinite half space. If an infinite plane wave strikes a panel it forces a bending wave in the panel whose wavelength is greater than or equal to the wavelength of the incident wave in air. Figure 3.1 represents an infinite plane sound wave incident on an infinite panel. The direction of propagation of the infinite plane sound wave is shown by the blue arrow. This direction of propagation is at an angle of θ to the normal to the panel. The normal to the panel is shown by the green dashed line. The wave front maxima are shown by the red lines. They are separated by the wavelength λ of the infinite plane sound wave.

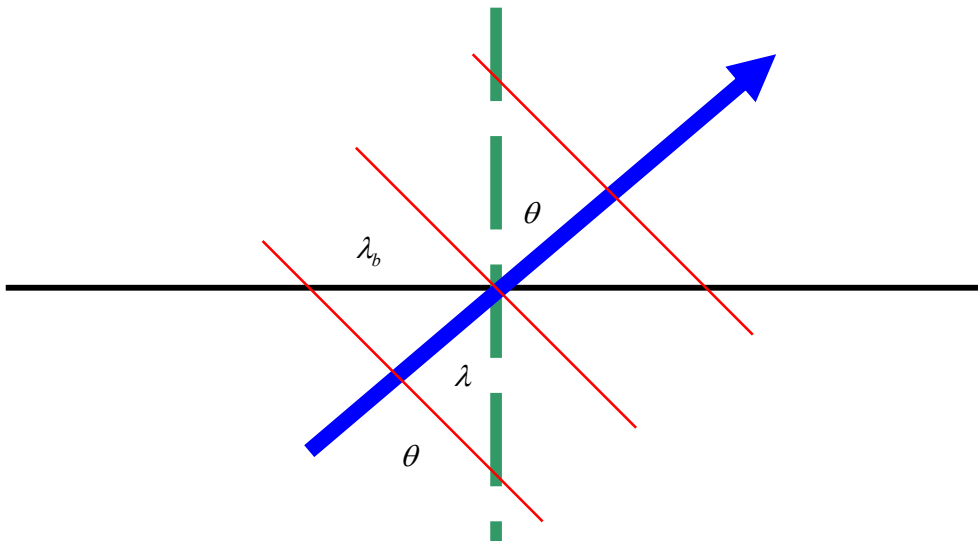


Figure 4.1. Infinite plane sinusoidal sound wave incident on an infinite panel.

The distance between the wave front maxima measured along the panel is

$$\lambda_b = \frac{\lambda}{\sin \theta} \quad (4.1)$$

where λ_b is the wavelength of the bending wave that the incident sound wave produces on the panel.

Since the wave number is

$$k = \frac{2\pi}{\lambda} \quad (4.2)$$

$$k \sin \theta = k_b \quad (4.3)$$

The frequencies of the incident sound wave, the forced bending wave and the transmitted sound wave must all be equal. If the particle velocity of the transmitted infinite plane sound wave is u , the component of the particle velocity normal to the panel is $u \cos \theta$.

Continuity dictates that the transmitted sound wave pressure and the pressure exerted by the panel to create the transmitted sound wave are the same pressure p . If the density of the air is ρ_0 and the speed of sound in the air is c , then the characteristic impedance of air is [2]

$$Z_c = \frac{p}{u} = \rho_0 c \quad (4.4)$$

The fluid wave impedance experienced by the panel on its radiating side is

$$Z_{wf} = \frac{p}{v} = \frac{p}{u \cos \theta} = \frac{Z_c}{\cos \theta} = \frac{\rho_0 c}{\cos \theta} \quad (4.5)$$

If the fluid wave impedance Z_{wf} is normalized by dividing it by the characteristic impedance Z_c , the normalized fluid impedance is

$$z_{wf} = \frac{Z_{wf}}{Z_c} = \frac{1}{\cos \theta} \quad (4.6)$$

The acoustic intensity radiated by the panel on the transmitted side is

$$I = \text{Re}(p_{rms} v_{rms}^*) = \text{Re}(Z_{wf}) v_{rms}^2 \quad (4.7)$$

The radiation efficiency σ is I/I_0 where I_0 is given by

$$I_0 = Z_c v_{rms}^2 \quad (4.8)$$

Thus combining equations (4.5) and (4.6) will give the radiation efficiency of the panel

$$\sigma = \frac{I}{I_0} = \frac{\text{Re}(Z_{wf})}{Z_c} = \text{Re}(z_{wf}) = \frac{1}{\cos \theta} \quad (4.9)$$

One important aspect of this result is that it cannot be correct for a finite size panel because it goes to infinity at grazing angles of incidence.

4.2 *Line Sources*

4.2.1 **Two Sources**

Firstly, the simplest case is two point sources, which are of equal amplitude and frequency separated by distance d as shown in figure 4.2 [43].

Parallel lines pointing to distant observer

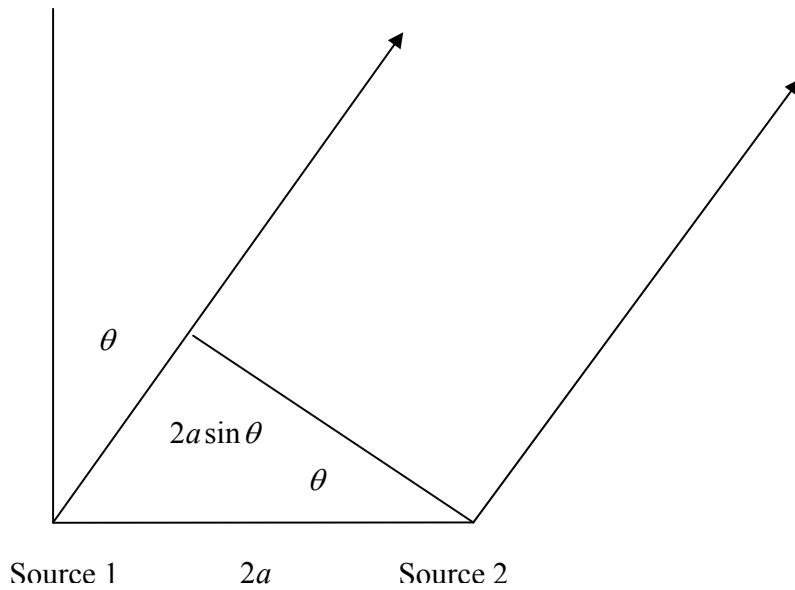


Figure 4.2. Two sources separated by distance $2a$

Since the distance to an observer is very large compared to $2a$, an observer will receive almost the same amplitude wave from each source and the lines from the two sources to the observer will be almost parallel.

Figure 4.2 shows that the wave from source 1 has to travel an extra distance of $2a \sin \theta$ where θ is the angle between normal to the line separating the two sources and the parallel lines from the sources to the observer. In this case θ is positive if source 2 is closer to the observer than source 1, with an assumption that the phase of source 2 leads the phase of source 1 by 2ψ [43].

The phase of the wave at the observer from source 2 leads the phase of the wave from source 1 by

$$2\delta = 2\psi + 2ka \sin(\theta) \quad (4.10)$$

If ω is the angular frequency of the two point sound sources, at time t , the amplitude of the sound at the distant observer is proportional to

$$\begin{aligned} \frac{\sin(\omega t) + \sin(\omega t + 2\delta)}{2} &= \sin(\omega t + \delta)\cos(\delta) \\ &= \frac{2\sin(\delta)\cos(\delta)}{2\sin(\delta)}\sin(\omega t + \delta) \end{aligned} \quad (4.11)$$

Using the following trigonometric identity

$$\begin{aligned} \sin 2\theta &= 2\sin\theta\cos\theta \\ &= \frac{\sin(2\delta)}{2\sin(\delta)}\sin(\omega t + \delta) \end{aligned} \quad (4.12)$$

Thus the amplitude of the sound at the distant observer is proportional to

$$\frac{\sin(2\delta)}{2\sin(\delta)} \quad (4.13)$$

4.2.2 Multiple Sources

In this section the equation for N sources is derived. Then N is allowed to tend to infinity to obtain the equation for a continuous line source. Assuming that there are N sources in a line of length $2a$, each of which has amplitude $\frac{1}{N}$.

There is distance $\frac{2a}{N-1}$ and the phase of $\frac{2\psi}{N-1}$ relative to the previous source.

The amplitude of the sound wave at a distant observer is proportional to

$$\frac{1}{N} \sum_{n=1}^N \sin[\omega t + 2(n-1)\delta] = \frac{\sin(N\delta)}{N \sin(\delta)} \sin[\omega t + (N-1)\delta] \quad (4.14)$$

where

$$2\delta = \frac{2\psi + 2ka \sin(\theta)}{N-1} \quad (4.15)$$

The above summation has been performed using formula 1.341.1 on page 29 of Gradshteyn and Ryzhik [45].

If N is large, then

$$N\delta \approx (N-1)\delta = \psi + ka \sin(\theta) \quad (4.16)$$

From which follows that

$$\delta = \frac{\psi + ka \sin(\theta)}{(N-1)} \ll 1 \text{ and } \sin(\delta) \approx \delta \quad (4.17)$$

The amplitude of the sound wave at the observer is proportional to

$$\begin{aligned} & \frac{\sin(N\delta)}{N \sin \delta} \sin[\omega t + (N-1)\delta] \\ &= \frac{\sin(\psi + ka \sin(\theta))}{\psi + ka \sin(\theta)} \sin(\omega t + \psi + ka \sin(\theta)) \end{aligned} \quad (4.18)$$

Therefore large N limit gives the result for a continuous line source of constant source strength over a length of $2a$ and a phase difference which varies linearly by a total amount of 2ψ over the length $2a$ of the continuous line source. The amplitude of sound at a distant observer is proportional to

$$\frac{\sin(\psi + ka \sin \theta)}{\psi + ka \sin \theta} \quad (4.19)$$

The phase difference ψ is due to a forced bending wave induced by a wave incident at an angle of ϕ

$$\psi = -k_b a = -ka \sin \phi \quad (4.20)$$

In this case the amplitude of the sound at a distant observer is proportional to

$$\frac{\sin [ka (\sin \theta - \sin \phi)]}{ka (\sin \theta - \sin \phi)} \quad (4.21)$$

4.3 *Infinite Strips*

An opening or thin panel in the form of an infinite strip was considered. This is shown in cross section in figure 4.3 [19]. This situation is solved as a two dimensional problem.

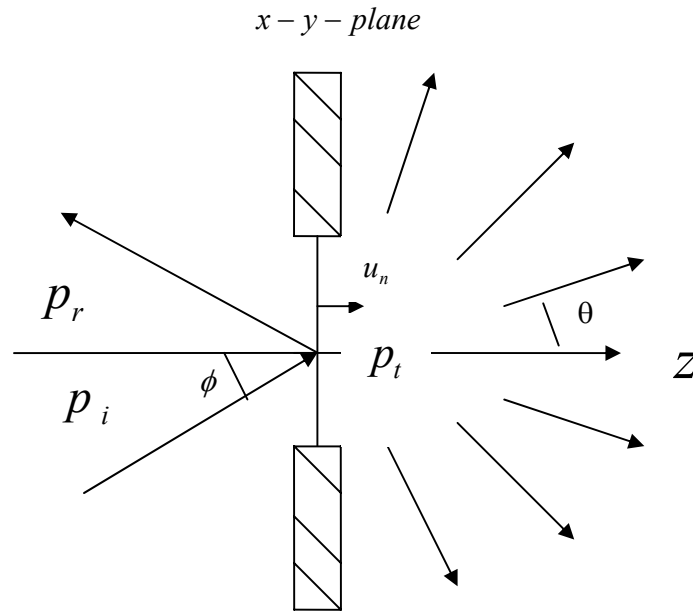


Figure 4.3. The reflection and transmission at a finite size opening or thin panel of a plane wave incident at an angle of ϕ to the normal.

The sound amplitude radiated at an angle θ due to sound incident at an angle ϕ on the other is proportional to

$$\frac{\sin [ka(\sin(\theta) - \sin(\phi))]}{ka(\sin(\theta) - \sin(\phi))} \quad (4.22)$$

The following approximations have been made

$$\sin(\theta) - \sin(\phi) = 2 \sin\left(\frac{\theta - \phi}{2}\right) \cos\left(\frac{\theta + \phi}{2}\right) \quad (4.23)$$

$$\rightarrow ka(\sin(\theta) - \sin(\phi)) = 2ka \sin\left(\frac{\theta - \phi}{2}\right) \cos\left(\frac{\theta + \phi}{2}\right) \quad (4.24)$$

Since $\sin x \approx x$ for small x , then for $\theta - \phi$ small

$$\approx ka(\theta - \phi) \cos(\phi) \quad (4.25)$$

The radiated power per unit length was of interest. This power per unit length is proportional to the pressure squared. Integrating the pressure squared over all angles of θ will give the power per unit length radiated due to a wave incident at an angle of ϕ . The approximation was used on the assumption that any contribution beyond the $\pm \frac{\pi}{2}$ limits is fairly small. The range of validity of this approximation will be investigated later. While this approximation is clearly not correct for low values of ka , the formula obtained for radiation efficiency will be altered later so that it tends to the correct result for a square of side $2a$ at low values of ka . The power per unit length is proportional to

$$\int_{-\frac{\pi}{2}}^{\frac{\pi}{2}} p^2 d\theta \approx \int_{-\infty}^{\infty} p^2 d\theta \quad (4.26)$$

From integral 3.821.9 on page 446 of Gradshteyn and Ryzhik [45]

$$\int_0^{\infty} \frac{\sin^2(mx)}{(x)^2} = |m| \frac{\pi}{2} \quad (4.27)$$

Thus
$$\int_0^{\infty} \frac{\sin^2(mx)}{(mx)^2} = \frac{\pi}{2|m|} \quad (4.28)$$

and
$$\int_{-\infty}^{\infty} \frac{\sin^2(mx)}{(mx)^2} = \frac{\pi}{|m|} \quad (4.29)$$

With these approximations, the total radiated sound power per unit length of strip is proportional to

$$= \int_{-\infty}^{\infty} \frac{\sin^2[ka(\theta - \phi)\cos\phi]}{[ka(\theta - \phi)\cos\phi]^2} d\theta \quad (4.30)$$

$$= \int_{-\infty}^{\infty} \frac{\sin^2(ka\theta\cos(\phi))}{[ka\theta\cos(\phi)]^2} d\theta \quad (4.31)$$

$$= \frac{\pi}{ka\cos(\phi)} \quad (4.32)$$

It is now necessary to investigate the range of validity of equation (4.32). The maximum value of the integrand in equation (4.30) is 1 when θ equals ϕ .

4.3.1 Argument 1

The integrand in equation 4.30 is replaced with a rectangular function which is equal to 1 when θ is within $\frac{\pi}{2ka\cos(\phi)}$ of ϕ and is zero otherwise as shown in figure 4.4. This function

has the same maximum value as the integrand since $\left(\frac{\sin x}{x}\right)^2 \rightarrow 1$ as $x \rightarrow 0$ and the same integral was the integrand. For this replacement function the change to the limits of integration is only valid if the nonzero part of the replacement function lies between $-\pi/2$ to $\pi/2$.

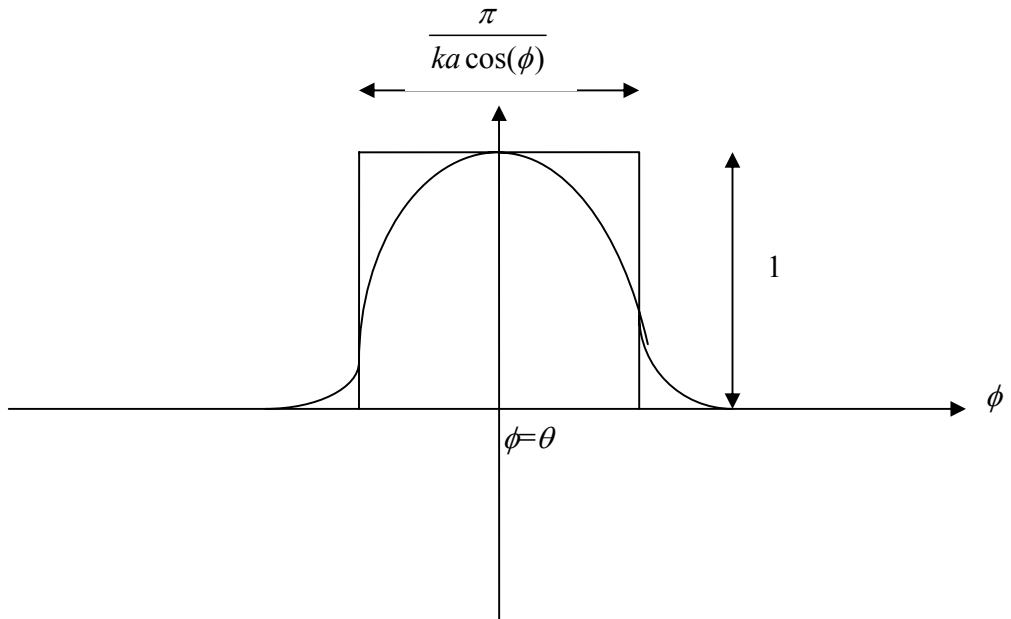


Figure 4.4. Approximation of $\frac{\sin^2 [ka(\theta - \phi) \cos \phi]}{[ka(\theta - \phi) \cos \phi]^2}$ with a rectangular function

4.3.2 Argument 2

Since integration is actually only up to $\pm \frac{\pi}{2}$, the result is only even approximately correct if

the non-zero range of the rectangular function does not include $\pm \frac{\pi}{2}$.

$$|\phi| + \frac{\pi}{2ka \cos(\phi)} \leq \frac{\pi}{2} \quad (4.33)$$

Rearranging the equation

$$\frac{\pi}{2ka \cos(\phi)} \leq \frac{\pi}{2} - |\phi| \quad (4.34)$$

The factor 2 in front of $ka \cos(\phi)$ in equation (4.34) gives half of the width of the rectangular function. At $\phi = \frac{\pi}{2}$ only half of the integral is included as shown in figure 4.5.

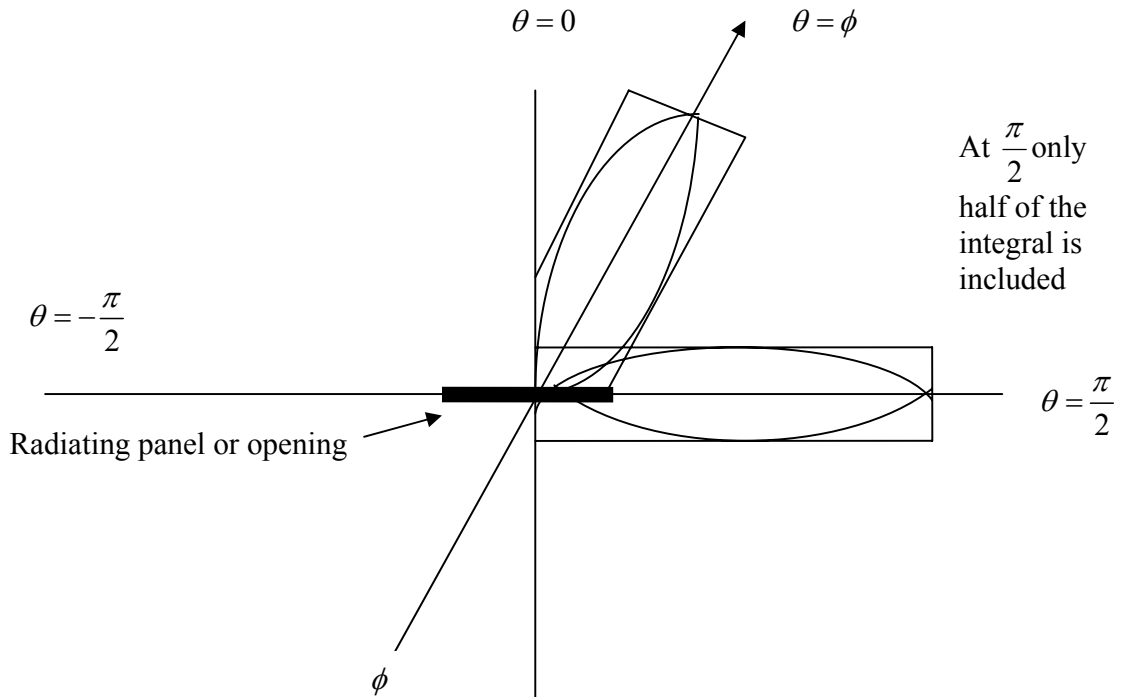


Figure 4.5. Only half of the integral is included at $\theta = \frac{\pi}{2}$ as shown in this polar diagram of the integrand.

There are two arguments for ϕ close to $\frac{\pi}{2}$. One is when

$$\cos \phi \approx \frac{\pi}{2} - \phi \quad (4.35)$$

and the other argument is when

$$\frac{\pi}{2} - \phi \approx \cos \phi \quad (4.36)$$

For ϕ close to $\frac{\pi}{2}$ when $\cos\phi \approx \frac{\pi}{2} - \phi$, substituting equation (4.35) into equation (4.34)

gives

$$\frac{\pi}{2ka\left(\frac{\pi}{2} - \phi\right)} \leq \frac{\pi}{2} - \phi \quad (4.37)$$

$$\frac{\pi}{2ka} \leq \left(\frac{\pi}{2} - \phi\right)^2 \quad (4.38)$$

$$\sqrt{\frac{\pi}{2ka}} \leq \frac{\pi}{2} - \phi \quad (4.39)$$

$$\phi \leq \frac{\pi}{2} - \sqrt{\frac{\pi}{2ka}} \quad (4.40)$$

For ϕ close to $\frac{\pi}{2}$ when $\frac{\pi}{2} - \phi \approx \cos\phi$, substituting equation (4.36) into equation (4.34) gives

$$\frac{\pi}{2ka \cos\phi} \leq \cos\phi \quad (4.41)$$

$$\frac{\pi}{2ka} \leq \cos^2\phi \quad (4.42)$$

$$\cos\phi \geq \sqrt{\frac{\pi}{2ka}} \quad (4.43)$$

$$|\phi| \leq \arccos\left(\sqrt{\frac{\pi}{2ka}}\right) \quad (4.44)$$

Thus equation (4.32) is only valid in the range given by equation (4.44).

Referring back to figure 4.4 and argument 1, one can see that even when $\phi = 0$ and $\cos(\phi) = 1$ the integral must be less than or equal to π . This is because the maximum value of the integrand in equation (4.30) is one, the maximum value of the integral before the limits are extended is $\pi/2 - (-\pi/2) = \pi$.

$$\therefore \frac{\pi}{ka \cos(\phi)} = \frac{\pi}{ka} \leq \pi \quad (4.45)$$

$$\therefore ka \geq 1 \quad (4.46)$$

This means that the approximations can only be valid if ka is greater than or equal to one.

The argument where $\frac{\pi}{2} - \phi \approx \cos \phi$ gives the value of the integral at the limiting angle

defined by $\cos \phi_l = \sqrt{\frac{\pi}{2ka}}$ as

$$\frac{\pi}{ka \cos \phi} = \frac{\pi}{ka} \sqrt{\frac{2ka}{\pi}} \quad (4.47)$$

$$= \sqrt{\frac{2\pi}{ka}} \quad (4.48)$$

It is also possible to approximate the integral if $|\phi| = \pi/2$. Because of symmetry in the equations we only need to consider the case $\phi = \pi/2$. If $\phi = \frac{\pi}{2}$

$$\text{then} \quad ka(\sin(\theta) - \sin(\phi)) = ka \left(\sin(\theta) - \sin\left(\frac{\pi}{2}\right) \right) \quad (4.49)$$

With $\sin\left(\frac{\pi}{2}\right) = 1$ and by using the following identity

$$\sin \theta = \cos\left(\frac{\pi}{2} - \theta\right) \quad (4.50)$$

gives

$$ka(\sin(\theta) - \sin(\phi)) = ka \left[\cos\left(\frac{\pi}{2} - \theta\right) - 1 \right] \quad (4.51)$$

If $\frac{\pi}{2} - \theta$ is small and only the first two terms of the

$\cos \theta = 1 - \frac{\theta^2}{2} + \frac{\theta^4}{4} - \dots$ expansion are used

$$\approx ka \left[1 - \frac{1}{2} \left(\frac{\pi}{2} - \theta \right)^2 - 1 \right] \quad (4.52)$$

Substituting $y = \frac{\pi}{2} - \theta \rightarrow \frac{ka}{2} y^2$, it follows that the integral becomes

$$\int \frac{\sin^2\left(\frac{ka}{2} y^2\right)}{\left(\frac{ka}{2} y^2\right)^2} dy \quad (4.53)$$

Using integral number 3.852.3 on page 464 of Gradshteyn and Ryzhik [45]

$$\int_0^{\infty} \frac{\sin^2(a^2 x^2)}{x^4} dx = \frac{2\sqrt{\pi}}{3} a^3 \quad (4.54)$$

gives

$$= \frac{1}{\left(\frac{ka}{2}\right)^2} \frac{2\sqrt{\pi}}{3} \left(\frac{ka}{2}\right)^{3/2} \quad (4.55)$$

$$= \frac{2}{3} \sqrt{\frac{2\pi}{ka}} \quad (4.56)$$

This is 2/3 of the maximum value at $\cos \phi = \sqrt{\frac{\pi}{2ka}}$.

4.4 *Finite size square panels*

From equations 4.8 and 4.9, the power radiated into a half space by a panel of surface area S is

$$P_t = |u_n|^2 \cdot S \cdot \rho c \cdot \sigma \quad (4.57)$$

where $u_n = u_{iz} + u_{rz} = u_{tz}$ is the normal rms component of the particle velocity. The velocities are positive in the direction of the z-axis, and the indices i, r and t refer to incident, reflected and transmitted wave, respectively [19].

The radiated power is

$$P_t = |u_n|^2 \cdot S \cdot \rho c \cdot \text{Re}\{z_{wf}\} \quad (4.58)$$

where

$$\text{Re}\{z_{wf}\} = \rho c \sigma$$

The short-wave-theory or infinite-panel-theory implies that for values $ka \rightarrow \infty$, the dotted curve in figure 4.6 corresponds to $\sigma = \frac{1}{\cos \phi}$. The short-wave-theory or infinite-panel-theory is only valid if the wavelength of the sound is short compared to the dimensions of the panel. As $\theta \rightarrow 90^\circ$, $\sigma \rightarrow \infty$ and the radiation impedance tends to infinity

$$\begin{aligned} z_{wf} \approx \text{Re}\{z_{wf}\} = \rho c \sigma &\rightarrow \frac{\rho c}{\cos \phi} \quad \text{for } ka \rightarrow \infty \\ &\rightarrow \infty \quad \text{for } \theta \rightarrow 90^\circ \end{aligned} \quad (4.59)$$

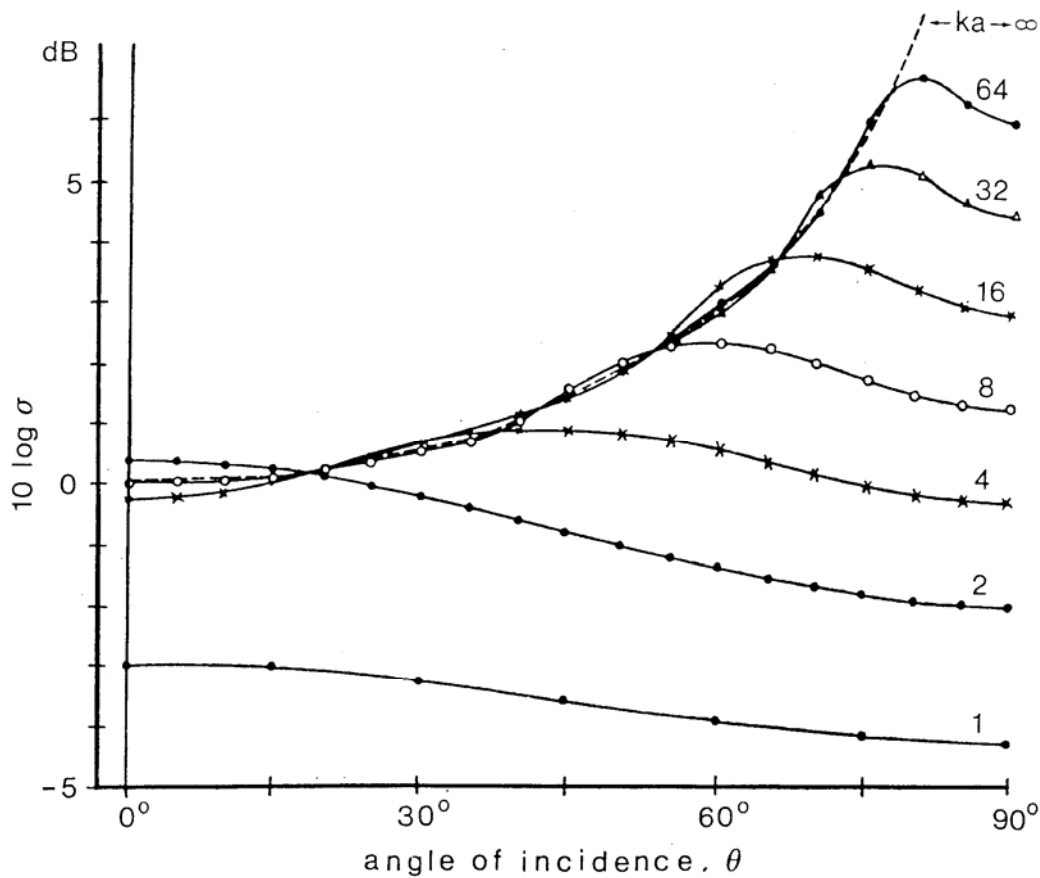


Figure 4.6. Calculated values of radiation efficiency. Square panel with incidence in x-z plane [4].

In practice, for a real panel, ka will always have a finite value. Figure 4.6 shows that when $ka \gg 1$, σ increases with ϕ like a dotted curve until a certain value, where σ remains finite, even for $\phi = 90^\circ$. When ka decreases, the influence of ϕ on σ is reduced.

For $ka < 2$, σ decreases with decreasing ka to values less than unity, and ϕ loses its importance. When $ka \ll 1$, the following approximation applies:

$$\operatorname{Re}\{z_i\} \approx \rho c \sigma \rightarrow \frac{2\rho c}{\pi} (ka)^2 \text{ for } ka \ll 1 \quad (4.60)$$

In order to calculate the radiation efficiency for $ka \ll 1$ of the square panel it was assumed that the same result for radiation efficiency will be produced if the impedance for a pulsating

hemisphere with the same surface area as square of side $2a$ was calculated. The argument was that, because of the symmetry for the plane in the middle of the hemisphere and the small size of the source compared to the wavelength of the sound, the impedances of the spherical and square sources are the same. The critical factor was the volume velocity, the product of the linear velocity and surface area.

Hence, the area of hemisphere with radius r is area $2\pi r^2$ and area of the square is $(2a)^2$.

Equating those areas gives

$$2\pi r^2 = (2a)^2 = 4a^2 \quad (4.61)$$

$$r^2 = \frac{2}{\pi} a^2 \quad (4.62)$$

Now at very low frequencies the real part of the normalized specific acoustic impedance for sphere of radius r is $k^2 r^2$

$$k^2 r^2 = \frac{2}{\pi} k^2 a^2 \quad (4.63)$$

Thus the radiation efficiency of the square panel is

$$\sigma = \frac{\text{Re}(Z_{wf})}{Z_c} = k^2 r^2 = \frac{2}{\pi} k^2 a^2 \quad (4.64)$$

The radiation efficiency of the square panel is combined with the radiation efficiency of the strip by inverting both efficiencies, adding them together and inverting the result of the addition.

$$\sigma(\phi) = \begin{cases} \frac{1}{\frac{\pi}{2k^2a^2} + \cos \phi} & \text{if } |\phi| \leq \phi_l \\ \frac{1}{\frac{\pi}{2k^2a^2} + \frac{3 \cos \phi - \cos \phi_l}{2}} & \text{if } \phi_l < |\phi| \leq \frac{\pi}{2} \end{cases} \quad (4.65)$$

In equation (4.65) the result has been interpolated linearly in $\cos \phi$ between the result at $|\phi| = \phi_l$ and the result at $|\phi| = \frac{\pi}{2}$. The argument was that $\frac{1}{\cos \phi}$ is correct up to the limiting angle ϕ_l and above this limiting angle it was shown that at 90 degrees the value is 2/3 of the value at the limiting angle.

The values in between were approximated by a straight line as a function of $\cos \phi$. The results are shown in figure 4.7.

The radiation efficiency averaged over all angles of incidence ϕ is

$$\langle \sigma \rangle = \int_{-\frac{\pi}{2}}^{\frac{\pi}{2}} \sigma(\phi) \sin \phi d\phi \quad (4.66)$$

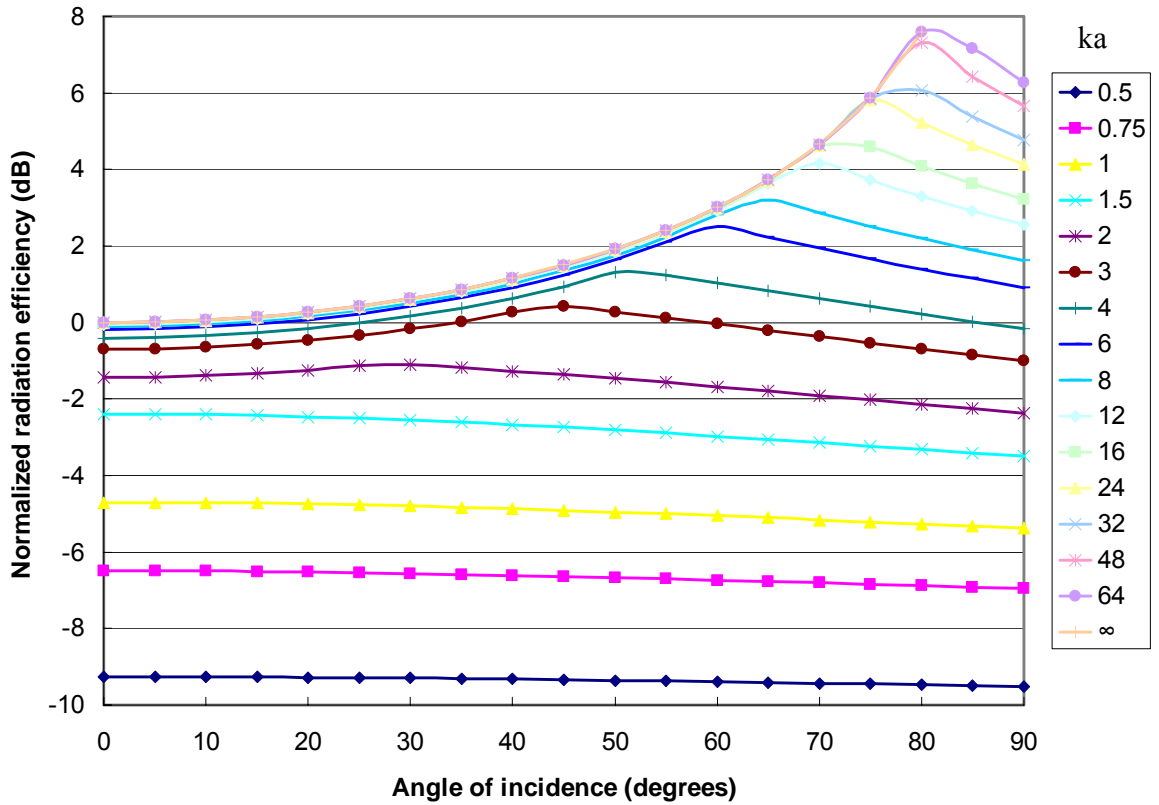


Figure 4.7. Radiation efficiency as a function of the angle of incidence and the values of ka shown in the legend.

Sato [4] calculated values of $\sigma(ka)$ in decibels (dB) for a square wall at all angles where he integrated those values to find their average value $\langle \sigma(ka) \rangle$ over all angles of incidence. The radiation efficiency given by equation (4.65) and Sato's numerically calculated radiation efficiency results were compared. Comparison showed that the equation (4.65) is always between -1.8dB and $+1.1\text{ dB}$ of Sato's numerical results. The biggest errors resulted from the combination of the high frequency and low frequency results in the region of $ka = 2$. Rindel's [19] approximations differs from Sato's tabulated results by between -1.4 dB and $+0.9\text{ dB}$, but it is too complicated to be easily analytically integrated.

The approximate expression for radiation efficiency was integrated to obtain the average value of radiation efficiency over all angles of incidence.

$$\int_{-\frac{\pi}{2}}^{\frac{\pi}{2}} \sigma(\phi) \sin \phi d\phi \quad (4.67)$$

To evaluate this integral, the following substitutions were made

$$y = \frac{\pi}{2(ka)^2} \quad g = \cos \phi$$

$$dg = -\sin \phi d\phi$$

Substituting $g = \cos \phi$ when $dg = -\sin \phi d\phi$ gave

$$= -\int_1^0 \sigma(g) dg = \int_0^1 \sigma(g) dg$$

$$= \int_{g_l}^1 \frac{dg}{y+g} + \int_0^{g_l} \frac{dg}{y+(3g_l-g)} \quad (4.68)$$

The cosine of the limiting angle was denoted as g_l . The radiation efficiency at 90° will be equal to $2/3$ of its value at the limiting angle if y is insignificant. At the limiting angle the radiation efficiency is equal to $1/(y+g_l)$ and at $g_l=0$ which corresponds to 90° , $1/(y+\frac{3}{2}g_l)$

is produced. In order to get $\frac{2}{3}\left(\frac{1}{g_l}\right)$, $1.5 g_l$ at the bottom line of equation (4.68) is needed.

Clearly when $g=0$, $\frac{y+(3g_l-g)}{2}$ expression is equal to $1.5 g_l$, and when $g=g_l$, the expression

$y + \frac{(3g_l-g)}{2}$ is equal to $y+g_l$ which is what was expected.

$$= [\ln(y+g)]_{g_l}^1 + 2 \int_0^{g_l} \frac{dg}{2y+3g_l-g}$$

$$\begin{aligned}
&= \ln\left(\frac{y+1}{y+g_l}\right) - 2\left[\ln(2y+3g_l - g)\right]_0^{g_l} \\
&= \ln\left(\frac{y+1}{y+g_l}\right) - 2\ln\left(\frac{2y+2g_l}{2y+3g_l}\right) \\
&= \ln\left(\frac{y+1}{y+g_l}\right) + 2\ln\left(\frac{2y+3g_l}{2y+2g_l}\right)
\end{aligned} \tag{4.69}$$

Since we are dealing with finite panels not just openings one needs to implement the plate wave impedance which is

$$Z_{wp} = m\omega \left\{ j \left[1 - \left(\frac{k_s}{k_b} \right)^4 \right] + \eta \left(\frac{k_s}{k_b} \right)^4 \right\} \tag{4.70}$$

where k_s is the wave number of incident sinusoidal sound wave,

k_b is the wave number of the forced sinusoidal bending wave,

η is the damping loss factor,

m is the mass per unit area of the panel and

ω is the angular frequency.

Substituting the trace wave number, which is $k_s = k \sin \phi$, into equation (4.70) gives

$$Z_{wp} = m\omega \left\{ j \left[1 - \left(\frac{k \sin \phi}{k_b} \right)^4 \right] + \eta \left(\frac{k \sin \phi}{k_b} \right)^4 \right\} \tag{4.71}$$

The critical frequency is $\omega^2 = \frac{c^4 m}{D}$ where D is the bending stiffness of the plate, with fluid

wave number $k^4 = \left(\frac{\omega}{c} \right)^4$ and free bending wave equal to $k_b^4 = \frac{m\omega^2}{D}$. Substituting these into

equation (4.71) gives the following expression for the plate wave impedance

$$Z_{wp} = m\omega \left\{ j \left[1 - \left(\frac{\omega}{\omega_c} \right)^2 \sin^4 \phi \right] + \eta \left(\frac{\omega}{\omega_c} \right)^2 \sin^4 \phi \right\} \quad (4.72)$$

Combining the fluid wave impedance $Z_{wf} = \frac{\rho_0 c}{\cos \phi}$ with the plate wave impedance Z_{wp} gives

$$Z = \frac{p}{v} = 2\rho_0 c \sigma(\phi) + m\omega \left\{ j \left[1 - \left(\frac{\omega}{\omega_c} \right)^2 \sin^4 \phi \right] + \eta \left(\frac{\omega}{\omega_c} \right)^2 \sin^4 \phi \right\} \quad (4.73)$$

The reason for the factor 2 is that when sound pressure is applied onto the panel it vibrates and sound pressure is radiated on both sides of the panel. Thus the fluid wave impedance on both sides of the panel will be needed.

The first term of equation (4.73) does not include the imaginary part of the impedance. This is not a problem for the large panels. For finite size panels where ka values are small and the imaginary part is significant, this term will be much smaller than the impedance of the panel. For openings with a small values of ka , the impedance is relatively independent of angle of incidence ϕ and its value will have an insignificant effect on the directivity calculations.

CHAPTER 5

5. Relative Sound Level

The initial research of this thesis was the investigation of directivity patterns of different acoustic sources. One of the directivity patterns found is shown in figure 5.1.

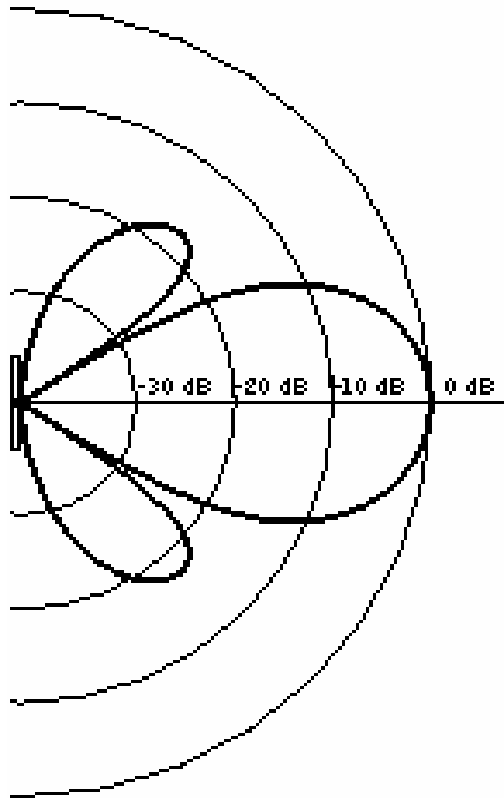


Figure 5.1. Directivity pattern for a circular piston in a large baffle when ka is large [46].

Figures 5.2 and 5.3 show different representations of the directivity pattern found in figure 5.1.

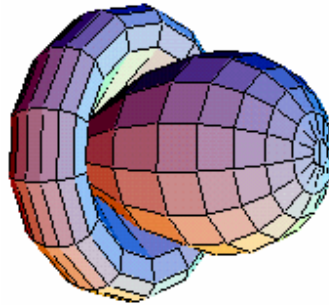


Figure 5.2. 3-D directivity pattern field for a circular piston in a larger piston when ka is large [46].

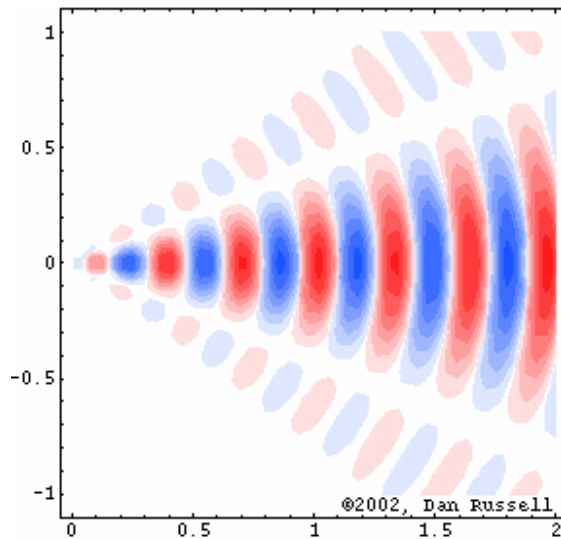


Figure 5.3. Animation of sound field for a circular piston in a larger piston when ka is large [47].

The color palette used to generate the *Mathematica* contour plots on this page was borrowed from Sparrow et al. [48].

Figure 5.1 shows the case when the frequency becomes high and ka becomes much greater than 1. Figure 5.1 represents measured directivity pattern for a loudspeaker when the frequency is at 10 kHz and ka is 9.34 [47]. At higher frequencies (10 kHz) the speaker radiates all of its sound in front. The sound level behind the speaker is almost 25 dB lower than the level in front, indicating that much more sound energy is being radiated directly in front and very little behind. The sound field radiated by the loudspeaker becomes narrower and side lobes appear. The pressure amplitude falls off rapidly as the distance from the central axis increases. The side lobes are much lower in amplitude than the main lobe where the darker the contour the higher the pressure and the louder the sound. It might be important to note that the sound waves in the side lobes have the opposite phase to the sound waves in the main lobe.

While investigating the radiation of sound Rindel found the directivity pattern $\left(\frac{\sin x}{x}\right)^2$ for a single frequency, where x is defined as in equation (5.1). This is shown in figure 5.4 [49].

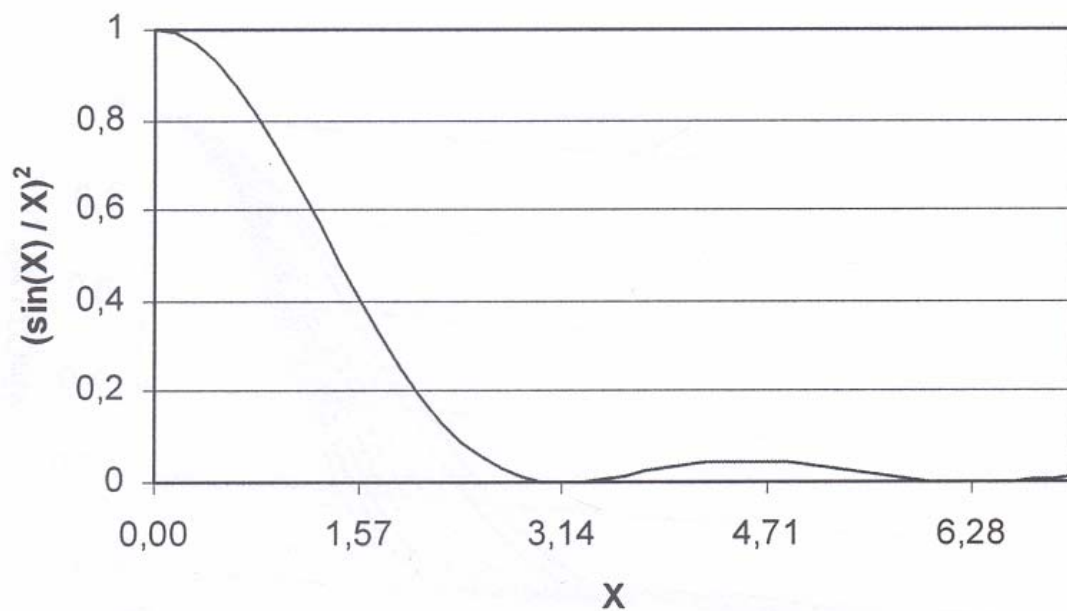


Figure 5.4. The radiation function $\left(\frac{\sin x}{x}\right)^2$ for a single frequency [49].

Figure 5.4 indicates that there are some side lobes, which occur when x is greater than 3.14. It appears that this supports the evidence presented in figure 5.3, which represents the case

when the frequency becomes high (ka equals 9.34). Side lobes are also seen in the measured result shown in figure 5.5.

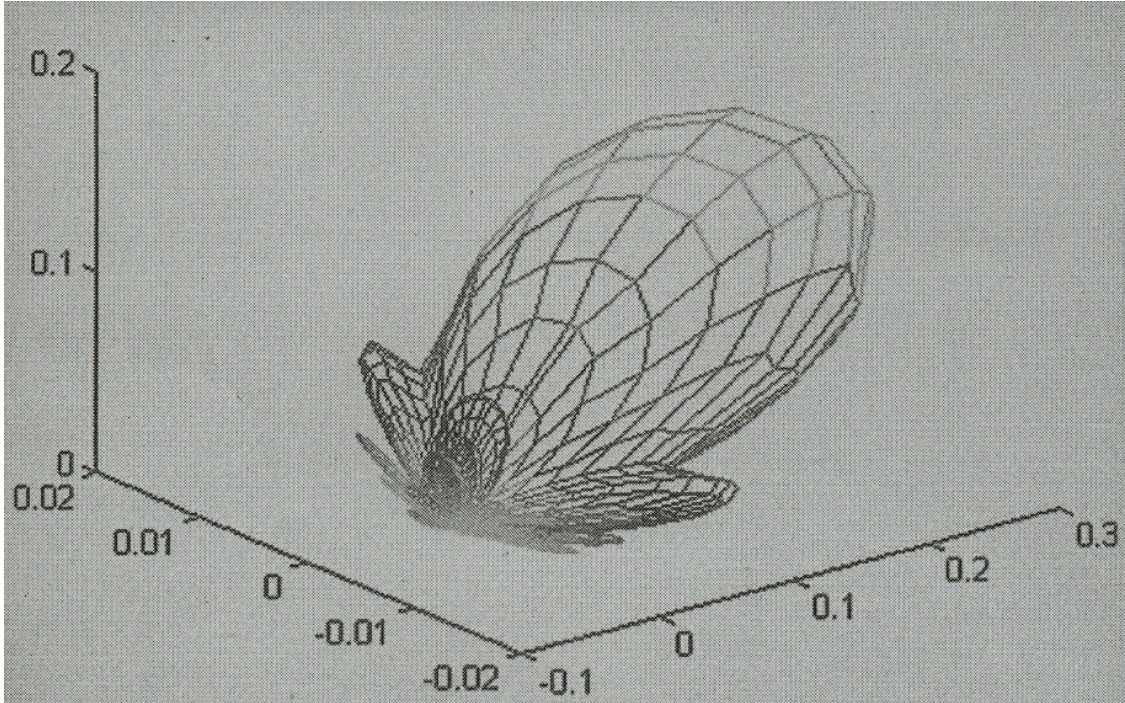


Figure 5.5. Measured radiation pattern from a plane surface [50].

Rindel assumed that the incident sound is a plane wave and the surface is rectangular with dimensions $2a \times 2b$ as shown in figure 5.6.

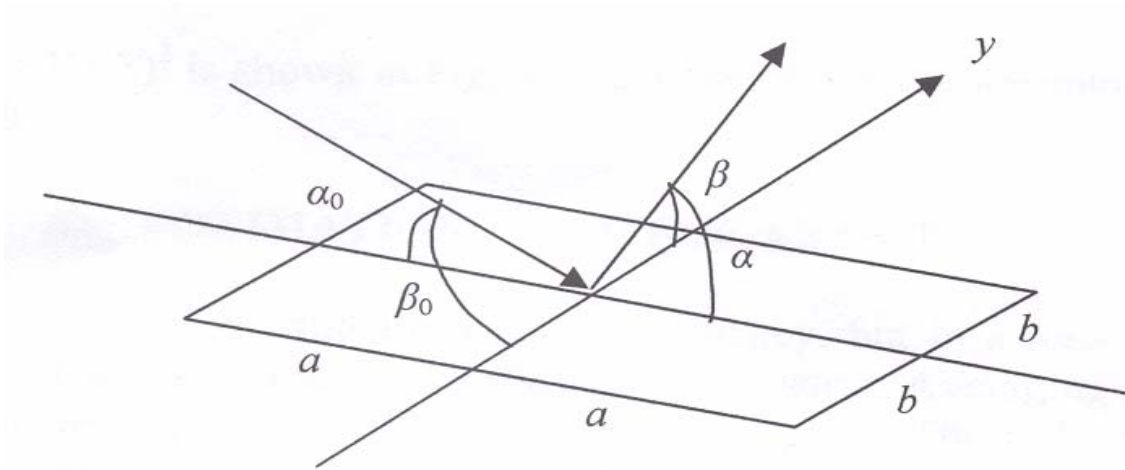


Figure 5.6. Definition of angles of incidence and reflection from a rectangular surface [49].

The angles α_0 and β_0 relative to the x and y axes describe a direction of propagation of the incident wave. The angles α and β relative to the x and y axes describe a direction on the receiver side [49]. Using the result for sound transmission through a rectangular opening as derived in [19], Rindel found the following expression:

$$x = ka(\cos \alpha - \cos \alpha_0) \quad (5.1)$$

Figures 5.1 and 5.5 produce very similar directivity patterns. Our calculation method was based on finding the sound amplitude, which is radiating into the half space for a particular angle. It could be shown that the parameter $ka(\sin(\theta) - \sin(\phi))$ in equation (4.22) is same as the x in equation (5.1).

5.1 *Analysis and comparison of the level of sound radiated as predicted by different models*

The thesis will not present a method for predicting the sound insulation at grazing angles. It will attempt to predict the level of sound radiated from a finite flat panel or finite opening in any particular direction relative to the level of sound radiated in the direction normal to the finite flat panel or finite opening.

5.1.1 The equations used for calculation

The effective impedance $Z_e(\phi)$ of a finite panel in an infinite baffle to a plane sound wave incident at an angle of ϕ to the normal to the panel is

$$Z_e(\phi) = Z_{wfi}(\phi) + Z_{wft}(\phi) + Z_{wp}(\phi) \quad (5.2)$$

where

$Z_{wfi}(\phi)$ is the wave impedance of the fluid as experienced by the finite panel in an infinite baffle, whose vibration is due a plane sound wave incident at an angle of ϕ to the normal to the panel, on the side from which the plane sound wave is incident (this is the fluid loading on the incident side),

$Z_{wft}(\phi)$ is the wave impedance of the fluid as experienced by the finite panel in an infinite baffle, whose vibration is due a plane sound wave incident at an angle of ϕ to the normal to the panel, on the side opposite to which the sound is incident (this is the fluid loading on the non-incident or transmitted side) and

$Z_{wp}(\phi)$ is the wave impedance of the finite panel in an infinite baffle to a plane sound wave incident at an angle of ϕ to the normal to the panel, ignoring fluid loading.

We will assume that the fluid wave impedances on both sides are the same and ignore the imaginary part of the fluid wave impedance. That is

$$Z_{wfi}(\phi) = Z_{wft}(\phi) = \rho c \sigma(\phi) \quad (5.3)$$

where ρ is the density of the fluid, c is the speed of sound in the fluid and $\sigma(\phi)$ is the radiation efficiency into the fluid of one side of the finite panel in an infinite baffle, whose vibration is due a plane sound wave incident at an angle of ϕ to the normal to the panel.

The rms normal velocity $v_{rms}(\phi)$ of the panel due to a plane sound wave incident at an angle of ϕ to the normal to the panel which exerts an rms pressure $p_{irms}(\phi)$ is

$$v_{rms}(\phi) = \frac{p_{irms}(\phi)}{2\rho c \sigma(\phi) + Z_{wp}(\phi)} \quad (5.4)$$

The transmitted rms sound pressure $p_{trms}(\theta, \phi)$ which is radiated by the panel on the non-incident side to a receiving point which is at an angle of θ to the normal to the centre of the panel and a large distance from the panel is

$$p_{trms}(\theta, \phi) \propto v_{rms}(\phi) \frac{\sin[ka(\sin \theta - \sin \phi)]}{ka(\sin \theta - \sin \phi)}$$

$$\propto \frac{p_{irms}(\phi)}{2\rho c \sigma(\phi) + Z_{wp}(\phi)} \frac{\sin[ka(\sin \theta - \sin \phi)]}{ka(\sin \theta - \sin \phi)} \quad (5.5)$$

where k is the wave number of the sound and $2a$ is the length of the panel in the direction of the source.

We now consider the case where sound is generated by a sound source in a room or duct. We assume that the sound pressure waves are incident at different angles ϕ with random phases and mean squared sound pressures which are proportional to a weighting function $w(\phi)$.

$$|p_{irms}(\phi)|^2 \propto w(\phi) \quad (5.6)$$

The weighting function is to account for the fact that sound waves at grazing angles of incidence will have had to suffer more wall collisions and therefore be more attenuated before reaching the panel. The total mean square sound pressure $|p_{Trms}(\theta)|^2$ at the receiving point is

$$|p_{Trms}(\theta)|^2 \propto \int_{-\frac{\pi}{2}}^{\frac{\pi}{2}} \frac{w(\phi)}{|2\rho c \sigma(\phi) + Z_{wp}(\phi)|^2} \left\{ \frac{\sin[ka(\sin \theta - \sin \phi)]}{ka(\sin \theta - \sin \phi)} \right\}^2 d\phi \quad (5.7)$$

We are also interested in the case when sound is incident from a source in a free field at an angle θ to the normal to the panel and the panel radiates at all angles ϕ into a room or duct. In this case the weighting function $w(\phi)$ is to account for the fact that sound waves radiated at grazing angles will have had to have more wall collisions and therefore be more attenuated before reaching a microphone near the middle of the room. In this second case, we have to integrate over all angles of radiation ϕ because of the reverberant nature of the sound. For this case, the impedance terms in the integral are functions of θ rather than ϕ and can be taken outside the integral. However in this study we have calculated both cases using the formula for the first case which is shown above. This is because both cases should be the same by the principle of reciprocity and it is not clear which form of the formula is more correct.

For large values of ka , the two cases of the formula will be similar. If ka is much greater than 1, the function

$$\left\{ \frac{\sin[ka(\sin \theta - \sin \phi)]}{ka(\sin \theta - \sin \phi)} \right\}^2 \quad (5.8)$$

has a sharp maximum at $\phi = \theta$ and is symmetrical in both θ and ϕ about the point $\theta = \phi$. We can exploit these facts by evaluating the impedance terms for the first case at $\phi = \theta$ and taking them out side the integral. This gives the formula for the second case.

The relative sound pressure level $L(\theta)$ in the direction θ is

$$L(\theta) = 20 \log_{10} (|p_{Trms}(\theta)|) - 20 \log_{10} (|p_{Trms}(0)|) \quad (5.9)$$

A weighting function was needed, because the assumption of diffuse field incidence did not agree with the experimental results in the literature. In this study, the following weighting function $w(\phi)$ was used.

$$w(\phi) = \begin{cases} \frac{1}{2} \left(1 + \cos \left(\frac{\pi\phi}{\phi_w} \right) \right) & \text{if } |\phi| < \phi_w \\ 0 & \text{if } |\phi| \geq \phi_w \end{cases} \quad (5.10)$$

This weighting function was chosen because it goes smoothly to zero at the weighting angle ϕ_w . Weighting functions based on physical models are being investigated by a more recent postgraduate student. Note that this weighting angle ϕ_w is different from the limiting angle ϕ_l which was introduced in chapter 4. ϕ_l is a function of ka which is used in the calculation the radiation efficiency $\sigma(\phi)$. ϕ_w is a parameter which is use to match the weighting function to the actually distribution of sound as determined by the best match between the theory and the directivity results from the literature. ϕ_w may need to be a function of frequency, angle of radiation (or incidence), size of panel, size of opening, room dimensions or duct length. However in this thesis we will try to use a constant value of ϕ_w when comparing with a particular set of experimental or theoretical data.

It is important to note that although the weighting angle ϕ_w can be greater than $\pi/2$, ϕ is only integrated over the range from $-\pi/2$ to $\pi/2$. Also, the weighting function does not have to be zero when ϕ is equal to $-\pi/2$ and $\pi/2$. Uniform weighting is obtained when ϕ_w is infinite.

In this study we use the radiation efficiency of a strip of width $2a$, which we approximate with the following equation (see equation (4.65)).

$$\sigma(\phi) = \begin{cases} \frac{1}{\frac{\pi}{2k^2a^2} + \cos \phi} & \text{if } |\phi| \leq \phi_l \\ \frac{1}{\frac{\pi}{2k^2a^2} + \frac{3 \cos \phi - \cos \phi}{2}} & \text{if } \theta_l < |\theta| \leq \frac{\pi}{2} \end{cases} \quad (5.11)$$

where

$$\phi_l = \arccos\left(\sqrt{\frac{\pi}{2ka}}\right) \quad (5.12)$$

and k is the wave number of the sound and $2a$ is the length of the panel in the direction of the source.

For an opening with no panel in an infinite baffle we put $Z_{wp}(\phi) = 0$. For a finite panel in an infinite baffle we use the infinite panel result for $Z_{wp}(\phi)$. This result is expected to be the correct result when averaged over frequency, because this approach gives the correct result for point impedances when averaged over frequency and position on a finite panel.

$$Z_{wp}(\phi) = m\omega \left\{ j \left[1 - \left(\frac{\omega}{\omega_c} \right)^2 \sin^4(\phi) \right] + \eta \left(\frac{\omega}{\omega_c} \right)^2 \sin^4(\phi) \right\} \quad (5.13)$$

where m is the surface density (mass per unit area) of the panel, η is the damping loss factor of the panel, ω_c is the critical frequency of the panel and ω is the angular frequency of the sound.

In this study the integral was performed by evaluating the integrand at 1° intervals from -90° to 90° and summing the values. In some cases, a constant value of attenuation relative to radiation in the normal direction was added to the calculated value to obtain better agreement at low frequencies. In one case, the attenuation relative to radiation in the normal direction was limited to a maximum value of attenuation by a method described later.

5.1.1.1 Why are openings and finite panels different?

The case when the sound is radiated from a room or duct is considered in this section. We assume that the sound is incident as described by the weighting function $w(\phi)$. The following analysis applies to finite size openings and finite size panels. Assumptions will be made which allow the approximation $\phi = \theta$. To show why openings and finite panels are different we make a further approximation. In the equation (5.7) for the total mean square sound pressure $|p_{Trms}(\theta)|^2$ at the receiving point we note that if ka is much greater than 1, the function

$$\left\{ \frac{\sin[ka(\sin \theta - \sin \phi)]}{ka(\sin \theta - \sin \phi)} \right\}^2 \quad (5.14)$$

has a sharp maximum at $\phi = \theta$. We exploit this fact by evaluating the rest of the integral at $\phi = \theta$ and taking it out side the integral. We then note that the integral that we are left with is proportional to the radiation efficiency $\sigma(\theta)$ of the finite panel. Thus

$$|p_{Trms}(\theta)|^2 \propto \frac{w(\theta)\sigma(\theta)}{|2\rho c\sigma(\theta) + Z_{wp}(\theta)|^2} \quad (5.15)$$

For an opening $Z_{wp}(\phi) = 0$ and we obtain

$$|p_{Trms}(\theta)|^2 \propto \frac{w(\theta)}{\sigma(\theta)} \quad (5.16)$$

For a finite panel $|Z_{wp}(\theta)|^2 \gg 2\rho c\sigma(\theta)$ and we obtain

$$|p_{Trms}(\theta)|^2 \propto \frac{w(\theta)\sigma(\theta)}{|Z_{wp}(\theta)|^2} \quad (5.17)$$

Apart from near coincidence $|Z_{wp}(\theta)|^2$ is independent of θ . Thus the result for a finite panel reduces to

$$|p_{Trms}(\theta)|^2 \propto w(\theta)\sigma(\theta) \quad (5.18)$$

If $ka \gg 1$ and $|\theta| < \phi_l$

$$\sigma(\theta) = \frac{1}{\cos(\theta)} \quad (5.19)$$

In this case, if $w(\theta)$ is constant, for an opening we obtain

$$|p_{Trms}(\theta)|^2 \propto \cos(\theta) \quad (5.20)$$

and for a finite panel we obtain

$$|p_{Trms}(\theta)|^2 \propto \frac{1}{\cos(\theta)} \quad (5.21)$$

Note that equation (5.21) is different from the solid piston results graphed in Figures 5.1 to 5.4.

Another possible simple weighing function is

$$w(\theta) \approx \cos(\theta) \quad (5.22)$$

With this weighting, our approximate results become

$$|p_{Trms}(\theta)|^2 \propto \cos^2(\theta) \quad (5.23)$$

for an opening and

$$|p_{Trms}(\theta)|^2 \text{ is independent of } \theta$$

for a finite panel except near coincidence. In both cases, the ratio of the result for an opening to the result for a finite panel is proportional to $\cos^2(\theta)$. Note that this result assumes $ka \gg 1$ and $|\theta| < \phi_l$ where ϕ_l is given by equation (5.12).

In this chapter, the prediction method described in section 5.1.1 is compared with experimental results and prediction methods for finite size openings and finite size panels from the literature. The weighting function given in equation (5.10) is used and the weighting angle ϕ_w is varied to obtain the best agreement. The weighting function and the weighting angle ϕ_w give an indication of the distribution of incident sound which is needed to produce the experimental results or the results of the predictive method. This will be a valuable guidance for future work which seeks to develop a physical model of the incident sound distribution in different situations. Results for all methods are presented on a logarithmic scale of Strouhal number. The Strouhal number is defined as the ratio of the distance across the finite flat panel or finite opening in the direction of radiation relative to the wavelength of the sound in the air.

5.1.2 Roberts experimental results and prediction method for finite openings

Roberts offered a simple prediction method for finite openings, which agreed with practical tests. This method was based on a concept of a flat discrete plane wave front expanding on all flanks at the velocity of sound, where the sound field was controlled by the frequency of the sound and the size of the generating surface. Roberts conducted the tests with sound radiating from an opening of a sliding window in the wall of room to outside. [7]. The size of the wall (baffle) in which the sliding window was mounted is not stated in [7]. The opening width was set at 75, 130, 300 and 600 millimetres and the opening height was 970 millimetres. The measurements were made at 0° and 90° to the normal to the opening at a distance of 1000 millimetres from the centre of the edge of the opening. The measurements were made in both the horizontal and vertical directions. It is important to note that Roberts' calculated directivity results were produced when his directivity coefficient (Dc) was equal to 0.5, which is appropriate for the sound emitting from low reverberant rooms through a free opening.

Roberts' measured sound level at 90° relative to the sound level at 0° with various opening widths were compared with the theory of section 5.1.1 for predicting the sound radiation. Figure 5.7 represents the sound level at 90° relative to the sound level at 0° with the weighting angle ϕ_w set at 78° . The weighting angle ϕ_w was introduced in equation (5.10). It should not be confused with the limiting angle ϕ_l which was introduced in chapter 4 in the calculation of the radiation efficiency.

In figure 5.7, the theory of section 5.1.1 is compared to Roberts' measured data.

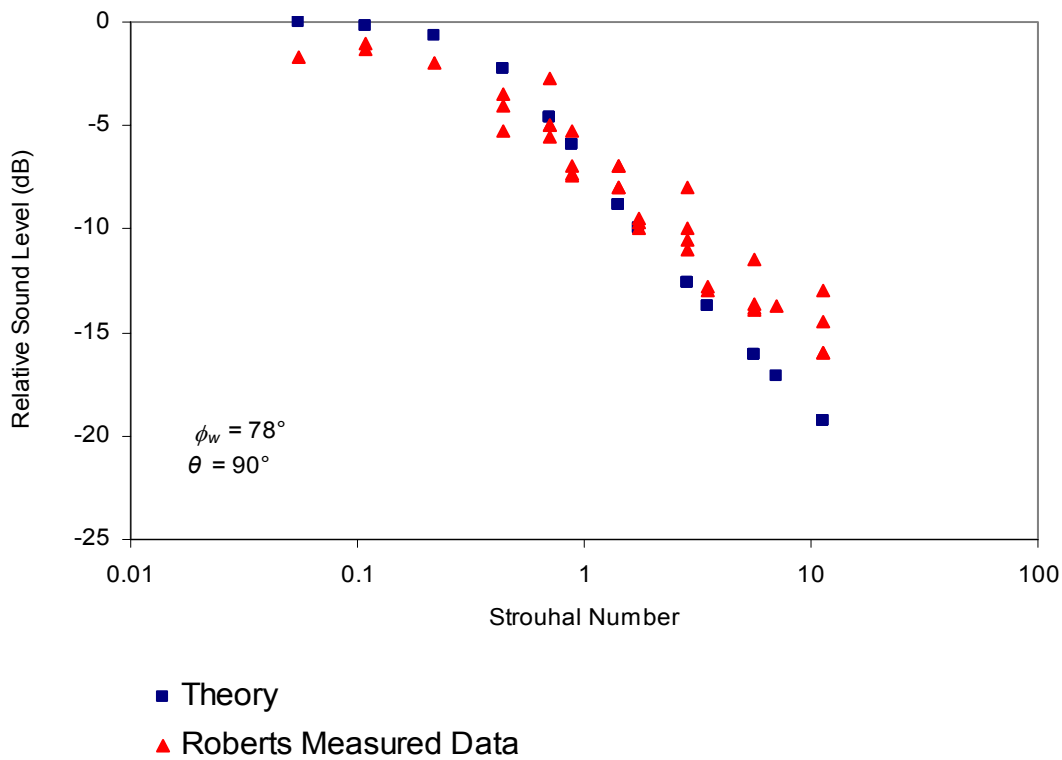


Figure 5.7. Comparison of Roberts experimental data with the theory of section 5.1.1 for the sound level at 90 degrees relative to the sound level at 0 degrees. The theory of section 5.1.1 is used with the weighting function using a weighting angle ϕ_w of 78 degrees.

At low Strouhal number the theory of section 5.1.1 exhibited a smaller relative sound level than Roberts' experimental data. In order to obtain reasonable agreement between the theory

of section 5.1.1 and the data presented by Roberts, a negative relative sound level constant was added to results of the theory of section 5.1.1

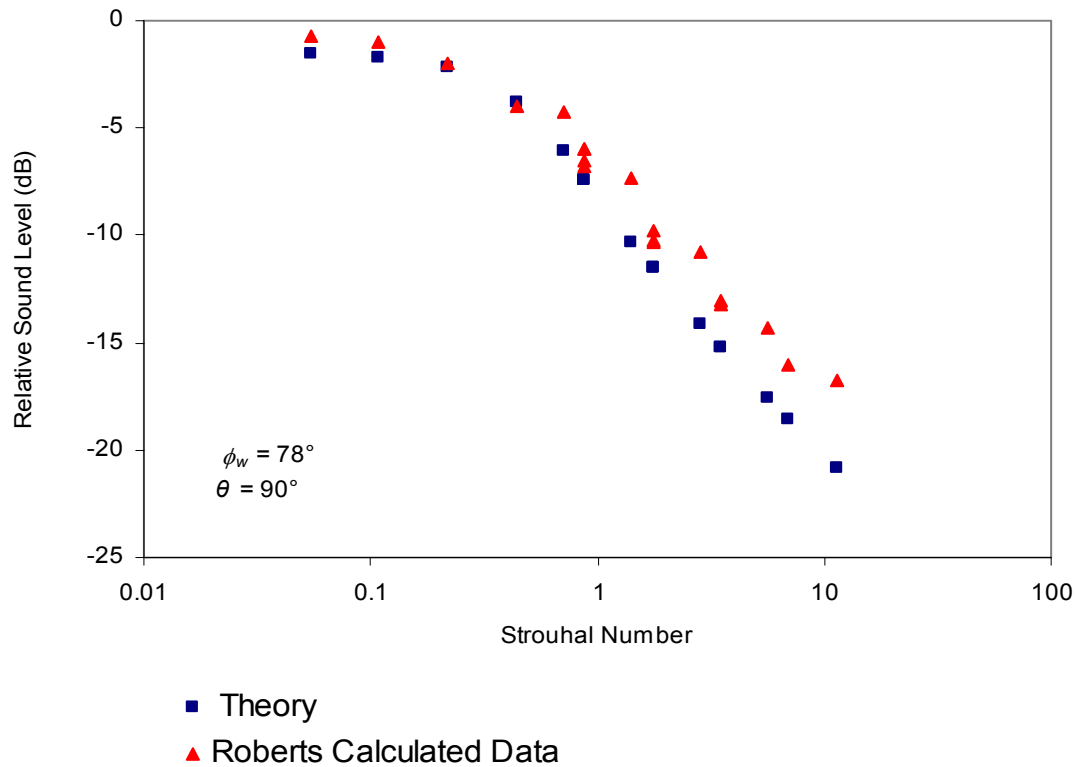


Figure 5.8. Comparison of Roberts calculated data with the theory of section 5.1.1 for the sound level at 90 degrees relative to the sound level at 0 degrees. The theory of section 5.1.1 is used with the weighting function using a weighting angle ϕ_w of 78 degrees. A negative relative sound level constant of -1.5 dB was added to results of the theory of section 5.1.1.

Figure 5.8 shows comparison of the theory of section 5.1.1 with Roberts calculated data. The constant of relative sound level was set to -1.5 dB because this gave the best agreement between theory and experiment. The relative sound level curves exhibit a similar pattern as in figure 5.7. Since we are interested in measured and practical tests, the theory of section 5.1.1 will be compared only to Roberts' measured data.

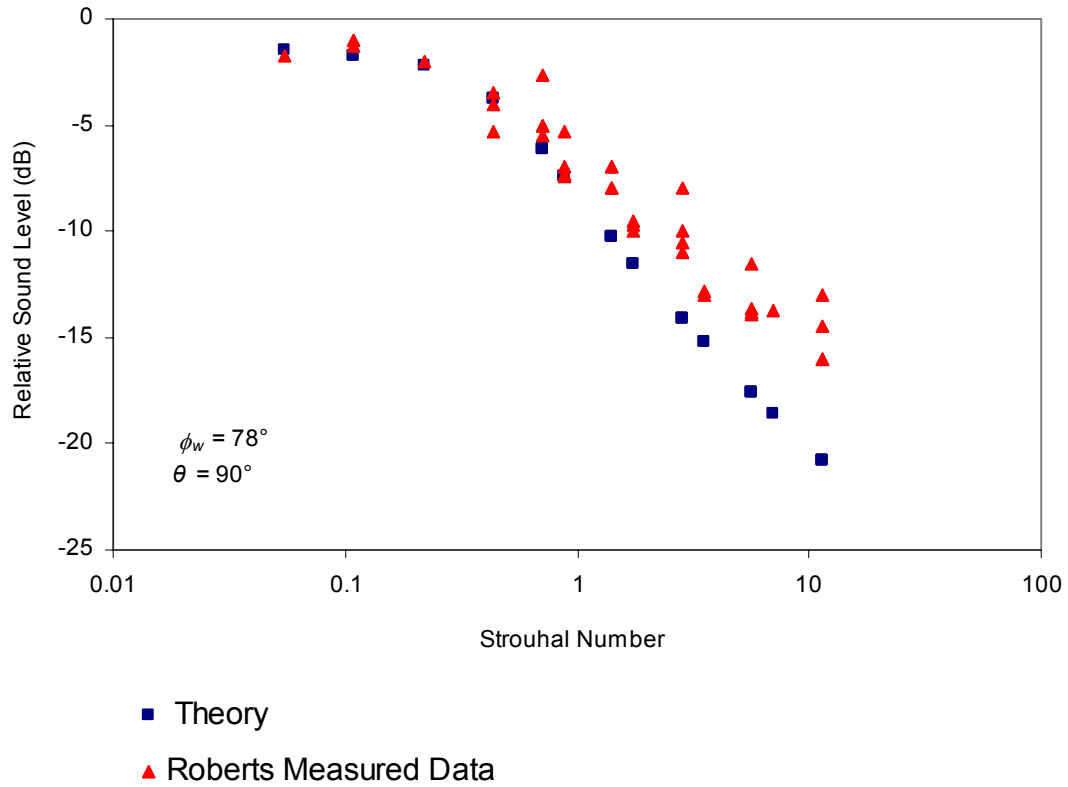


Figure 5.9. Comparison of Roberts measured data with the theory of section 5.1.1 for the sound level at 90 degrees relative to the sound level at 0 degrees. The theory of section 5.1.1 is used with the weighting function using a weighting angle ϕ_w of 78 degrees. A negative relative sound level constant of -1.5 dB was added to results of the theory of section 5.1.1.

Figure 5.9 represents the relative sound level at 90 degrees with the weighting angle at 78 degrees with the constant of relative sound level set to -1.5 dB. For some Strouhal numbers, Roberts has more than one measured value, which suggests experimental uncertainty in the relative sound level across the whole Strouhal number range.

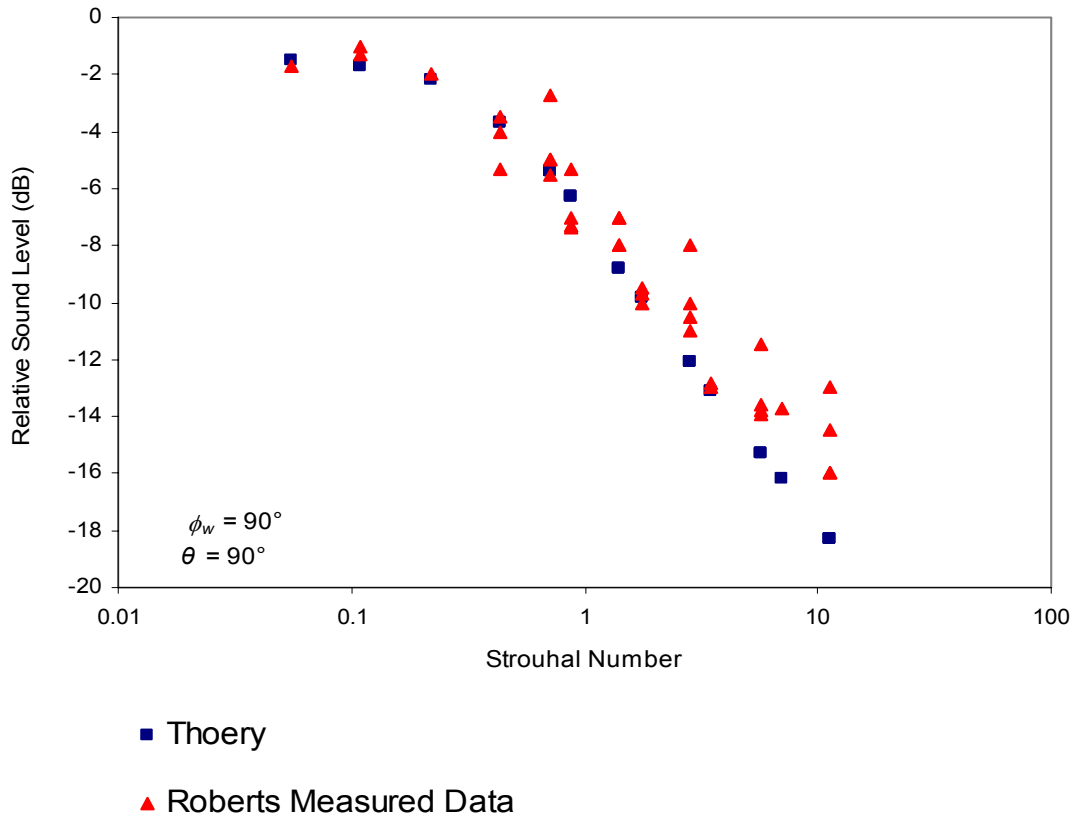


Figure 5.10. Comparison of Roberts measured data with the theory of section 5.1.1 for the sound level at 90 degrees relative to the sound level at 0 degrees. The theory of section 5.1.1 is used with the weighting function using a weighting angle ϕ_w of 90 degrees. A negative relative sound level constant of -1.5 dB was added to results of the theory of section 5.1.1.

Implementing the relative sound level constant improves the relative sound level at low Strouhal numbers. At the same time varying the weighting angle has an impact on the result at high Strouhal numbers. It is obvious that the theory of section 5.1.1 used with the weighting angle ϕ_w set at 90 degrees produces relative sound level values for 90 degrees which compare better to the measured data than the theory of section 5.1.1 used with the weighting angle ϕ_w set at 78 degrees.

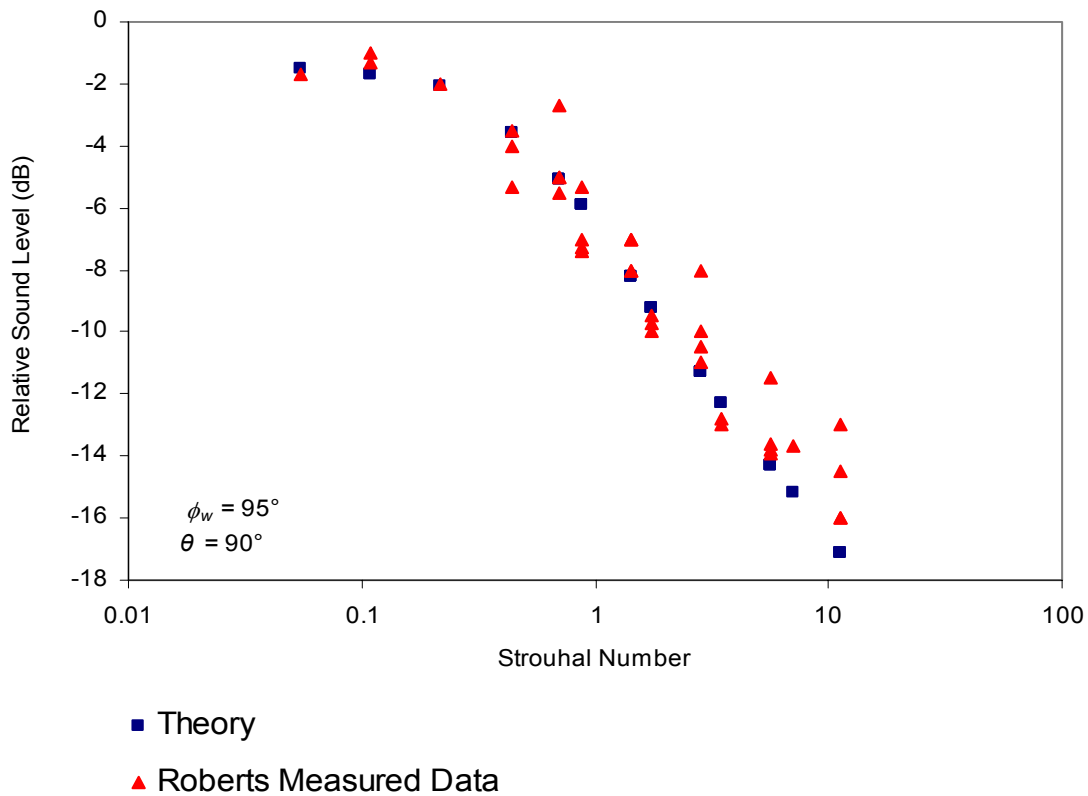


Figure 5.11. Comparison of Roberts measured data with the theory of section 5.1.1 for the sound level at 90 degrees relative to the sound level at 0 degrees. The theory of section 5.1.1 is used with the weighting function using a weighting angle ϕ_w of 95 degrees. A negative relative sound level constant of -1.5 dB was added to results of the theory of section 5.1.1.

The relative sound level curve at 90 degrees with a weighting angle at 95 degrees is very similar to that of figure 5.10 where the weighting angle was set to 90 degrees. The only difference is that relative sound level curve for the theory of section 5.1.1 seems to be decreasing compared to the measured values. This trend will in fact become more emphasized as we continue to increase the weighting angle. Note that the integration over φ in theory of section 5.1.1 is only performed from -90 degrees to 90 degrees even though the weighting angle ϕ_w of the weighting function is greater than 90 degrees.

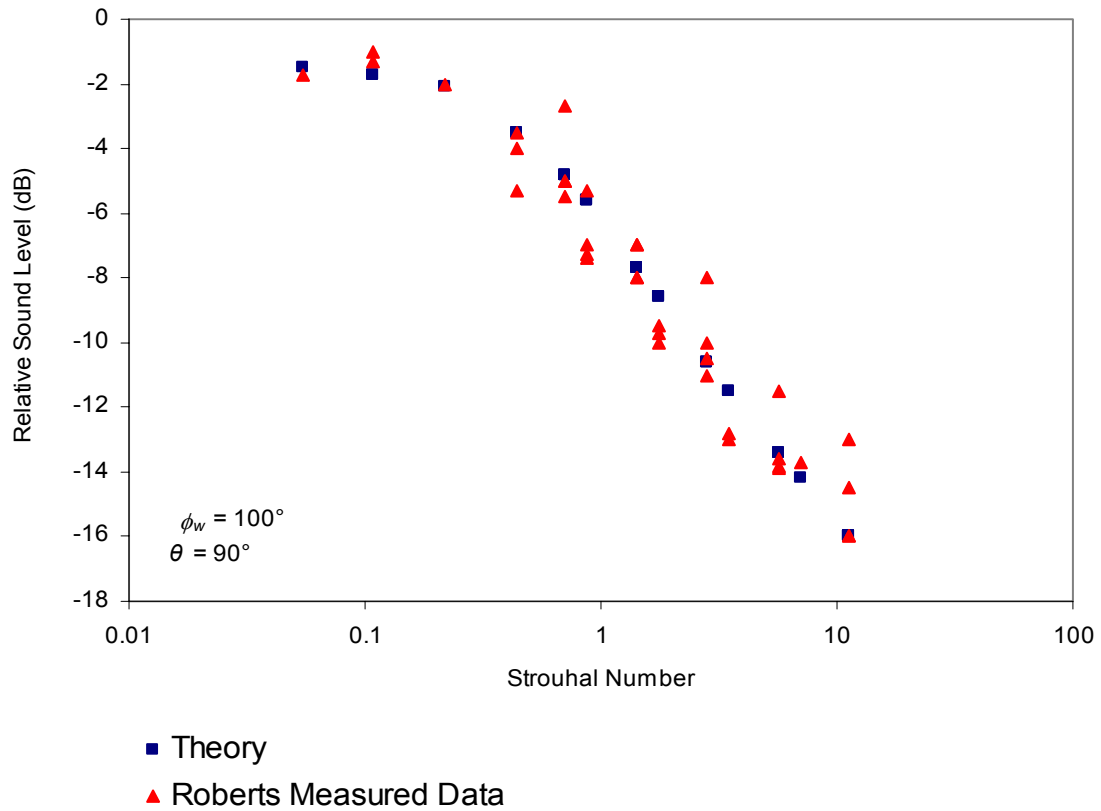


Figure 5.12. Comparison of Roberts measured data with the theory of section 5.1.1 for the sound level at 90 degrees relative to the sound level at 0 degrees. The theory of section 5.1.1 is used with the weighting function using a weighting angle ϕ_w of 100 degrees. A negative relative sound level constant of -1.5 dB was added to results of the theory of section 5.1.1.

With the increase in the weighting angle the predicted values decrease.

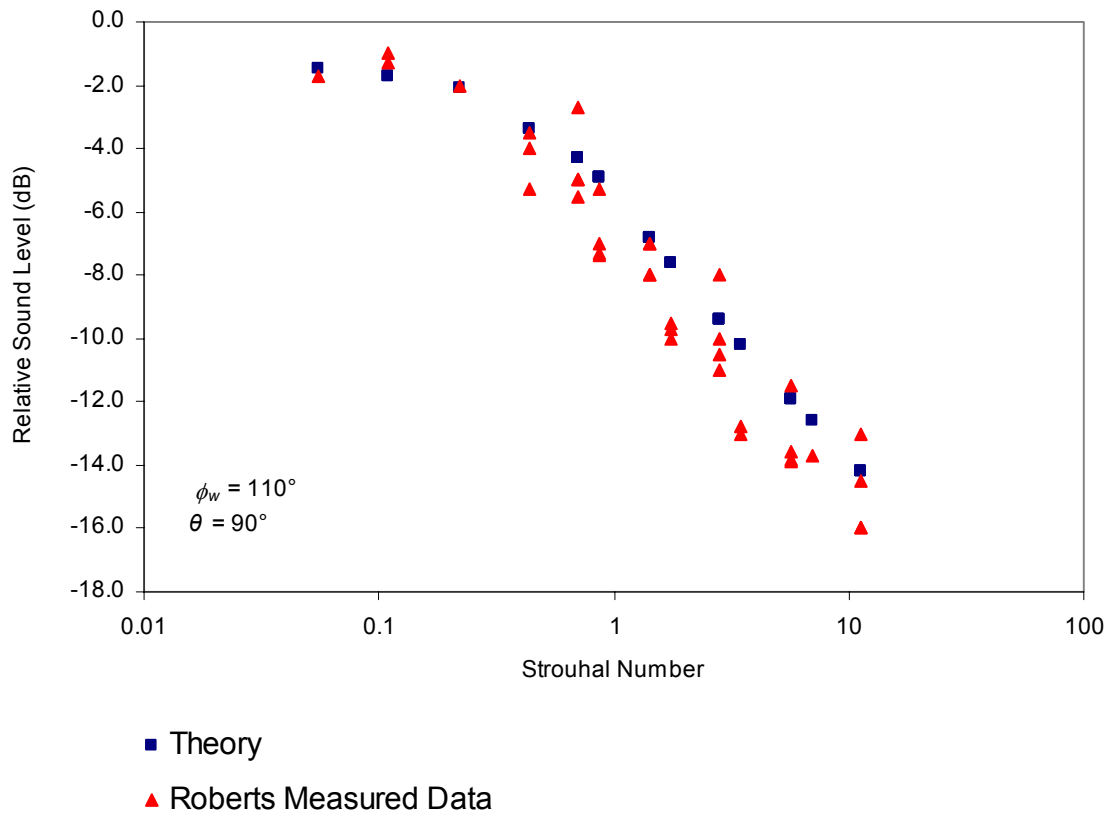


Figure 5.13. Comparison of Roberts measured data with the theory of section 5.1.1 for the sound level at 90 degrees relative to the sound level at 0 degrees. The theory of section 5.1.1 is used with the weighting function using a weighting angle ϕ_w of 110 degrees. A negative relative sound level constant of -1.5 dB was added to results of the theory of section 5.1.1.

An increase in the weighting angle not only affects the relative sound level at high Strouhal numbers but also has an impact on relative sound level as width of the opening increases because this increases the Strouhal number for a fixed frequency.

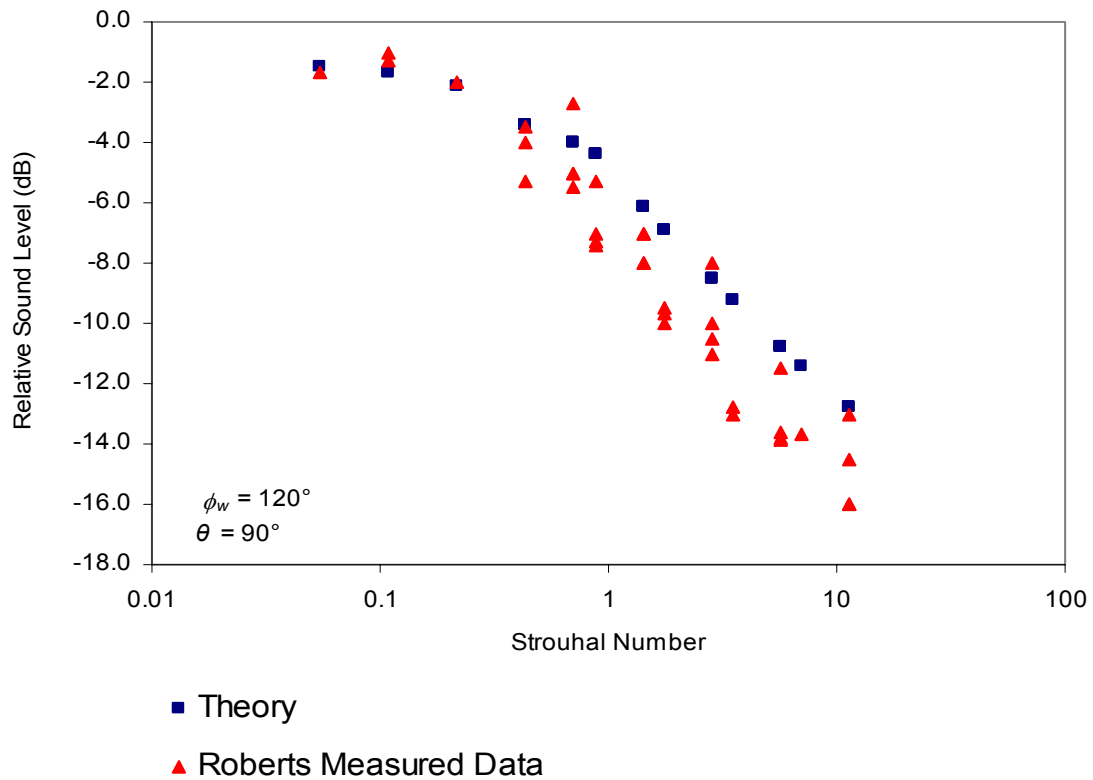


Figure 5.14. Comparison of Roberts measured data with the theory of section 5.1.1 for the sound level at 90 degrees relative to the sound level at 0 degrees. The theory of section 5.1.1 is used with the weighting function using a weighting angle ϕ_w of 120 degrees. A negative relative sound level constant of -1.5 dB was added to results of the theory of section 5.1.1.

Figure 5.14 represents the relative sound level at 90 degrees with the weighting angle set at 120 degrees. It is obvious that the difference becomes more extreme with the increase of the weighting angle. A weighting angle set at 100° gives the best results when the theory of section 5.1.1 is compared to Roberts' practical test.

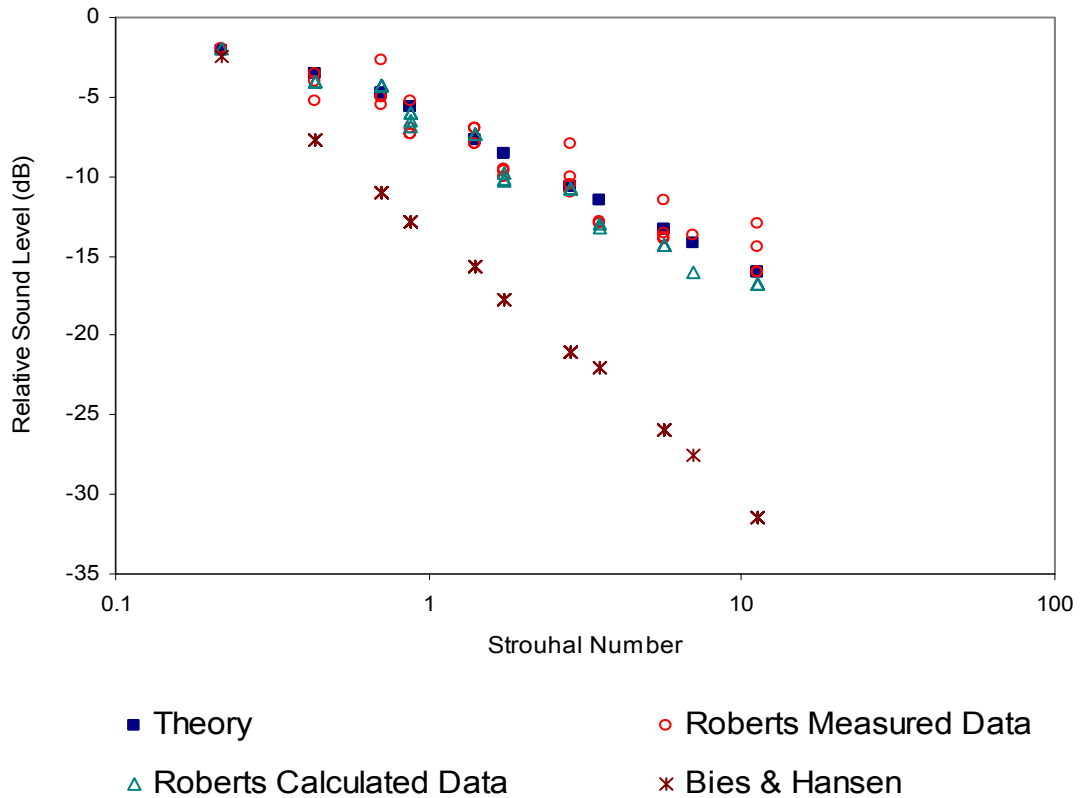


Figure 5.15. Comparison of different data with the theory of section 5.1.1 for the sound level at 90 degrees relative to the sound level at 0 degrees. The theory of section 5.1.1 is used with the weighting function using a weighting angle ϕ_w of 100 degrees. A negative relative sound level constant of -1.5 dB was added to results of the theory of section 5.1.1.

Models being compared in figure 5.15 have the same 0.5 m width of the opening. Bies & Hansen's [16] model is more directional as the other two models. The primary difference is that Bies and Hansen's model has investigated the directivity from the exit of a duct. Only plane waves propagate when the duct is less than 0.5 wavelengths wide. For ducts of greater dimensions than these, higher modes may propagate as well as plane waves. Higher order modes have been included in the theory of acoustic ducts by various authors [8, 53, and 54].

5.1.3 Rindel's experiment results for finite openings and panels

The theory of section 5.1.1 was compared with the experimental research of Rindel. It covered the transmission of traffic noise through windows. It has been done by comparing the external or outdoor noise level to the internal room level [19]. Rindel made 1:4 scale model measurements on the sound insulation of windows installed in one wall of a box in an anechoic room. The sound was incident from outside the box at an angle normal to the window. The window was mounted in an opening measuring 420 millimetres wide by 300 millimetres high by 75 millimetres deep. The wall of the box containing the window was part of the baffle measuring 3800 millimetres wide by 3100 millimetres high. The loudspeaker was 4000 millimetres from the middle of the front of the opening.

The theory of section 5.1.1 was used to calculate the relative sound level for sound travelling from indoors to outdoors. By reciprocity the results should be the same. Rindel measured the sound pressure level (SPL) for each window as a function of frequency and then calculated the external transmission loss (E) for the 0°, 45°, 75° and 90° angles of incidence. The following formula was used:

$$E = L_{out} - L'_{in} + correction \quad (5.24)$$

where $L_{out} \left[\frac{dB}{20\mu Pa} \right]$ is the sound pressure level measured outside the window as a function of the frequency and the angle of incidence,

$L'_{in} \left[\frac{dB}{20\mu Pa} \right]$ is the sound pressure level inside the window corrected with respect to the background noise and

$correction[dB]$ is the correction for the area of the specimen and the volume of the receiving room.

Rindel applied a background correction. For windows with very high sound insulation, he had to increase the power fed to the loudspeaker in order to measure the sound pressure in the receiving room with a reasonable accuracy. This only occurred at the highest frequencies.

$$L'_{in} = 10 \log \left(10^{\frac{L_{in}}{10}} - 10^{\frac{L_b}{10}} \right) \quad (5.25)$$

where $L_{in} \left[\frac{dB}{20 \mu Pa} \right]$ is the sound pressure level measured inside window as a function of the frequency and the angle of incidence,

$L_b \left[\frac{dB}{20 \mu Pa} \right]$ is the sound pressure level of the background noise.

Our calculation method was based on finding the sound, which is radiating into the half space for the particular angle. Emphasis was put on investigation at grazing incidence ($\phi = 90^\circ$) since with simple theories of sound insulation as angle tends to 90° the radiation efficiency goes to infinity. The transmission loss decreases with increasing angle relative to the normal and tends to vanish at grazing incidence.

5.1.3.1 Opening

The specific property of an opening in a thin baffle is that the ‘panel’ does not exist. It is a fictive, mass-less panel:

$$Z_w = 0 \quad (5.26)$$

The basic formula for the calculation of transmission loss is:

$$R = 10 \log \frac{|Z_1 + Z_w + Z_t|^2}{2 \bullet 4 \bullet \rho c \bullet \text{Re}\{Z_t\}} \quad (5.27)$$

Very often, the dimensions of the panel are so large ($ka \gg 1$) that the following equation is a good approximation:

$$R = 10 \log \left(\left| 1 + \frac{Z_w}{2 \bullet \rho c \bullet \sigma} \right|^2 \bullet \frac{\sigma}{2} \right) \quad (5.28)$$

where Z_w depends upon the type of panel, while σ is influenced by the type of the incident sound field and the dimensions of the panel.

The results of Rindel's measured data and the theory of section 5.1.1 directivity comparison for the opening are shown in figure 5.16.

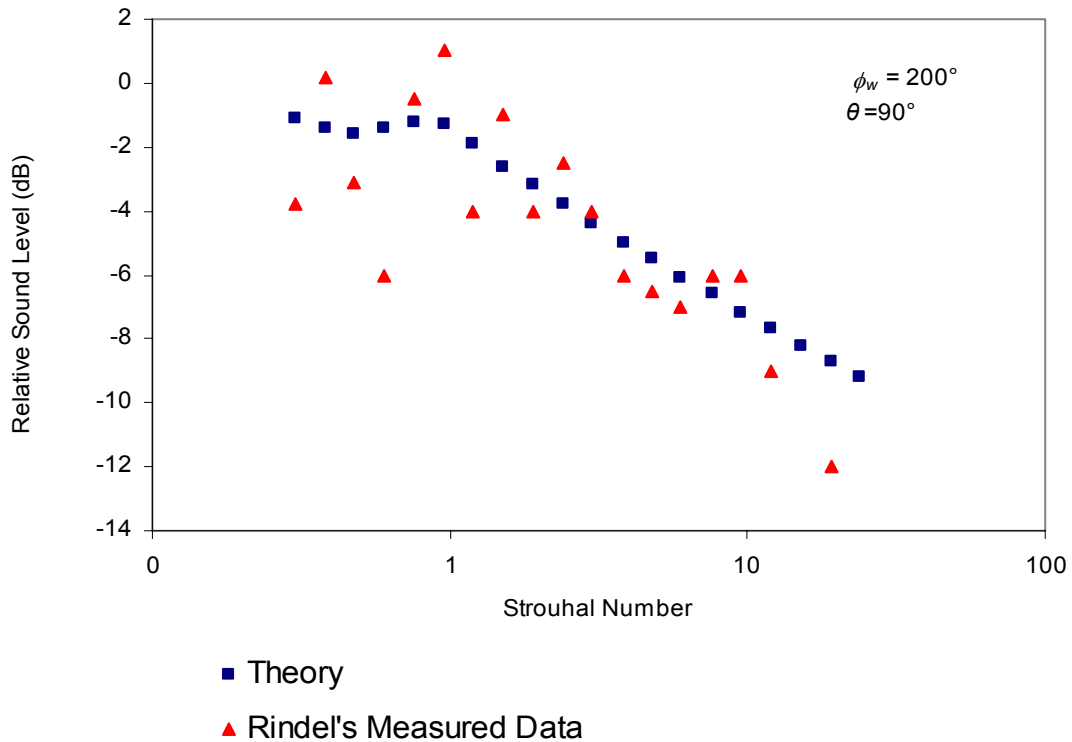


Figure 5.16. Comparison of Rindel's measured data with the theory of section 5.1.1 for the sound level at 90 degrees relative to the sound level at 0 degrees. The theory of section 5.1.1 is used with the weighting function using a weighting angle ϕ_w of 200 degrees.

The Strouhal number range is from 0.3 to 24. Length of the window is set to 1.6m. Rindel used a wooden frame with the inside dimensions 42 cm x 30 cm (1.64 m x 1.230 m in full scale). The thickness of the frame was 7.5 cm (30 cm in full scale) which corresponded to the thickness of the wall of the receiving room. The weighting angle of the weighting function for all three angles compared (90°, 75° and 45°) is 200.

The relative sound level curve at 90° produced by the theory of section 5.1.1 is somewhat smoother than the curve produced by Rindel. This is especially noticeable at low Strouhal number, particularly the dip at Strouhal number 0.6 and the peak at Strouhal number 1.

Between Strouhal number 0.6 and Strouhal number 0.75 there is a difference of 5.5 dB where the difference for our curve for the same Strouhal numbers is 0.2 dB. Overall the curves show very similar relative sound level across the Strouhal number range. Rindel's curve is missing a relative sound level value for Strouhal numbers 15 and 24.

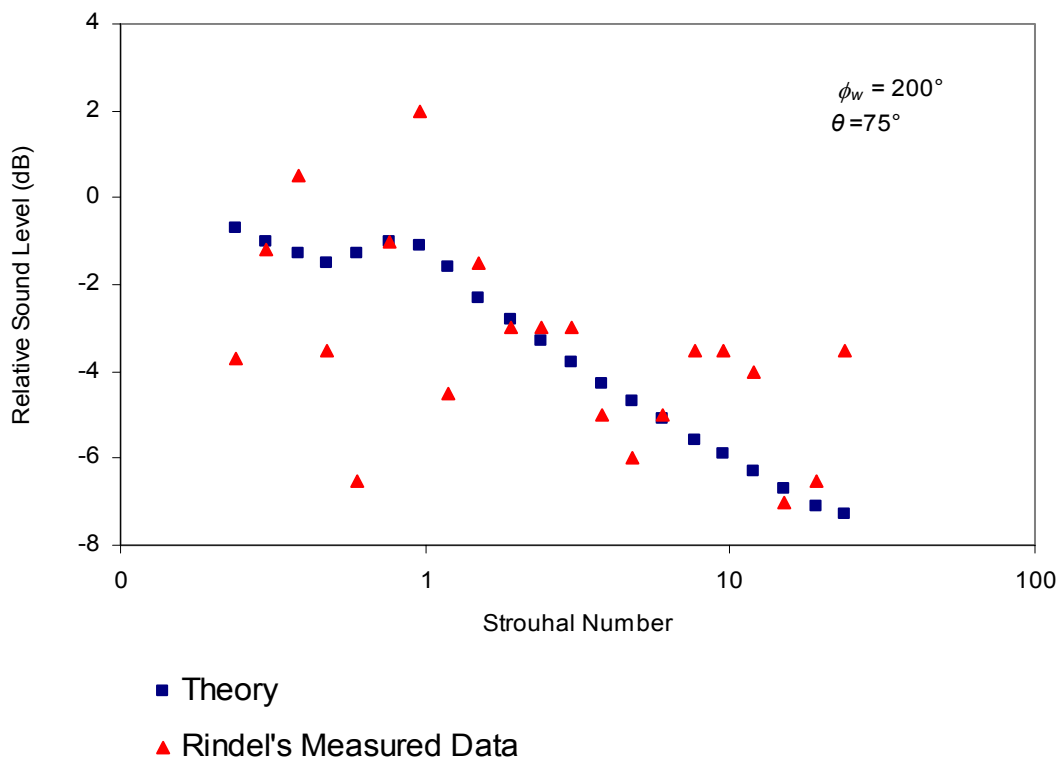


Figure 5.17. Comparison of Rindel's measured data with the theory of section 5.1.1 for the sound level at 75 degrees relative to the sound level at 0 degrees. The theory of section 5.1.1 is used with the weighting function using a weighting angle ϕ_w of 200 degrees.

If we compare the figure 5.17 curves to those of figure 5.16 we can see that they have similar shapes. The difference is that Rindel's curve for relative sound level at 75° has more peaks and dips across the whole Strouhal number range.

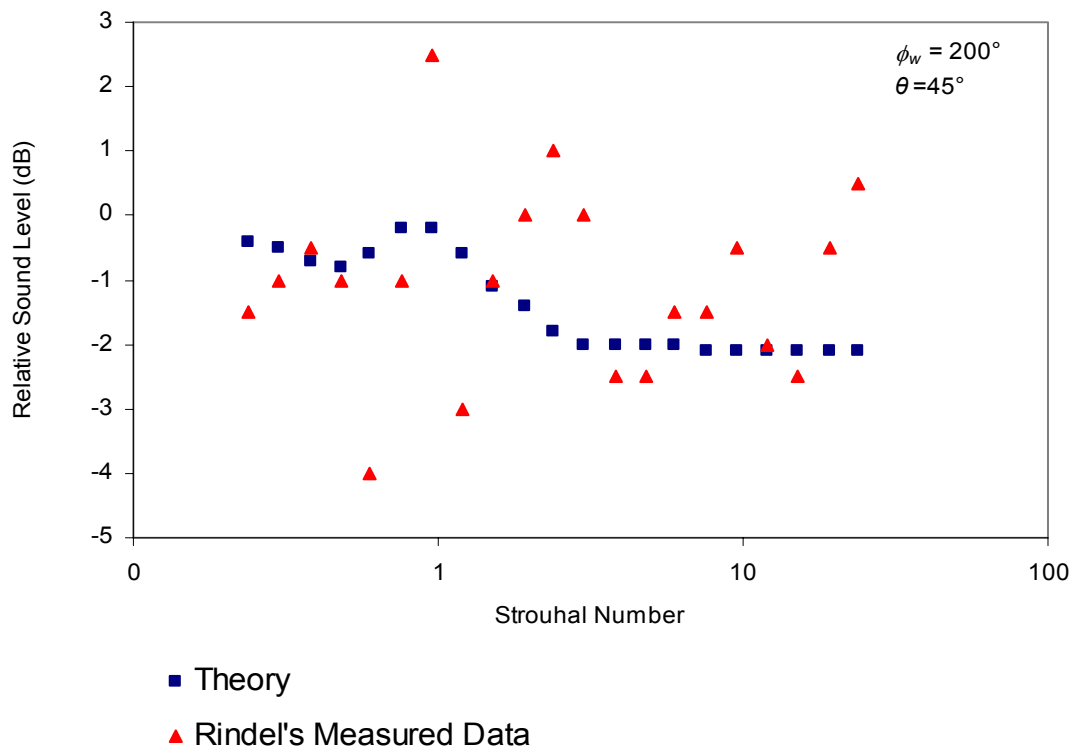


Figure 5.18. Comparison of Rindel's measured data with the theory of section 5.1.1 for the sound level at 45 degrees relative to the sound level at 0 degrees. The theory of section 5.1.1 is used with the weighting function using a weighting angle ϕ_w of 200 degrees.

The relative sound level curves at 45° have similar shapes as those for 75°. The difference is that from Strouhal number 4 through to Strouhal number 24, the theory of section 5.1.1 has a flat response.

5.1.3.2 A thin single panel

Most single leaf panels are very thin compared to the wavelength of the sound in the solid leaf material [25]. When the panel is a thin single panel the specific acoustic impedance (transmission impedance) of the panel well below the critical frequency is [40]

$$Z_w = j\omega m \quad (5.29)$$

where m is the mass per unit area of the panel

ω is the angular frequency.

The calculations presented in this thesis actually use equation (5.13).

In the case of Rindel's and Stead's experimental data, the relative sound level at an angle θ is the indoor sound level due to sound incident at an angle θ minus the indoor sound level due to sound incident at right angles to the panel or opening. Figure 5.19 represents the relative sound level at 90° for a thin single panel 4 mm thick. There is a problem at a low Strouhal numbers. The weighting angle ϕ_w was set at 120 degrees. Setting it to 200 degrees would compare better at low Strouhal numbers but would compromise the peak at the critical frequency. Rindel came across the same difficulty. Irregularities were found for nearly all the windows. One important reason is the standing waves in the niches of the specimen holder on either side of the specimen. According to Rindel the two lower frequencies of resonance in the niches of the specimen holder on either side of the specimen opening are within the 1/3 octave bands 400 Hz and 630 Hz (100 Hz and 160 Hz full scale).

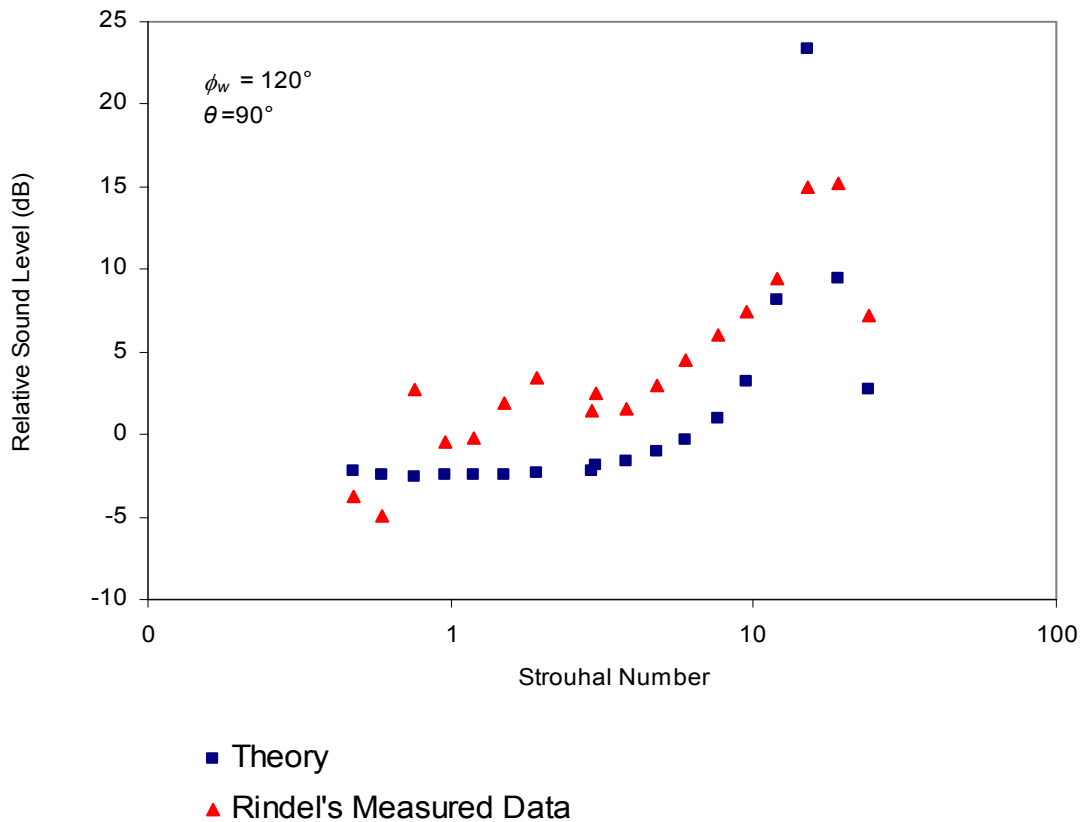


Figure 5.19. Comparison of Rindel's measured data with the theory of section 5.1.1 for the sound level at 90 degrees relative to the sound level at 0 degrees. The theory of section 5.1.1 is used with the weighting function using a weighting angle ϕ_w of 120 degrees.

The critical frequency worked out to be 3150 Hz, which corresponds to a Strouhal number of 15. The transmission loss (TL) at the critical frequency is dependent on the damping, which is characterized by the damping loss factor (η) [16]. Bies & Hansen in the "Properties of materials" (Appendix B) list the loss factor for glass as being 0.0006 to 0.02. Our damping loss factor is 0.01. When the stiffness of the panel is taken into account, the effect of coincidence occurs. The product of the critical frequency with the thickness of the glass is assumed to be 12 m/s in our calculations. The peak in figure 5.19 is due to coincidence which occurs at the critical frequency for 90 degree incidence and radiation.

5.1.3.3 Coincidence Region

Coincidence for single walls was first analyzed by Cremer [1]. According to Cremer when the stiffness of the panel is taken into account, the effect of coincidence occurs. The lowest frequency at which coincidence occurs is called the critical frequency. Coincidence occurs when the incident sound wave (air borne) speed c and speed of the free bending wave of the panel (structure borne) c_b are equal [16]. The critical frequency can be calculated using following equations [9]:

$$f_c = \left(\frac{c^2}{2\pi} \right) \sqrt{\left(\frac{m}{B} \right)} \text{Hz} \quad (5.30)$$

$$f_c = \left(\frac{0.55c^2}{c_L h} \right) \text{Hz} \quad (5.31)$$

where h is the thickness of the panel

B is the bending stiffness of the panel

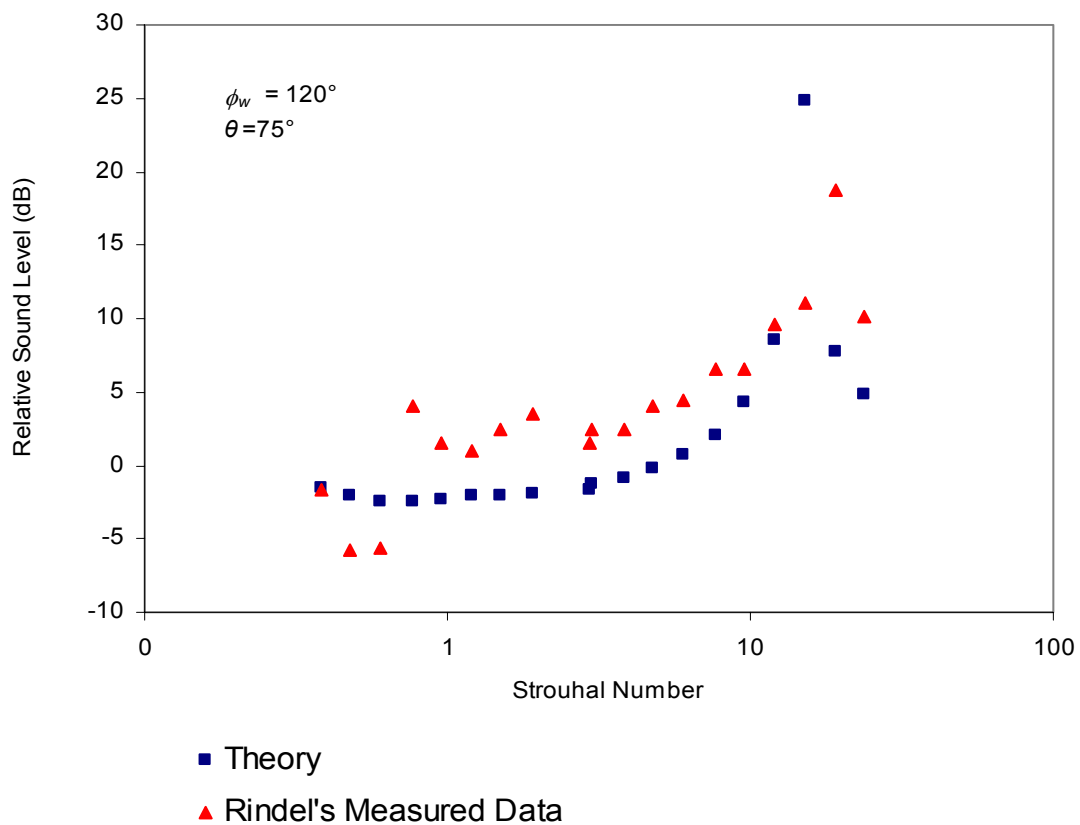


Figure 5.20. Comparison of Rindel's measured data with the theory of section 5.1.1 for the sound level at 75 degrees relative to the sound level at 0 degrees. The theory of section 5.1.1 is used with the weighting function using a weighting angle ϕ_w of 120 degrees.

The relative sound level at 75° is very similar to relative sound level at 90° with the coincidence frequency at 3150 Hz, which corresponds to a Strouhal number of 15.

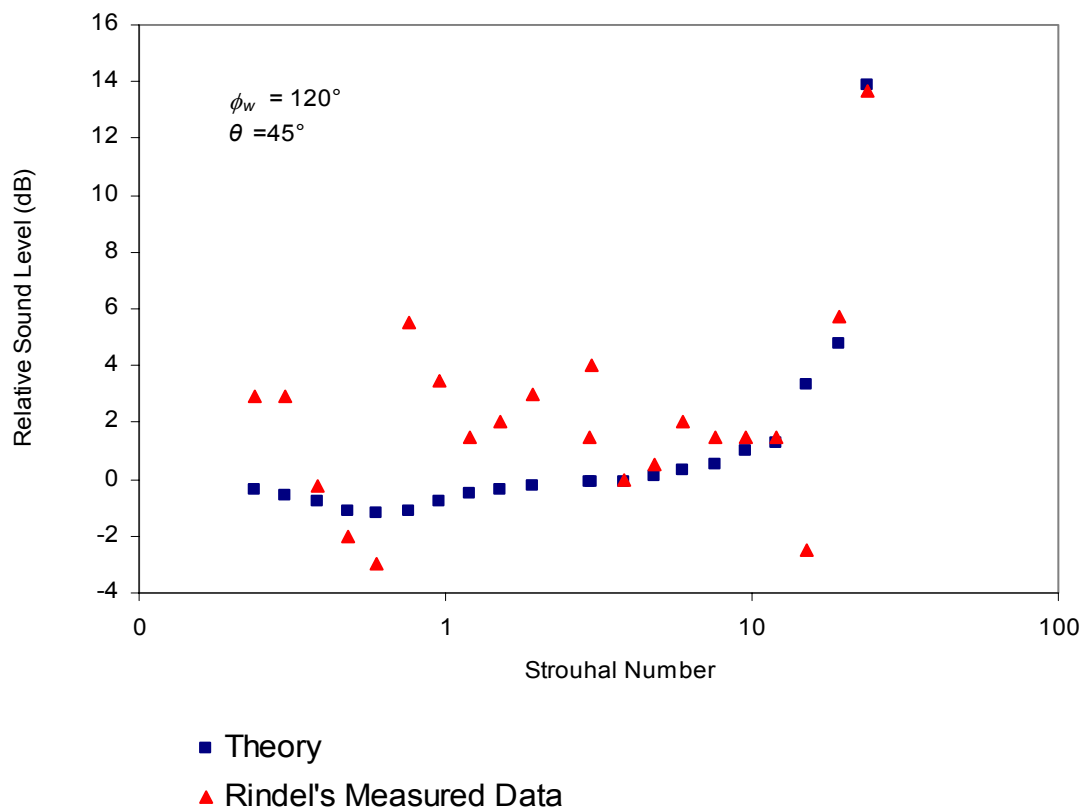


Figure 5.21. Comparison of Rindel’s measured data with the theory of section 5.1.1 for the sound level at 45 degrees relative to the sound level at 0 degrees. The theory of section 5.1.1 is used with the weighting function using a weighting angle ϕ_w of 120 degrees.

The relative sound level at 45° is somewhat different to curves of the other two angles. At low Strouhal number Rindel’s relative sound level curve predicts sharp peaks and dips. The difference between Strouhal number 0.6 and Strouhal number 0.75 is about 9 dB. The coincidence frequency peak has moved to 5000 Hz, Strouhal number 24, which is expected and predicted by the relevant theory. As the angle of incidence decreases the coincidence frequency increases. The coincidence frequencies of the 90° and 75° curves are the same at 3150 Hz, whereas the coincidence frequency of the 45° relative sound level curve has been shifted to 5000 Hz.

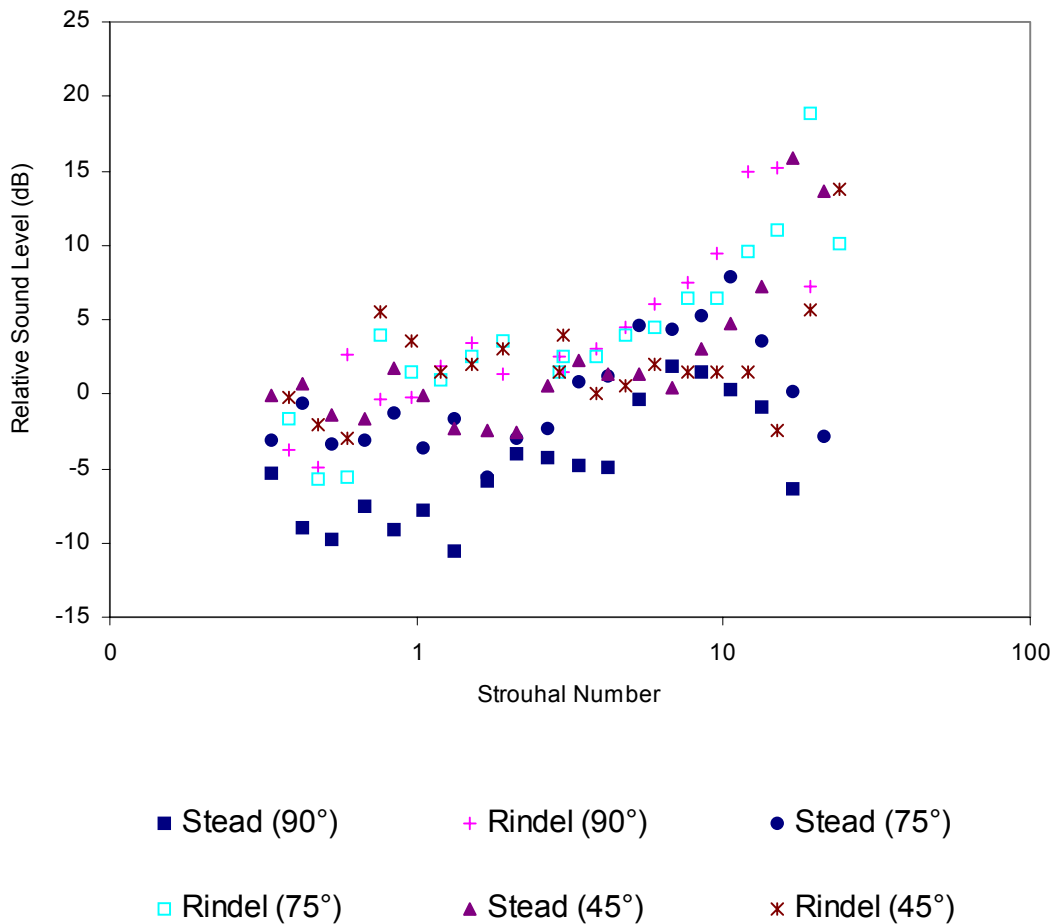


Figure 5.22. Rindel vs. Stead.

Stead [21] also made measurements on a window. His measurements are discussed in section 5.1.4. Figure 5.22 shows a relative sound level comparison between Rindel’s and Stead’s data. Overall, Rindel produced higher relative sound level values across the whole Strouhal number range and especially at high Strouhal numbers. Rindel’s relative sound level curve for 45° had an unexpected dip at Strouhal number 17. The critical frequency is at 3150 Hz, Strouhal number 15. The primary difference between the two models is in the thickness of the glass. Stead used 6 mm glass whereas Rindel used 4 mm glass. Another difference is in the length of the window. Rindel used a window 1.64 m in length, whereas Stead used a window 1.45 m in length.

5.1.3.4 *A Thick Single Panel*

Rindel investigated different window constructions including 12 mm thick single panel. This section compares Rindel's measurements with 12 millimetres thick single panel with the theory of section 5.1.1. Figure 5.23 represents the relative sound level at 90°.

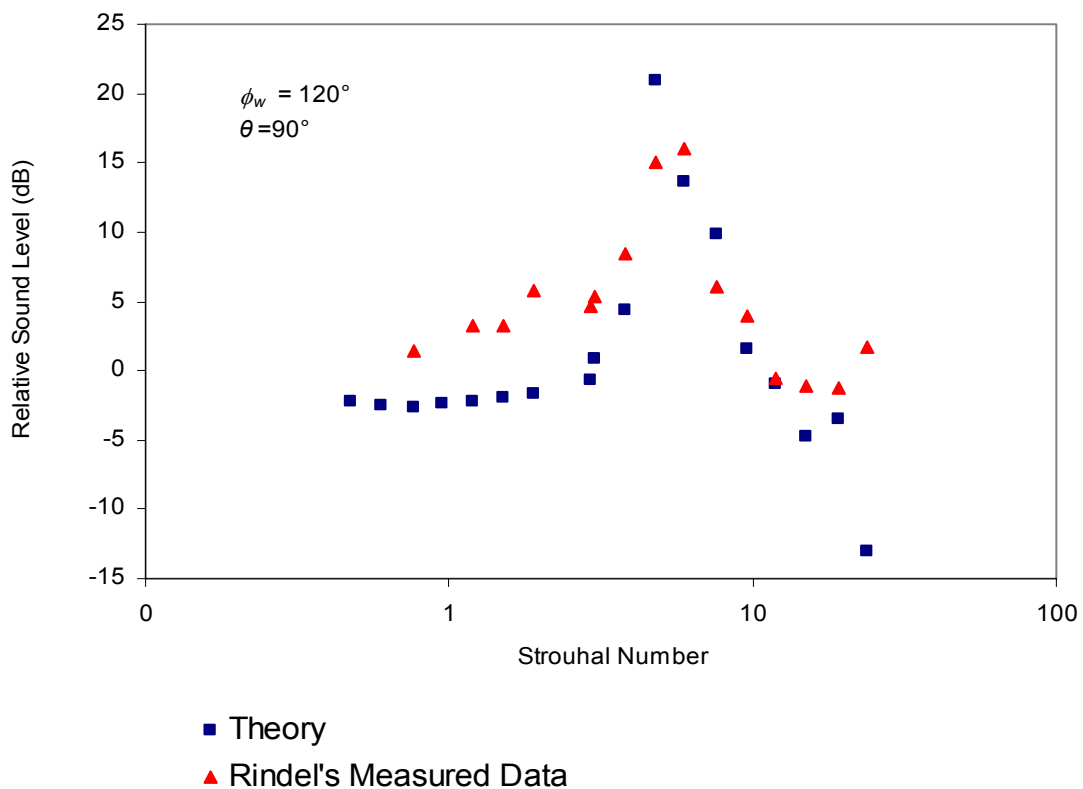


Figure 5.23. Comparison of Rindel's measured data with the theory of section 5.1.1 for the sound level at 90 degrees relative to the sound level at 0 degrees. The theory of section 5.1.1 is used with the weighting function using a weighting angle ϕ_w of 120 degrees.

The relative sound level at 90° shows a sharp peak around the critical frequency which is at 1000 Hz, Strouhal number 4.8.

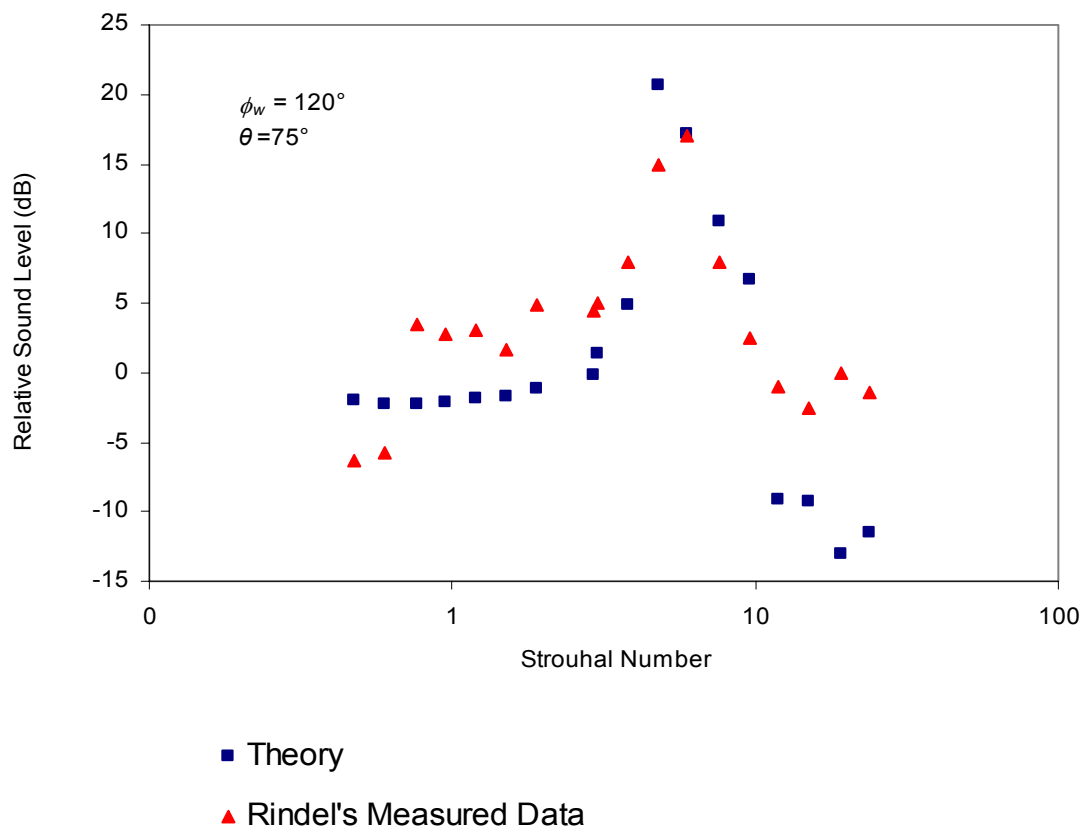


Figure 5.24. Comparison of Rindel's measured data with the theory of section 5.1.1 for the sound level at 75 degrees relative to the sound level at 0 degrees. The theory of section 5.1.1 is used with the weighting function using a weighting angle ϕ_w of 120 degrees.

The relative sound level curves at 75° are very similar to relative sound level curves at 90° with the coincidence frequency at 1000 Hz, Strouhal number 4.8.

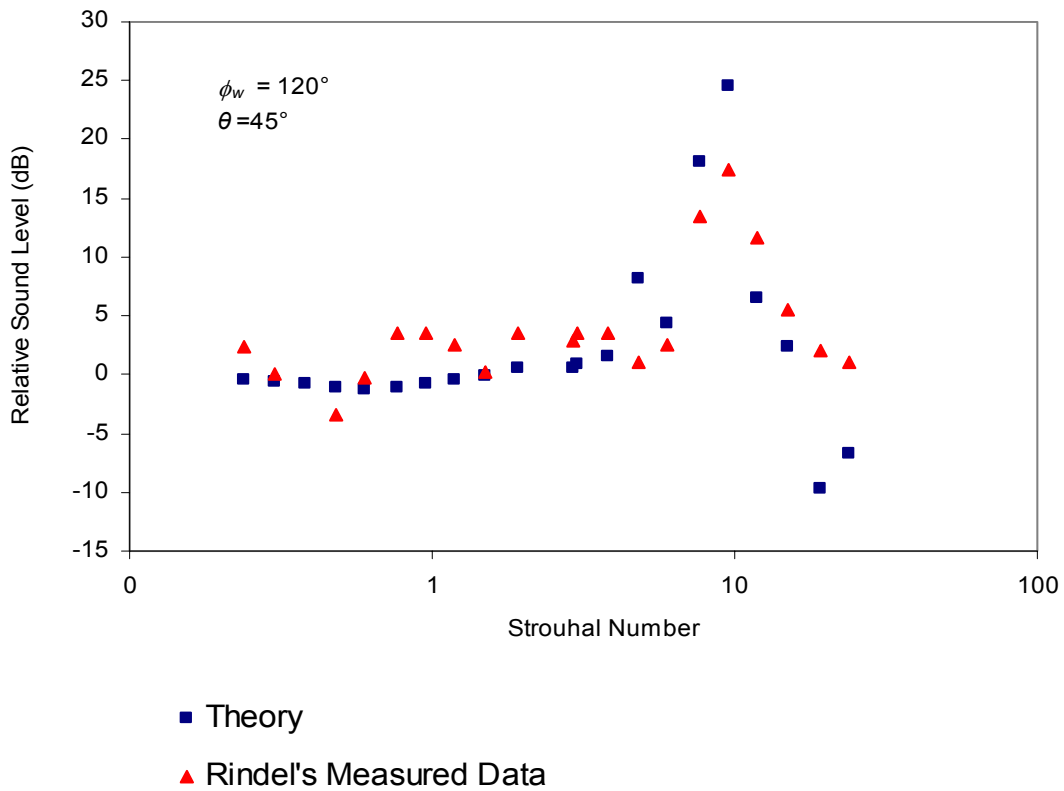


Figure 5.25. Comparison of Rindel’s measured data with the theory of section 5.1.1 for the sound level at 45 degrees relative to the sound level at 0 degrees. The theory of section 5.1.1 is used with the weighting function using a weighting angle ϕ_w of 120 degrees.

The relative sound level curve at 45° is somewhat different to curves of the other two angles. The coincidence frequency peak has been shifted to 2000 Hz, Strouhal number 9.6. This is because coincidence occurs at a higher frequency for an angle of incidence closer to normal incidence. The change from 90 degrees to 75 degrees is not sufficient to move the coincidence frequency to a lower third octave band.

5.1.4 Stead's experimental results for sound reduction through single isotropic glass panels of finite size

Stead [21] studied the sound transmission from outside a large building, whose façade served as a large baffle, into an office via a glass window. The sound was incident at an angle normal to the window from outside the room. This is the opposite direction to the theory of section 5.1.1, but because of the principle of reciprocity the theory is expected to give similar results as in the case of Stead's measurement results. The office was 5.12 m long, 2.88 m wide and 3 m high. The window was 2.12 high and 1.45 m wide. The window glass was 6 mm thick. The loudspeaker was located 20 m from the middle of the window. Sound transmission loss is a function of frequency. Bies and Hansen explained the typical transmission loss regions for a panel of finite size as shown in figure 5.26 [16].

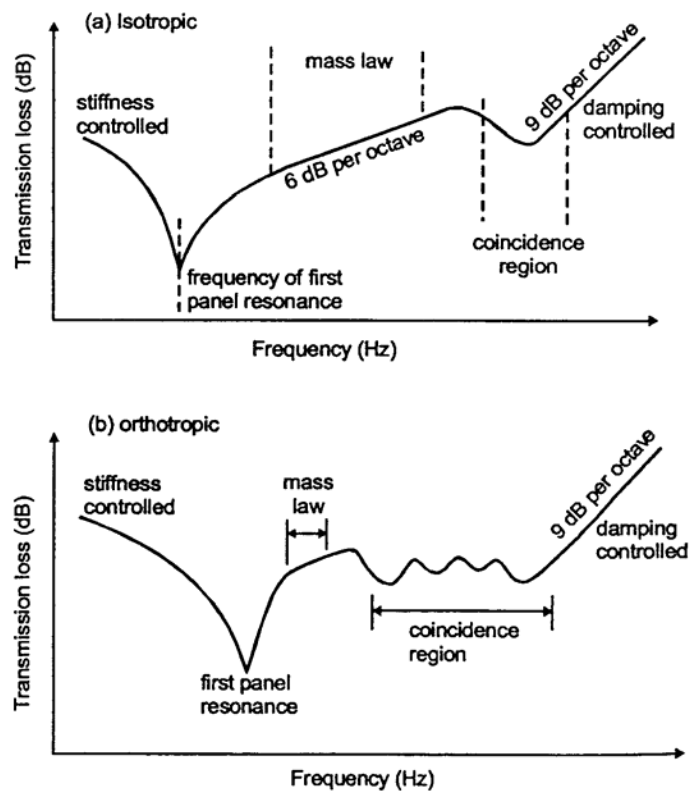


Figure 5.26. Typical TL as a function of frequency for a single panel.

The characteristic regions of the transmission loss spectrum are the stiffness controlled region, the mass law region, the coincidence region and the damping controlled region [16]. Panel mass and angle of sound incidence are the primary influences in the mass law region. The coincidence or critical frequency is determined by material properties and the angle of sound incidence and the dip minimum value is determined by the amount of damping in the panel. Panel damping also influences transmission loss above the coincidence region which is a damping controlled region.

Stead measured TL for varying angles of incidence, which have been corrected for the angle of incidence in accordance with the ISO 140, Part 5 [55]. Figure 5.27 presents directivity with sound incident at 90° for 6 mm glass. Stead set the speaker at 90° to the window when measuring the sound transmission loss at grazing incidence (sound at 90° to the window) [18].

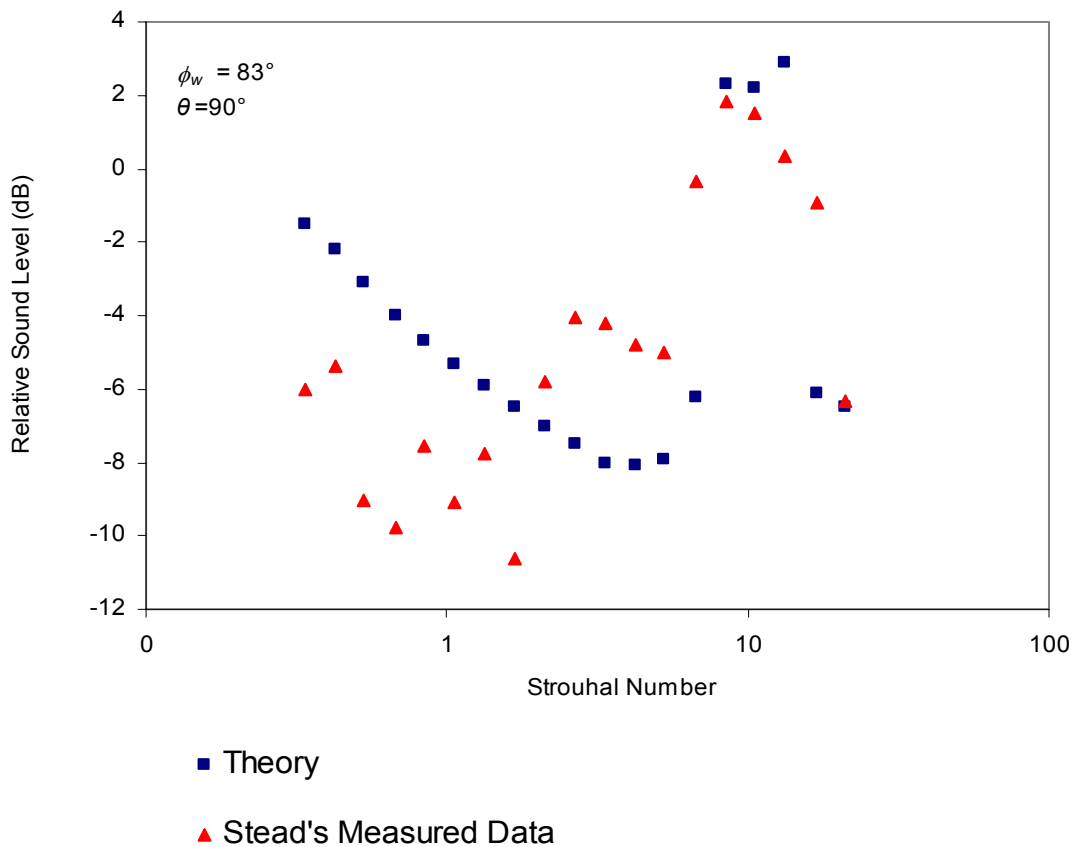


Figure 5.27. Comparison of Stead's measured data with the theory of section 5.1.1 for the sound level at 90 degrees relative to the sound level at 0 degrees. The theory of section 5.1.1 is used with the weighting function using a weighting angle ϕ_w of 83 degrees.

The relative sound level at 90° shows a broad peak around the critical frequency which is at 2500 Hz, Strouhal number 10.6. Above the coincidence region the panel damping influences the sound transmission loss and the relative sound level. A smaller weighting angle may be more appropriate for Stead's data than that used with Rindel's data. This is due to the difference in reverberant rooms. In his approach, Rindel used a box, which is more reverberant than the receiving room Stead used in his experimental setup.

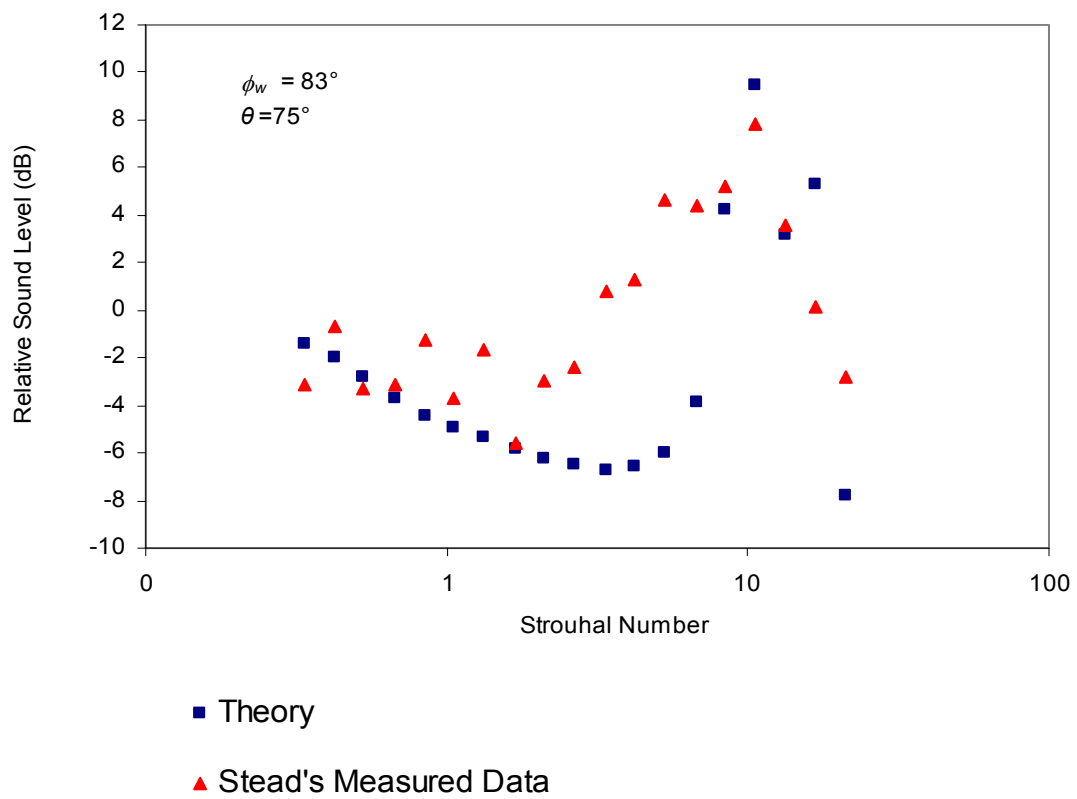


Figure 5.28. Comparison of Stead’s measured data with the theory of section 5.1.1 for the sound level at 75 degrees relative to the sound level at 0 degrees. The theory of section 5.1.1 is used with the weighting function using a weighting angle ϕ_w of 83 degrees.

The relative sound level at 75° is very similar to the relative sound level at 90° with coincidence frequency at 2500 Hz.

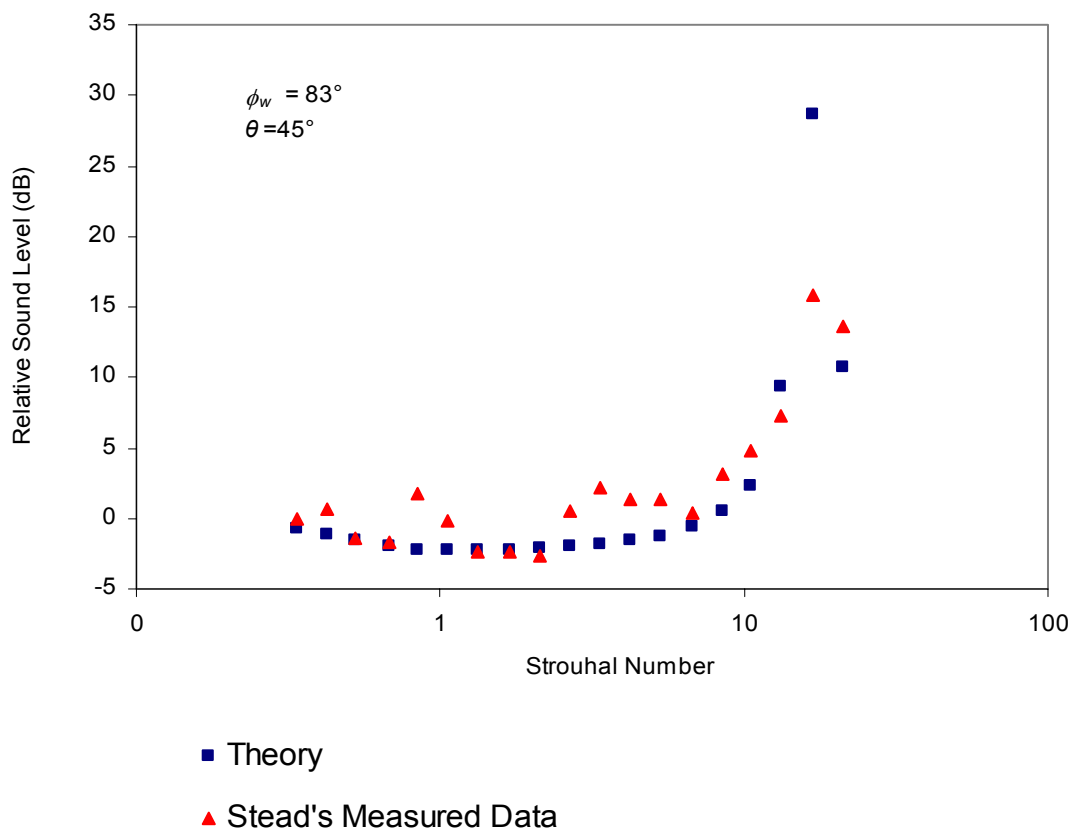


Figure 5.29. Comparison of Stead's measured data with the theory of section 5.1.1 for the sound level at 45 degrees relative to the sound level at 0 degrees. The theory of section 5.1.1 is used with the weighting function using a weighting angle ϕ_w of 83 degrees.

The relative sound level at 45° is somewhat different to curves of the other two angles. The coincidence frequency peak has been shifted to 5000 Hz as expected from the prediction method.

5.1.5 Bies & Hansen's directivity prediction model for an un baffled duct opening

Bies and Hansen's directivity of un baffled exhaust ducts was based on an experimental model investigation. The model is based on data for both rectangular and circular ducts and is presented in terms of Strouhal number based on frequency, and the geometric mean diameter of the duct for the angles measured from the centreline of the duct [16].

Higher order mode propagation occurs for values when the Strouhal number is greater than 0.5. That is when sound energy propagation in the duct is not entirely axial.

Cremer [1] proposed that in order to overcome the discrepancy found between calculations and measurements in the case of random incidence, the value of limiting angle should be ($\theta = 78^\circ$). Taking this into consideration it was reasonable to first consider a comparison with the weighting angle at 78 degrees. Figure 5.30 compares the relative sound level at 90 degrees with the weighting angle at 78 degrees.

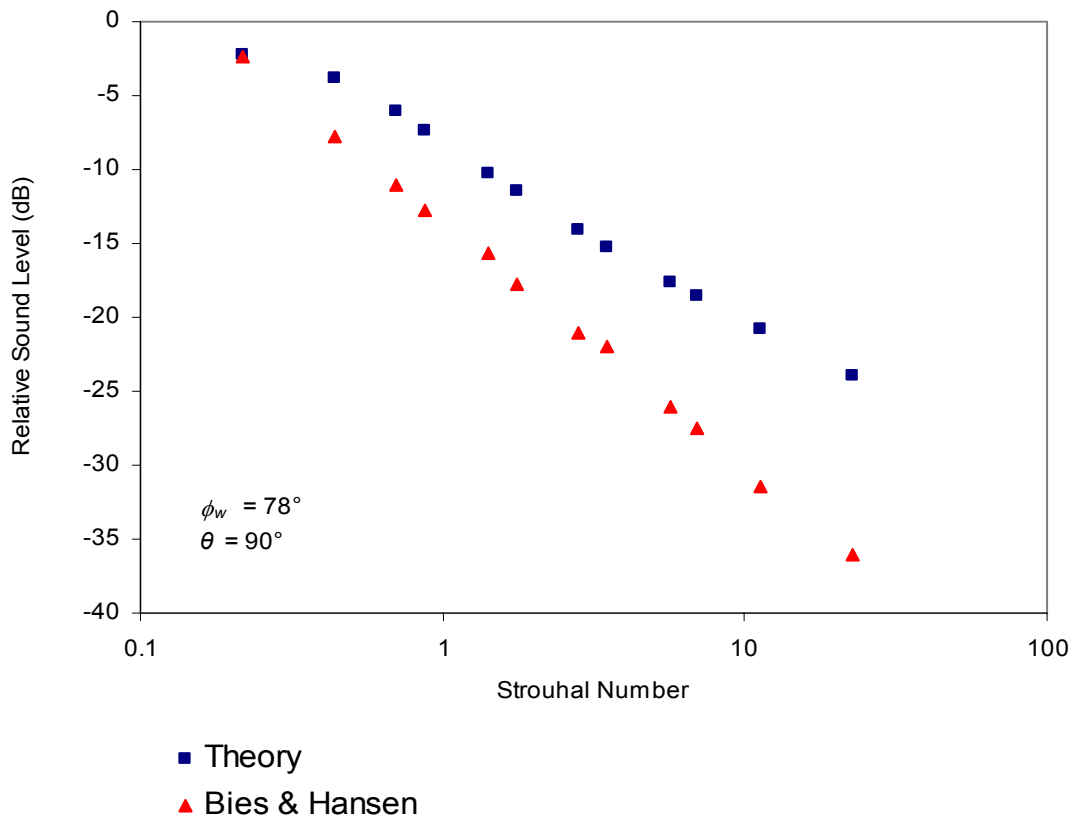


Figure 5.30. Comparison of Bies & Hansen's data with the theory of section 5.1.1 for the sound level at 90 degrees relative to the sound level at 0 degrees. The theory of section 5.1.1 is used with the weighting function using a weighting angle ϕ_w of 78 degrees. A negative relative sound level constant of -1.5 dB was added to results of the theory of section 5.1.1.

The agreement between the two models across the whole Strouhal number range is not quite satisfactory. It was necessary to change the weighting angle, which is one of the factors affecting directivity.

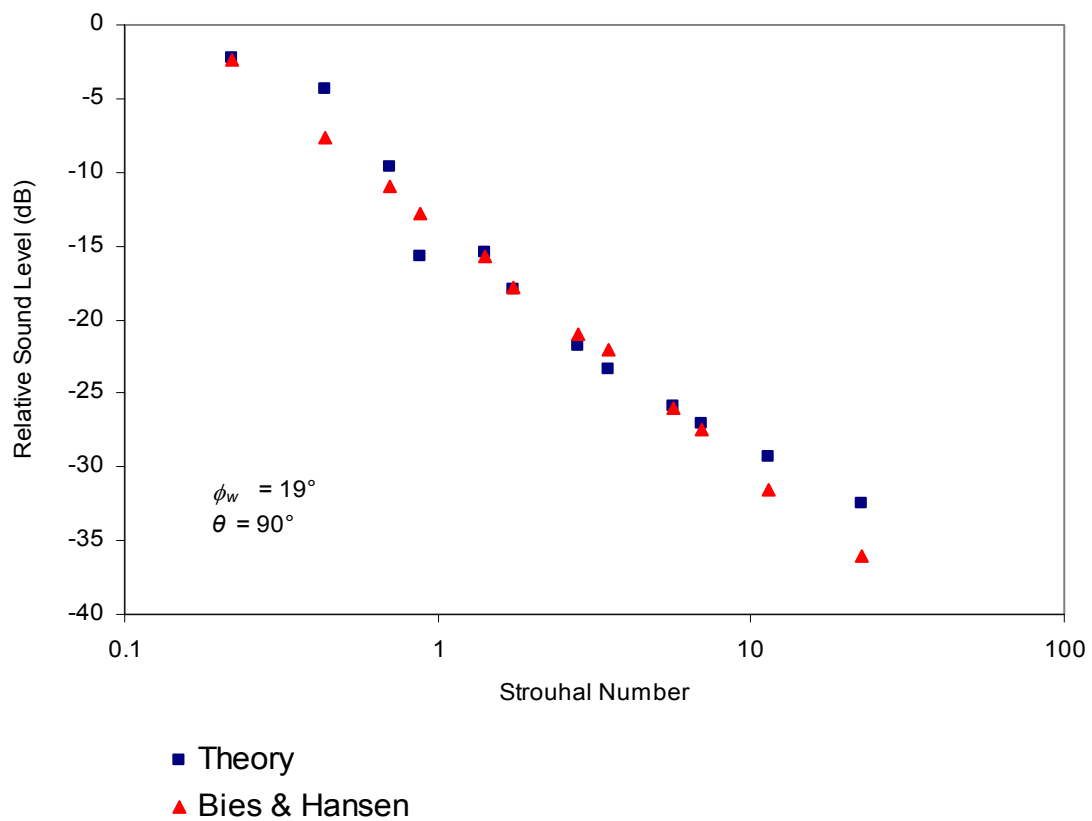


Figure 5.31. Comparison of Bies & Hansen’s data with the theory of section 5.1.1 for the sound level at 90 degrees relative to the sound level at 0 degrees. The theory of section 5.1.1 is used with the weighting function using a weighting angle ϕ_w of 19 degrees. A negative relative sound level constant of -1.5 dB was added to results of the theory of section 5.1.1.

The agreement between the two models when weighting angle is changed to 19 degrees is seen to be quite satisfactory, as shown in figure 5.31. One of the significant aspects of this comparison is the weighting angle. In order for the theory of section 5.1.1 to be valid the weighting angle should be the same and consistent throughout the comparison process. Therefore, a weighting angle of 55 degrees will be used, which seems to work best for all radiation angles.

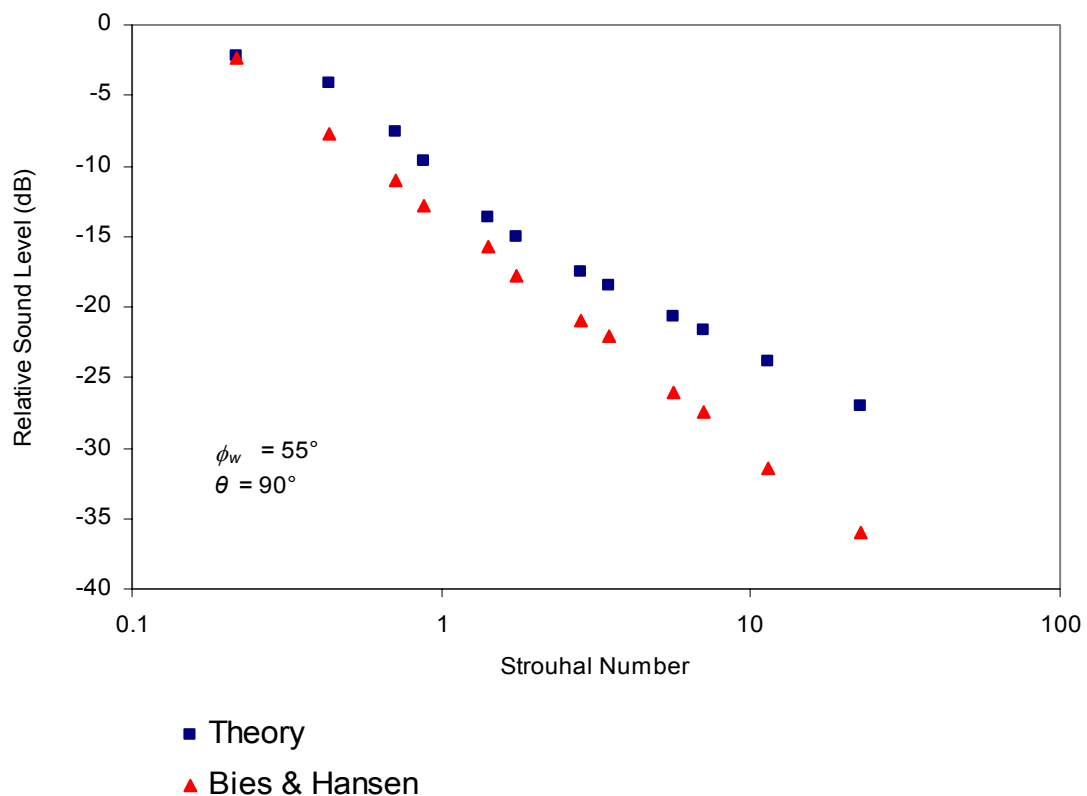


Figure 5.32. Comparison of Bies & Hansen’s data with the theory of section 5.1.1 for the sound level at 90 degrees relative to the sound level at 0 degrees. The theory of section 5.1.1 is used with the weighting function using a weighting angle ϕ_w of 55 degrees. A negative relative sound level constant of -1.5 dB was added to results of the theory of section 5.1.1.

Figure 5.32 shows that for relative sound level at 90 degrees with the weighting angle at 55 degrees the differences between the curves are somewhat bigger than in figure 5.31. For large Strouhal numbers the relative sound level differences between the two models is as much as 9 dB.

The weighting angle ϕ_w is likely to be smaller for a duct than for a room. In a duct, compared to a room, we would expect less sound energy to be incident on the opening at 90 degrees. This is because plane wave propagation is likely to be dominant in a duct, especially for low values of Strouhal number and long ducts.

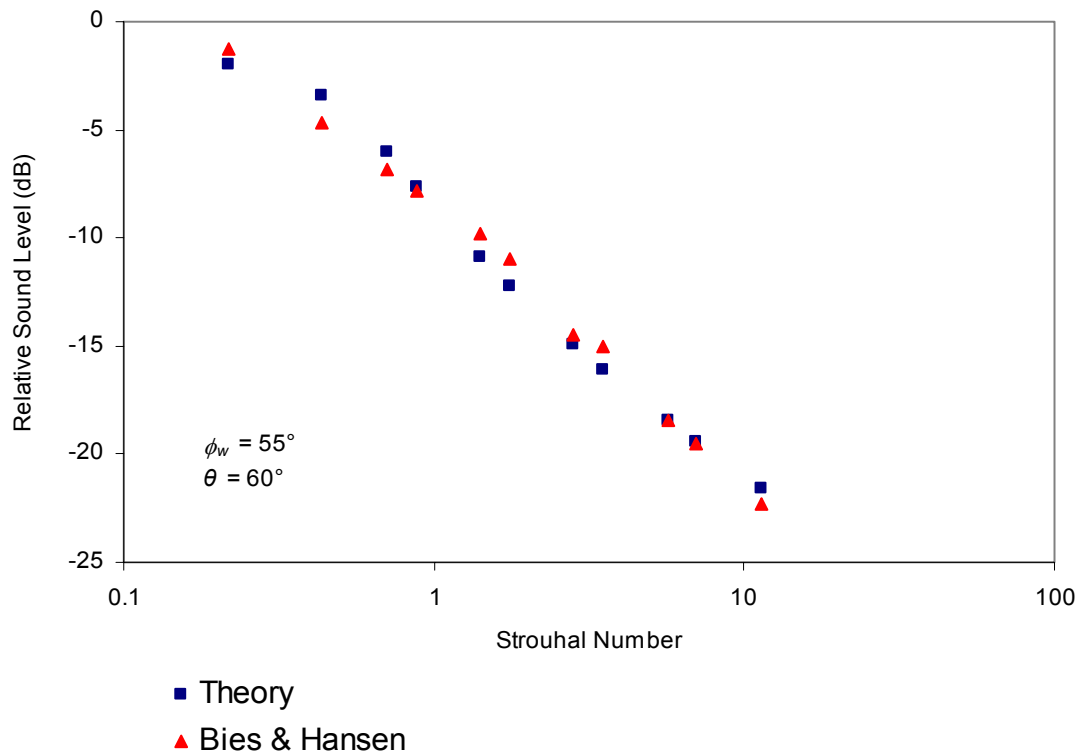


Figure 5.33. Comparison of Bies & Hansen’s data with the theory of section 5.1.1 for the sound level at 60 degrees relative to the sound level at 0 degrees. The theory of section 5.1.1 is used with the weighting function using a weighting angle ϕ_w of 55 degrees. A negative relative sound level constant of -1.5 dB was added to results of the theory of section 5.1.1.

Figure 5.33 shows that there is not great deal of difference between the relative sound level curves. In fact, the agreement between the two models for directivity at 60 degrees is quite satisfactory.

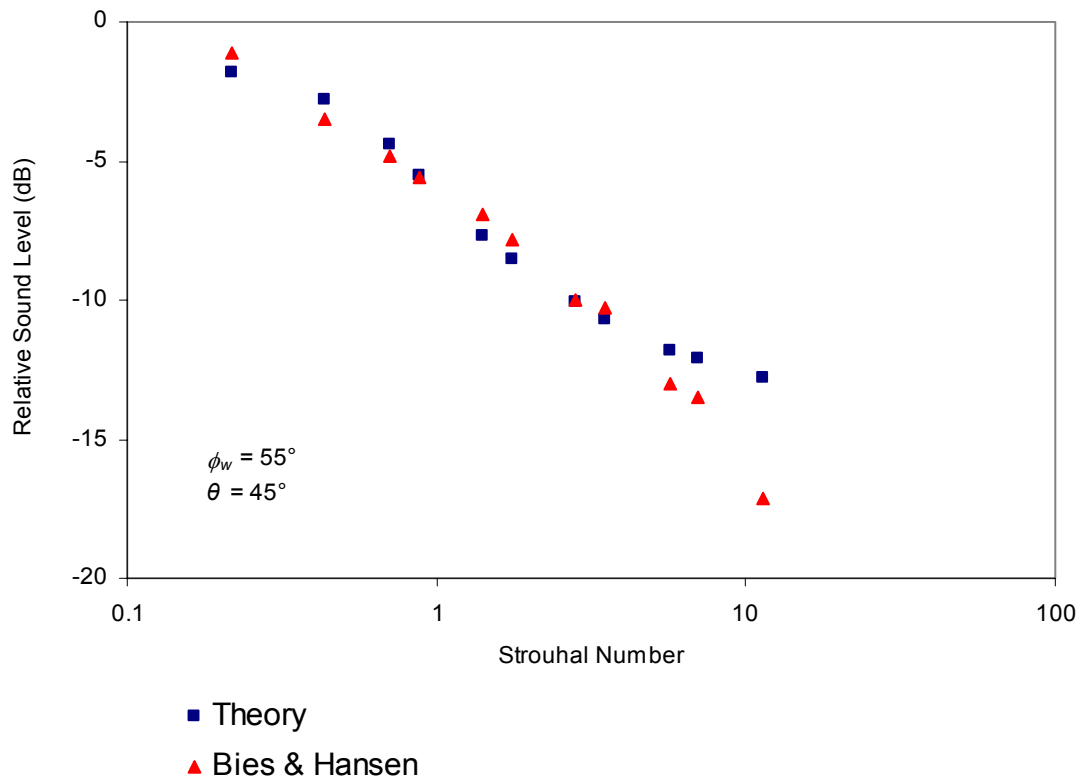


Figure 5.34. Comparison of Bies & Hansen’s data with the theory of section 5.1.1 for the sound level at 45 degrees relative to the sound level at 0 degrees. The theory of section 5.1.1 is used with the weighting function using a weighting angle ϕ_w of 55 degrees. A negative relative sound level constant of -1.5 dB was added to results of the theory of section 5.1.1.

For a relative sound level at 45 degrees the difference is obvious only for large Strouhal numbers. The difference is as much as 4.3 dB.

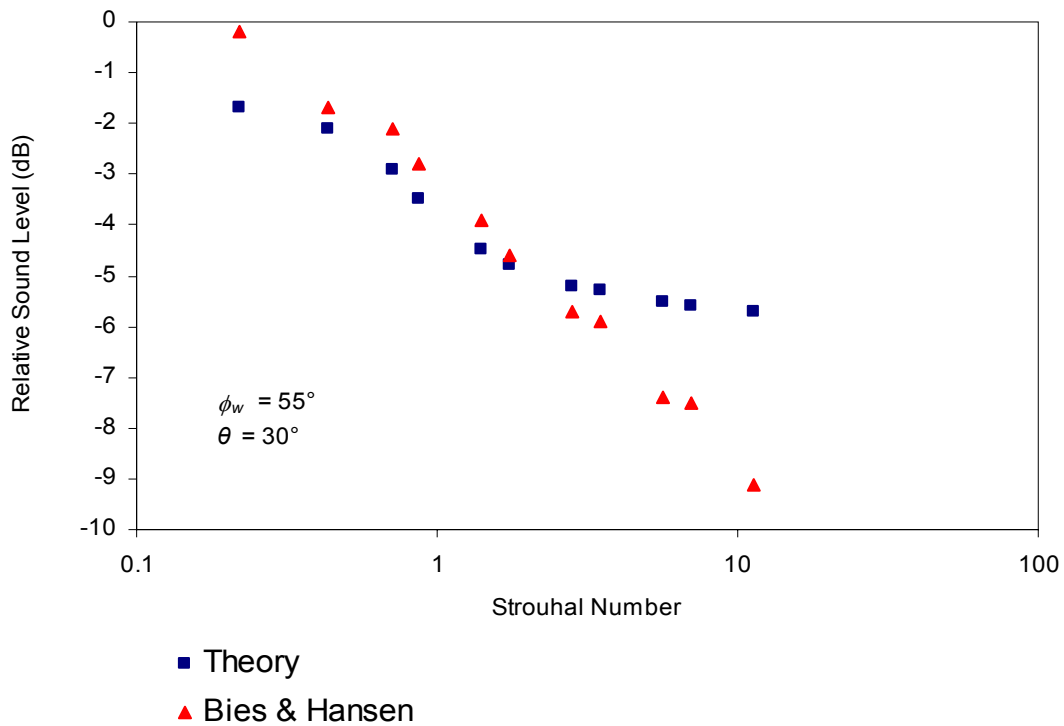


Figure 5.35. Comparison of Bies & Hansen’s data with the theory of section 5.1.1 for the sound level at 30 degrees relative to the sound level at 0 degrees. The theory of section 5.1.1 is used with the weighting function using a weighting angle ϕ_w of 55 degrees. A negative relative sound level constant of -1.5 dB was added to results of the theory of section 5.1.1.

The weighting angle used for the relative sound level radiated at different angles was 55° , which overall, when implemented showed the best agreement between the two models being compared. It is also important to note that relative sound level constant of - 1.5 dB was added to our data. This is because the comparison showed that at low frequencies the theory of section 5.1.1 could not quite produce the same relative sound level as the Bies & Hansen’s model. By studying figures 5.30 to 5.34 it can be seen that the general shape of the curves except for the relative sound level at 30° , are the same for different angles. As the curves in figure 5.35 indicate, there is a difference in relative sound level across the whole Strouhal number range. For small Strouhal numbers, the difference in the relative sound level between the two models is as much as 1.5 dB, and for large Strouhal numbers as much as 3.4 dB. The difference for small openings is equal to relative sound level constant that was added in order to match the relative sound level curves for other radiation angles. Setting the weighting

angle to 43 degrees would give a much better relative sound level comparison at 30° between the two models, which would not be the case for all other radiation angles.

5.1.6 B & K Microphone

The frequency response of the microphone is determined by diaphragm mass, diaphragm stiffness, mechanical damping of the diaphragm and interference and diffraction effects at frequencies where the microphone diameter becomes of the same order as the wavelength. The free field correction is a function of frequency [56]. Figure 5.36 shows the correction for the B & K one-inch condenser microphone types, 4144 and 4145, which is without the normal protection grid. The figure gives curves for correcting the electrostatic actuator response for various angles of incidence. It should be noted that the microphone is un baffled.

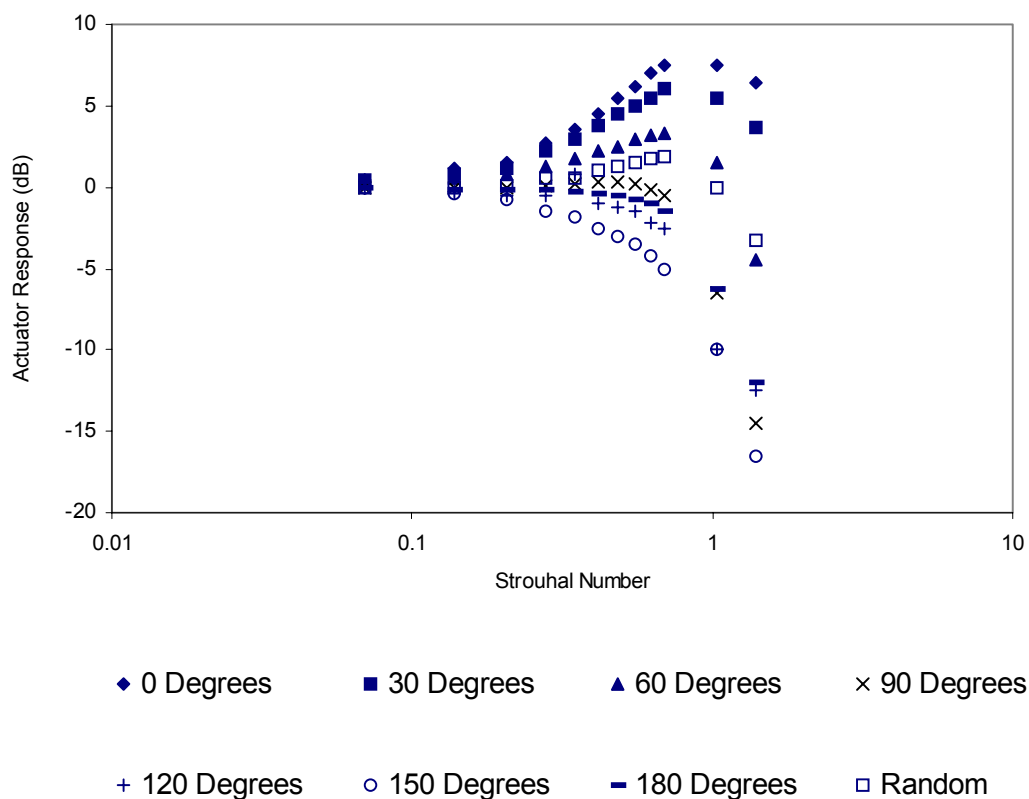


Figure 5.36. Free-Field Correction Curves.

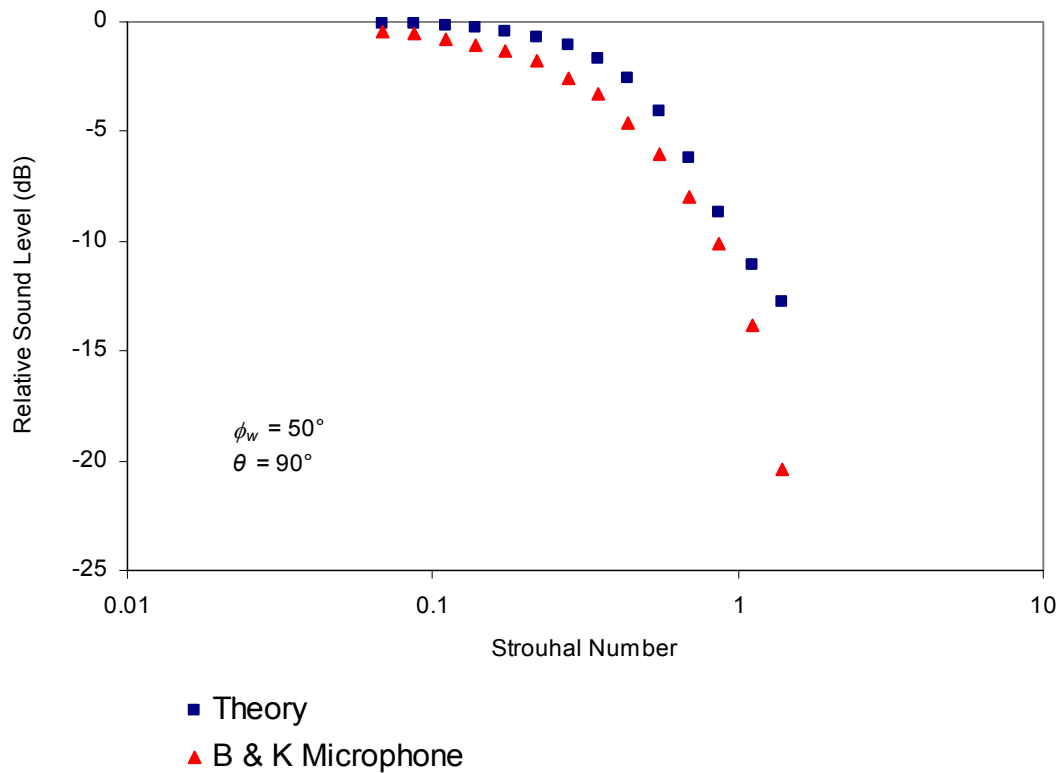


Figure 5.37. Comparison of Bruel & Kjaer microphone data with the theory of section 5.1.1 for the sound level at 90 degrees relative to the sound level at 0 degrees. The theory of section 5.1.1 is used with the weighting function using a weighting angle ϕ_w of 50 degrees.

The relative sound level at an angle θ for the one inch B&K microphone types 4144 and 4145 is defined as the free field correction for incidence at θ minus the free field correction for 0 degree incidence. These relative sound levels for different angles of incidence are compared to the theory of section 5.1.1 for an opening. Figure 5.38 represents the relative sound level at 90 degrees with a weighting angle at 50 degrees. It can be seen that overall, there is a very good agreement between the two models. The biggest difference is 7.6 dB when the Strouhal number is 1.4.

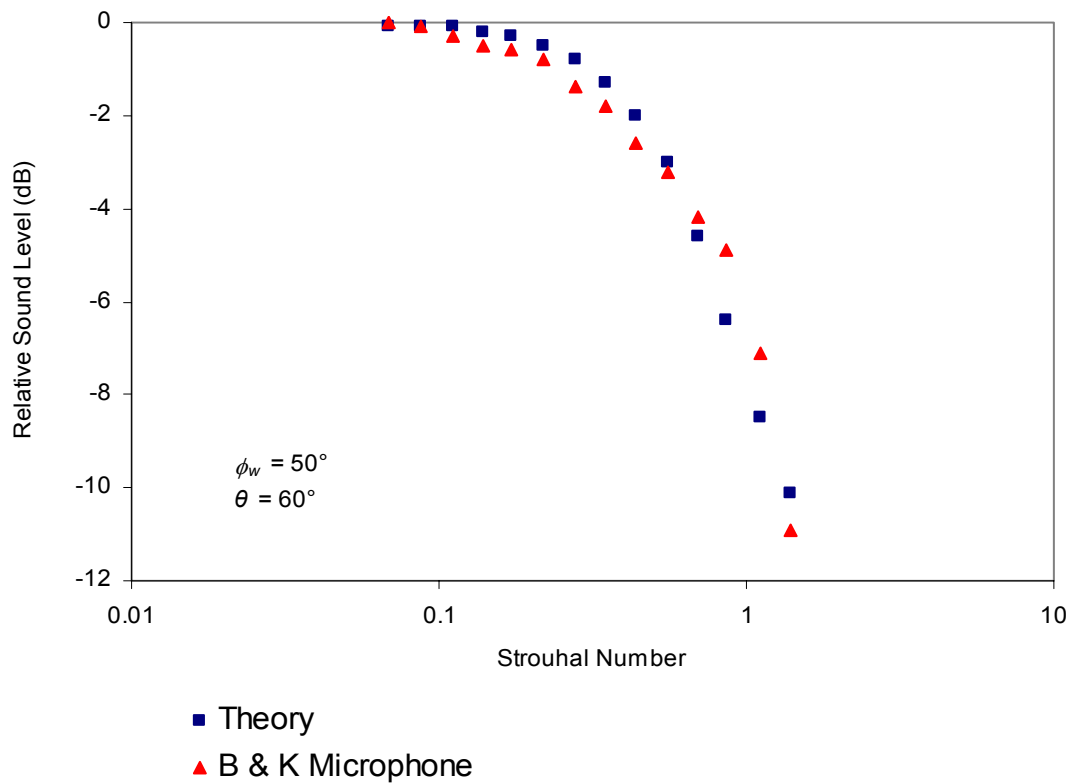


Figure 5.38. Comparison of Bruel & Kjaer microphone data with the theory of section 5.1.1 for the sound level at 60 degrees relative to the sound level at 0 degrees. The theory of section 5.1.1 is used with the weighting function using a weighting angle ϕ_w of 50 degrees.

The relative sound level curves at 60 degrees shown in figure 5.39 suggest that there is not a great deal of difference between the two models. In fact, the agreement is quite satisfactory.

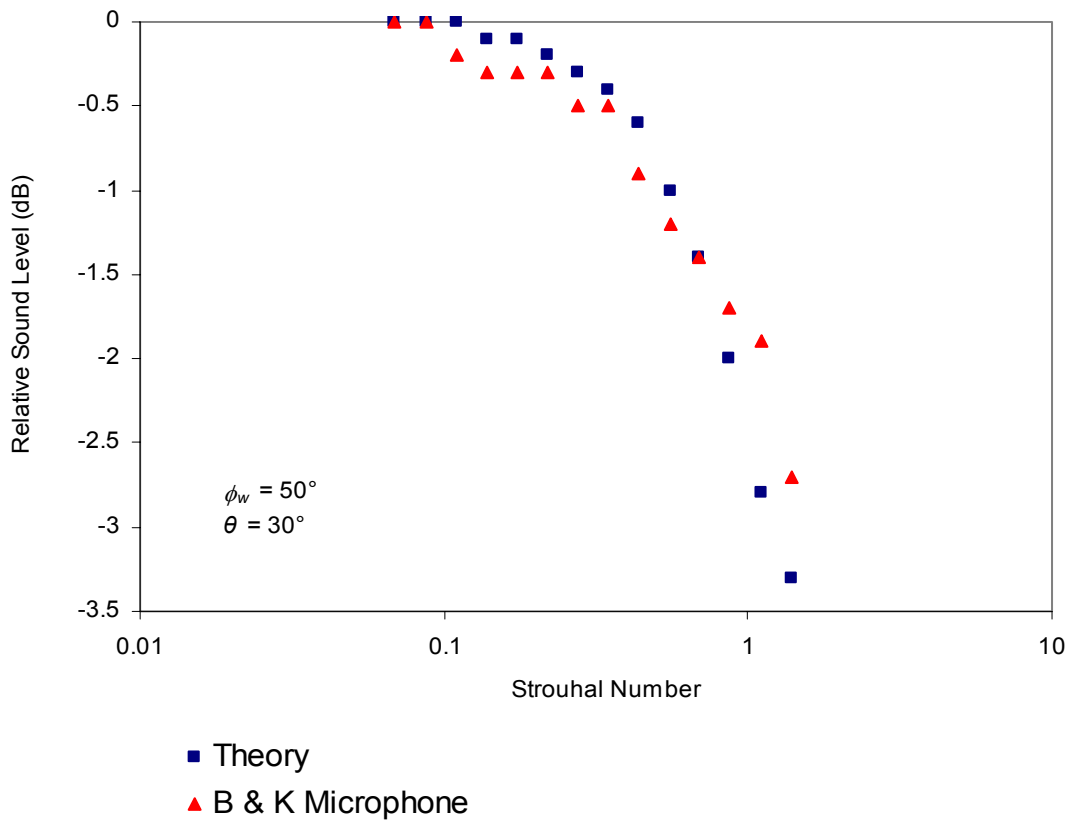


Figure 5.39. Comparison of Bruel & Kjaer microphone data with the theory of section 5.1.1 for the sound level at 30 degrees relative to the sound level at 0 degrees. The theory of section 5.1.1 is used with the weighting function using a weighting angle ϕ_w of 50 degrees.

Figure 5.39 shows another good agreement between the two models being compared. The general shape of the curves is the same for all angles investigated. Overall, the weighting angle at 55 degrees produced best agreement between the two models being compared.

5.1.7 Levine & Schwinger's analytic calculations on the radiation from an unflanged circular pipe

It is known that if the diameter is small compared to the wavelength, at the open end of a unbaffled pipe which has a circular cross section, nearly complete reflection of a dominant mode (plane) sound wave occurs [41]. The radiation characteristics of the pipe determine the absorption of energy from an externally incident plane wave. To describe the radiation characteristics of the pipe, Levine and Schwinger calculated the power-function, which compares the intensity of radiation in a given direction with that of an isotropically radiating point source of equal power output.

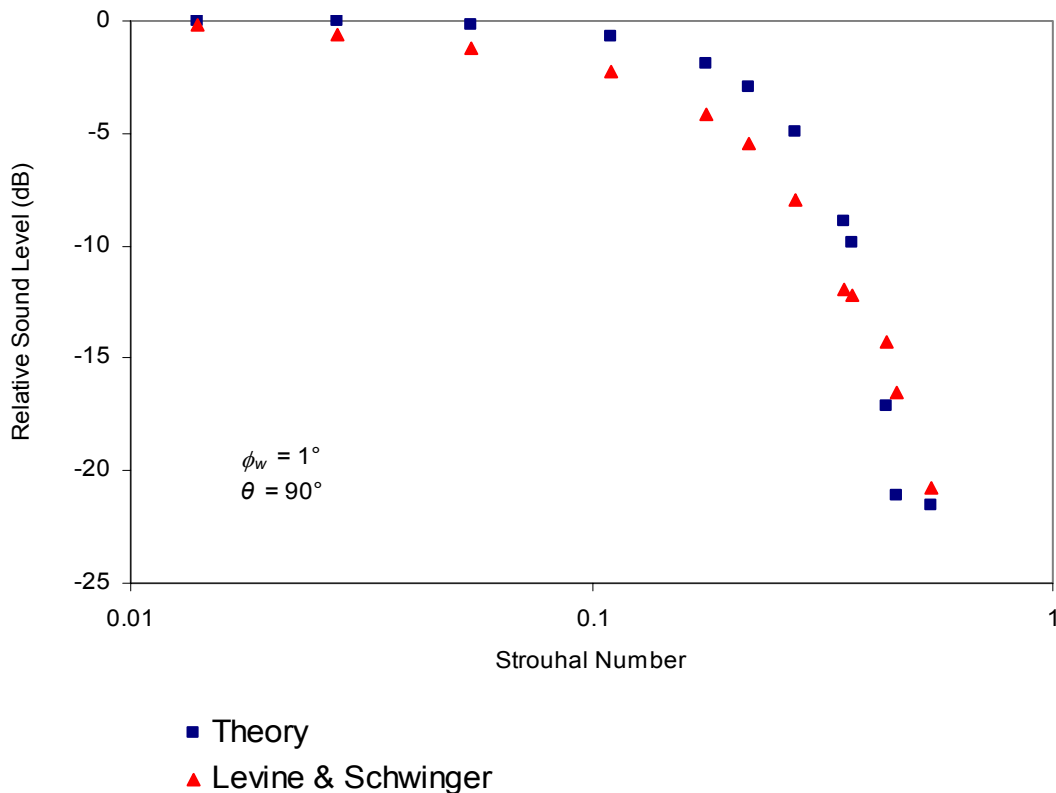


Figure 5.40. Comparison of Levine & Schwinger's data with the theory of section 5.1.1 for the sound level at 90 degrees relative to the sound level at 0 degrees. The theory of section 5.1.1 is used with the weighting function using a weighting angle ϕ_w of 1 degree.

Levine and Schwinger considered the situation in which only plane waves propagate in the pipe. That being the case a satisfactory comparison is produced only when the weighting angle is set to 1 degree. Because our spreadsheet calculations used 1 degree increments this sets the incident sound to be incident at 0° . At 90 degrees, the biggest relative sound level difference of 3.1 dB occurs when the Strouhal number is 0.28.

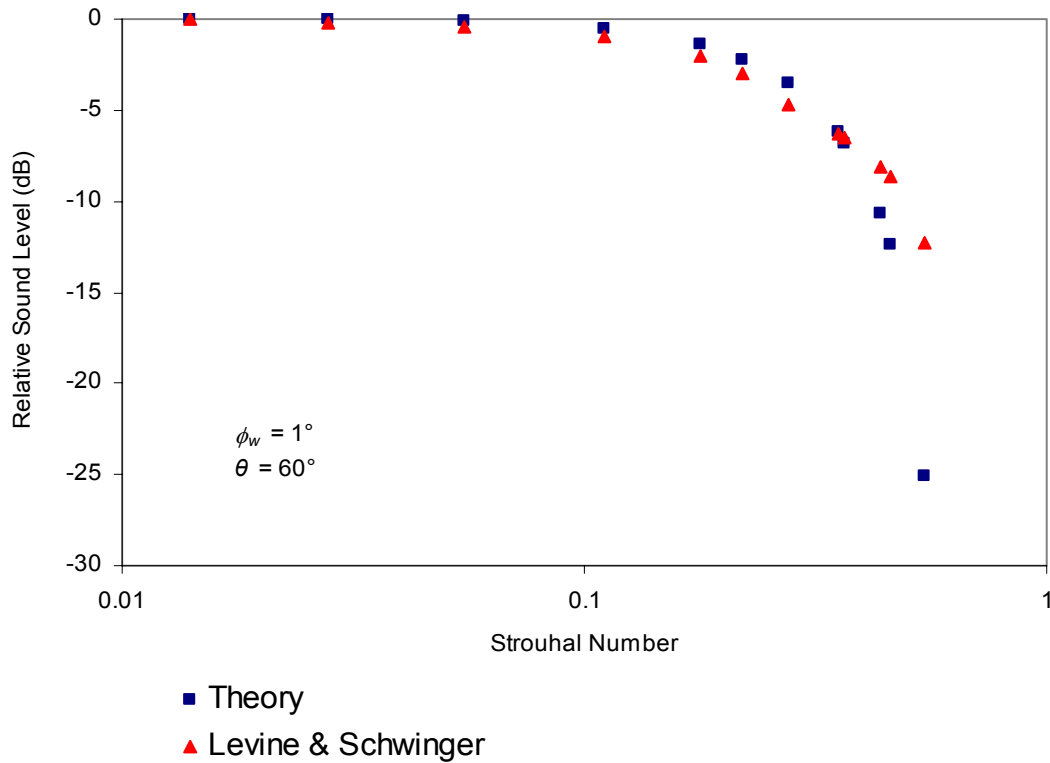


Figure 5.41. Comparison of Levine & Schwinger’s data with the theory of section 5.1.1 for the sound level at 60 degrees relative to the sound level at 0 degrees. The theory of section 5.1.1 is used with the weighting function using a weighting angle ϕ_w of 1 degree.

Figure 5.41 represents the relative sound level at 60 degrees with a weighting angle of 1 degree. Overall, there is a very good agreement between the two models. The biggest difference is 12.8 dB when the Strouhal number is 0.55.

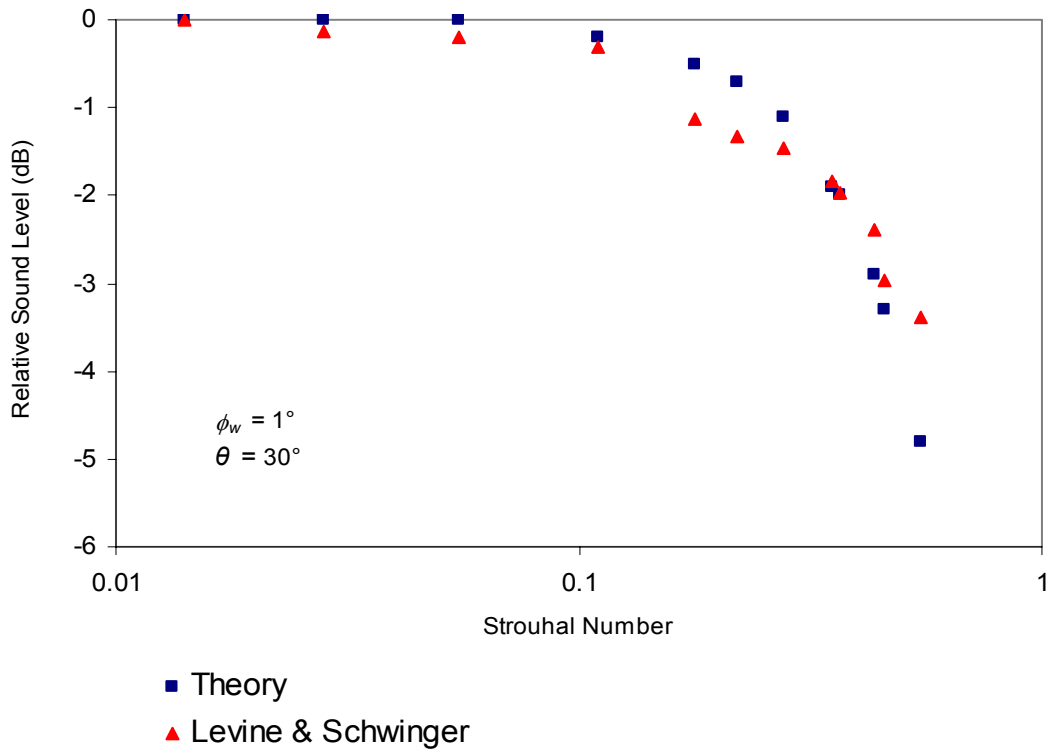


Figure 5.42. Comparison of Levine & Schwinger’s data with the theory of section 5.1.1 for the sound level at 30 degrees relative to the sound level at 0 degrees. The theory of section 5.1.1 is used with the weighting function using a weighting angle ϕ_w of 1 degree.

The relative sound level prediction models shown in figure 5.42 indicate generally good agreement for the relative sound level at 30 degrees. The relative sound level differences within the Strouhal number range from 0.18 through to 0.73 are small.

5.1.8 Environment Protection Authority experimental results on the directivity loss in a free field

The Environmental Protection Authority (EPA) model has also been investigated. The EPA model is based on a limited number of experimental results and the fitting of the model

curves to the experimental is now known to be very conservative [42]. A figure representing the directivity loss in a free field with its reference was acquired at the start of this research. From this figure it was possible to determine important information about the EPA model. It showed the sound pressure level (SPL) for a square un baffled duct area as a function of frequency for four angles relative to 0 degrees. SPL curves for 90 and 45 degrees relative to 0 degrees were investigated and compared to the theory of section 5.1.1.

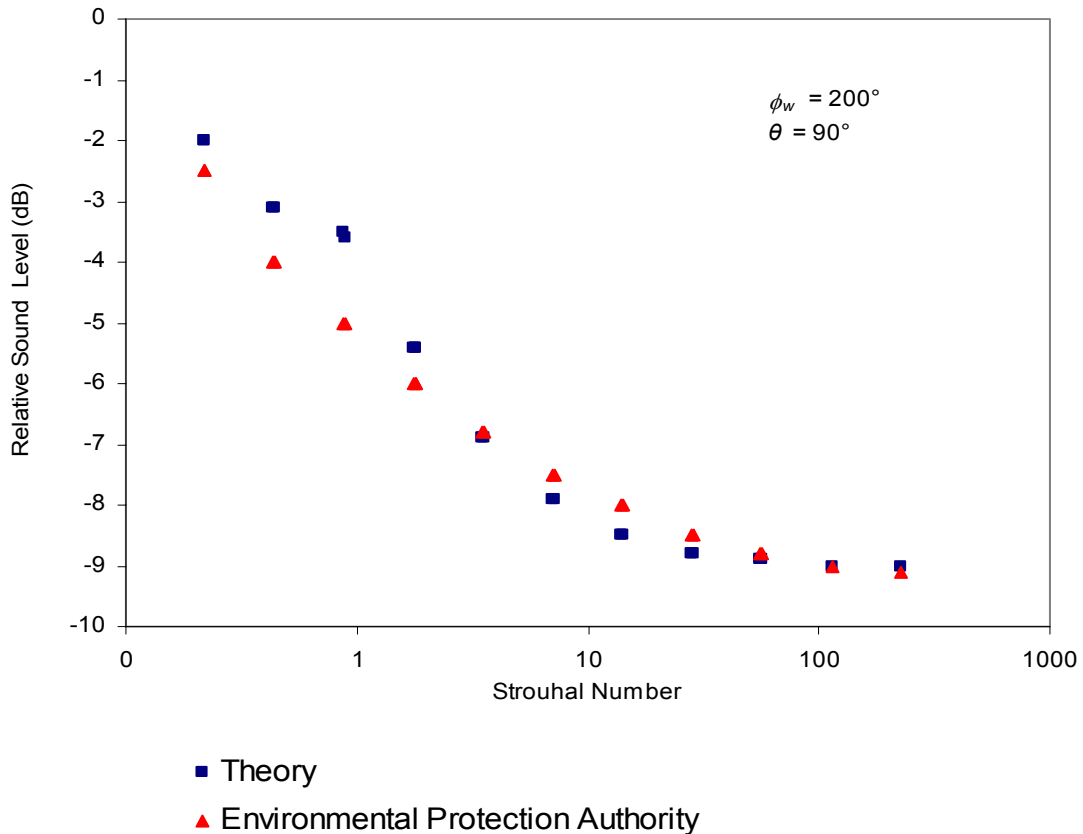


Figure 5.43. Comparison of Environmental Protection Authority data with the theory of section 5.1.1 for the sound level at 90 degrees relative to the sound level at 0 degrees. The theory of section 5.1.1 is used with the weighting function using a weighting angle ϕ_w of 200 degrees. A negative relative sound level constant of -1.5 dB was added to results of the theory of section 5.1.1.

Note that the integration over φ in theory of section 5.1.1 is only performed from -90 degrees to 90 degrees even though the weighting angle φ_w of the weighting function is greater than 90 degrees. Figure 5.43 showed that the EPA relative sound level curve asymptotes to a value of -9 dB.

In order to exhibit the same phenomenon, the following approach was used:

$$r_c = \left(r^n + \left(\frac{1}{8} \right)^n \right)^{\frac{1}{n}} \quad (5.32)$$

where $r = 10^{\frac{R}{10}}$

and R was the relative sound level at the angle of interest. This approach asymptotes the relative sound level to the maximum decrease.

After all the calculations were done the modified data for the theory of section 5.1.1 was compared to the data of the EPA. Figure 5.43 suggests that there was not a great deal of difference between the relative sound level curves. In fact the agreement between the two models for a relative sound level at 90 degrees was quite good. The biggest difference was 1.5 dB when the Strouhal number was 0.875.

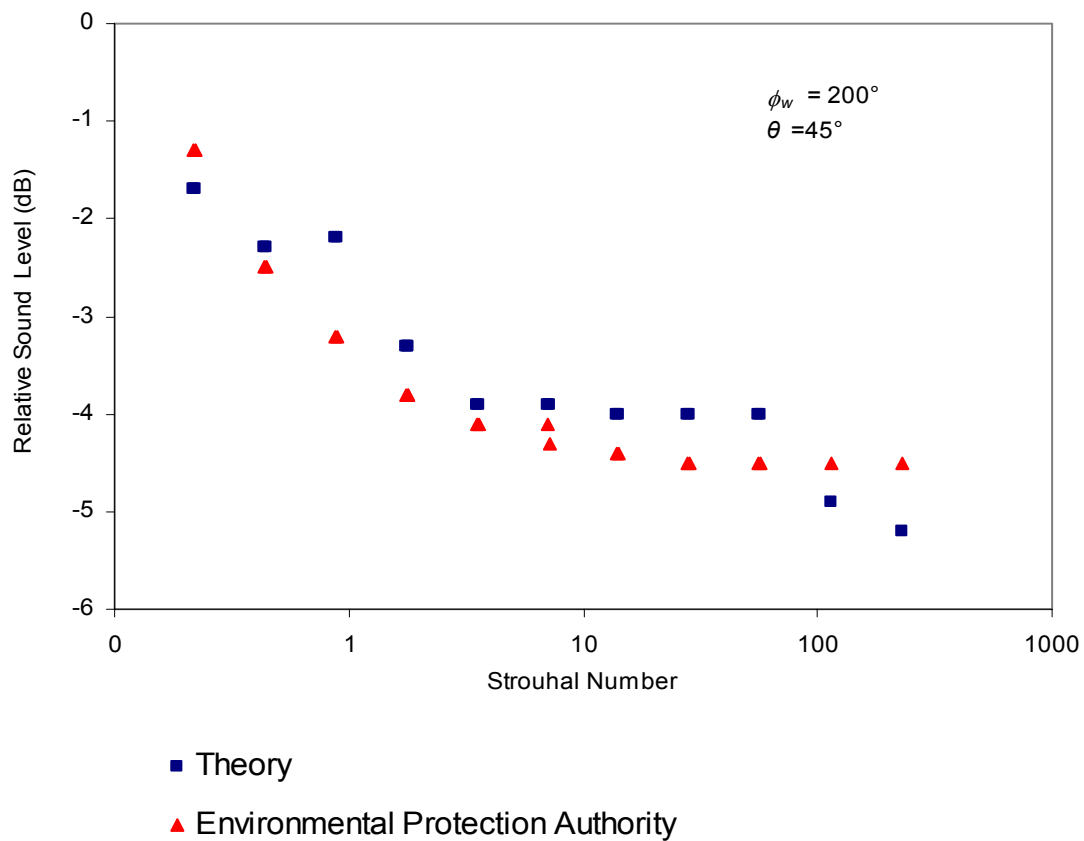


Figure 5.44. Comparison of Environmental Protection Authority data with the theory of section 5.1.1 for the sound level at 45 degrees relative to the sound level at 0 degrees. The theory of section 5.1.1 is used with the weighting function using a weighting angle ϕ_w of 200 degrees. A negative relative sound level constant of -1.5 dB was added to results of the theory of section 5.1.1.

Figure 5.44 represented the relative sound level at 45 degrees with a weighting angle at 200 degrees. Overall, there was a satisfactory agreement between the two models. The biggest difference was 1 dB when the Strouhal number was 0.875. The original reference for the EPA model would have enabled us to investigate it further and in greater detail.

5.1.9 Sharland's prediction model for sound radiation in ventilating systems

Sharland investigated and calculated the amount of noise radiated in ventilating system particularly through an atmospheric louvre fixed in a wall. The acoustic louvre is baffled by the wall. For example, schools or residential premises could have a noise problem, which is due to fan noise generated in ventilation ducting and then radiated to an adjacent property [39].

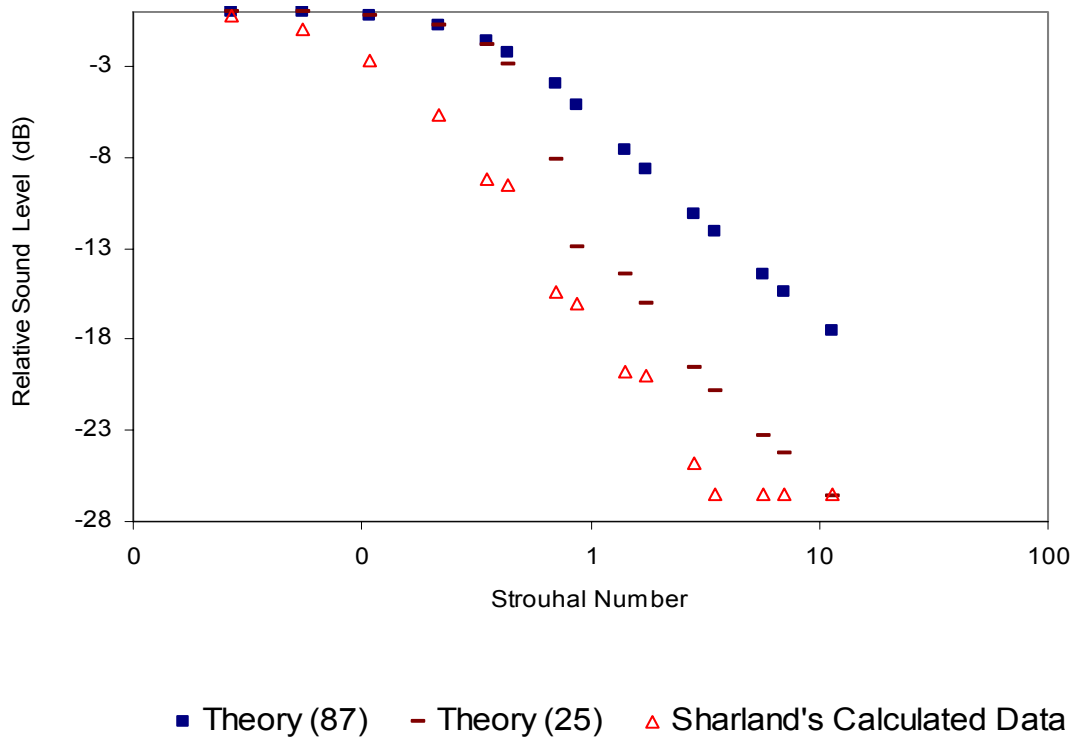


Figure 5.45. Comparison of Sharland's calculated data with the theory of section 5.1.1 for the sound level at 90 degrees relative to the sound level at 0 degrees. The theory of section 5.1.1 is used with the weighting function using a weighting angle ϕ_w of 87 and 25 degrees.

The theory of section 5.1.1 (87) and the theory of section 5.1.1 (25) represented relative sound level curves for the theory of section 5.1.1 at 90 degrees with weighting angles at 87° and 25° respectively. The weighting angle of 87° with no relative sound level constant added

was used for all angles for the two model comparison. That did not work well for the relative sound level at 90 degrees. A weighting angle set at 25 degrees produced a more satisfactory result. At a Strouhal number of 11, the difference between the two models was as little as 0.1 dB. For the rest of the Strouhal number range the difference was somewhat bigger, but the overall shape of the relative sound level curves for the two models was very similar.

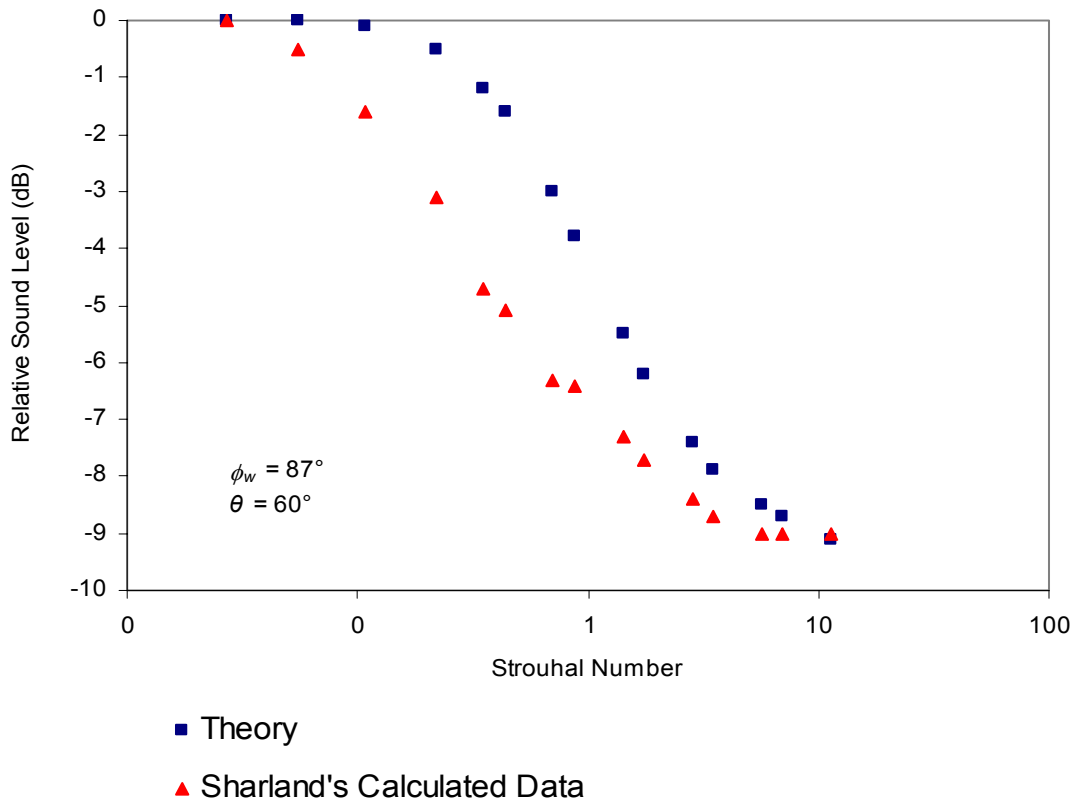


Figure 5.46. Comparison of Sharland’s calculated data with the theory of section 5.1.1 for the sound level at 60 degrees relative to the sound level at 0 degrees. The theory of section 5.1.1 is used with the weighting function using a weighting angle ϕ_w of 87 degrees.

The relative sound level curves for 60 degrees were very similar to the relative sound level curves for 90 degrees in terms of relative sound level difference across the Strouhal number range. At Strouhal numbers 0.35 and 0.44, the difference was as much as 3.5 dB and at a Strouhal number 11.3, the difference between the two models was as little as 0.1 dB.

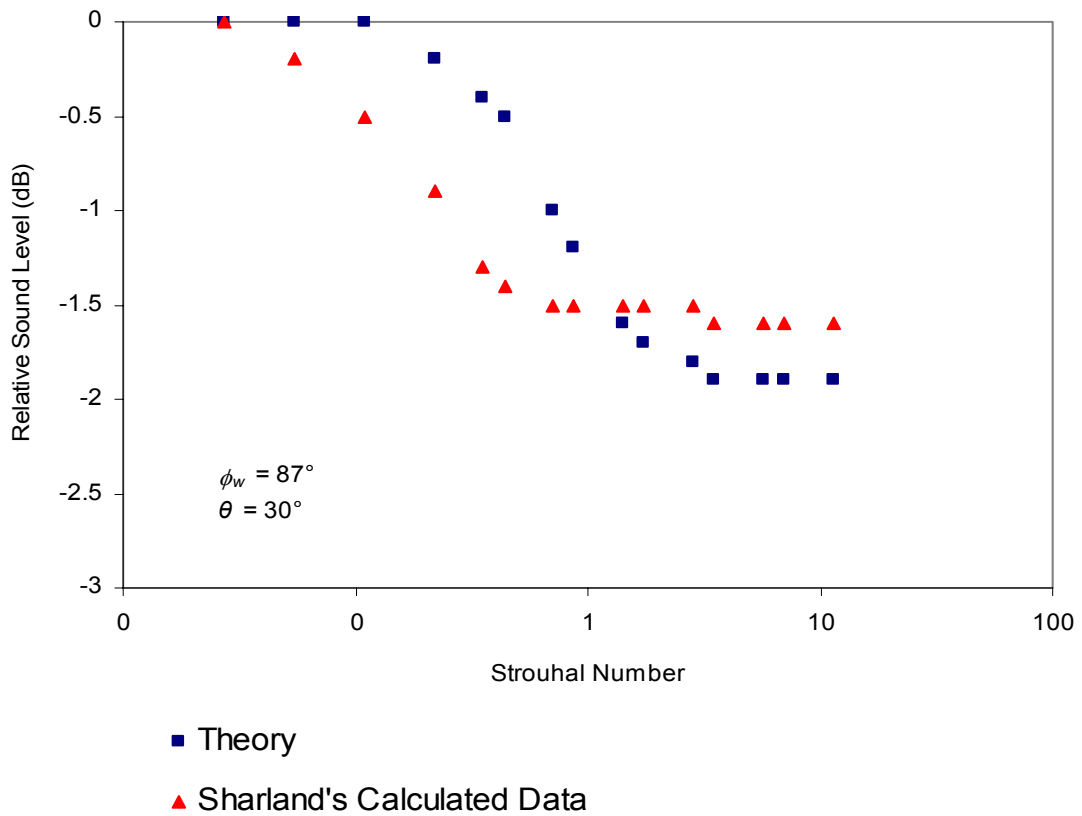


Figure 5.47. Comparison of Sharland’s calculated data with the theory of section 5.1.1 for the sound level at 30 degrees relative to the sound level at 0 degrees. The theory of section 5.1.1 is used with the weighting function using a weighting angle ϕ_w of 87 degrees.

Figure 5.47 shows the relative sound level at 30 degrees with a weighting angle at 87 degrees. The result was satisfactory considering that the biggest difference in the relative sound level for the two models was 0.9 dB at Strouhal numbers 0.35 and 0.44.

5.1.10 Woods' directivity prediction model for louvers and grilles

The directivity of a source depends on the size of the source and the frequency of the sound. As the frequency increases, the directivity of a source increases. For constant frequency, the directivity increases as source size increases [2]. Directivity is different in the horizontal and vertical directions for a rectangular source such as an open window or louvre because of the different sizes of the sources. In fact, since not all the sound is radiated, especially at low frequency, an end correction loss must be implemented in order to calculate the corrected values of the sound power level [40]. Woods presented two tables of data from which a sound pressure level at a distance can be obtained directly. One table gives the directivity at ($\theta = 0$) for either horizontal bearing or vertical bearing of an observation point from the centre of the louvre and the other table gives the directivity correction for a bearing angle away from the normal axis of the atmospheric louvre or grille. To estimate the SPL at a particular distance, one needs to take the attenuation value given in dB and subtract this from the sound power level (SWL) of the source, which will be corrected if necessary for end reflection loss. Using this procedure sound pressure level values were calculated for the required angles and compared to the theory of section 5.1.1. The acoustic louvre is baffled by the wall in which it is mounted.

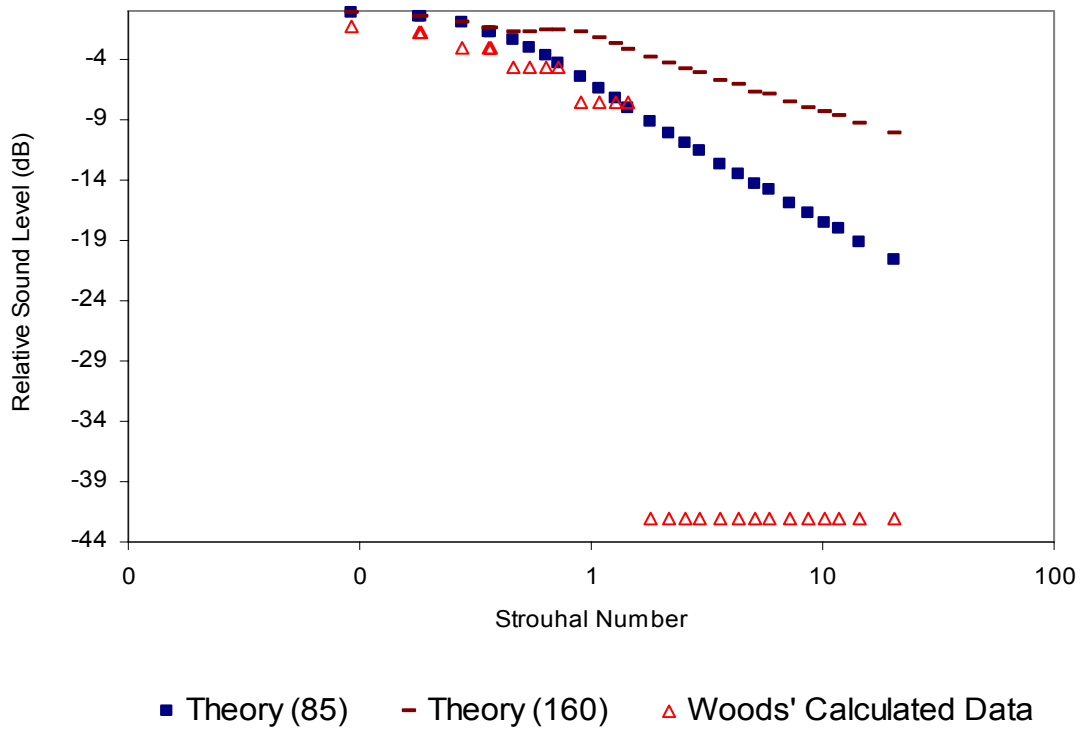


Figure 5.48. Comparison of Woods’ calculated data with the theory of section 5.1.1 for the sound level at 90 degrees relative to the sound level at 0 degrees. The theory of section 5.1.1 is used with the weighting function using a weighting angle ϕ_w of 85 and 160 degrees.

The theory of section 5.1.1 (85) and the theory of section 5.1.1 (160) represented the relative sound level curves for the theory of section 5.1.1 at 90 degrees with weighting angles at 85° and 160° respectively. A weighting angle of 160° with no relative sound level constant added was used for all angles for the two model comparison. That did not work well for the relative sound level at 90 degrees. A weighting angle set at 85 degrees produced a more satisfactory result, at least for low Strouhal numbers. At Strouhal number 1.8 through to 20.4, Woods predicted that the relative sound level asymptoted to a value of -44 dB. The theory of section 5.1.1 clearly did not predict the same relative sound level at high Strouhal numbers. It predicted that at Strouhal number 20.4 the relative sound level was -20.7 dB. At Strouhal numbers 0.092 through to 0.28 there was no difference at all between the two models.

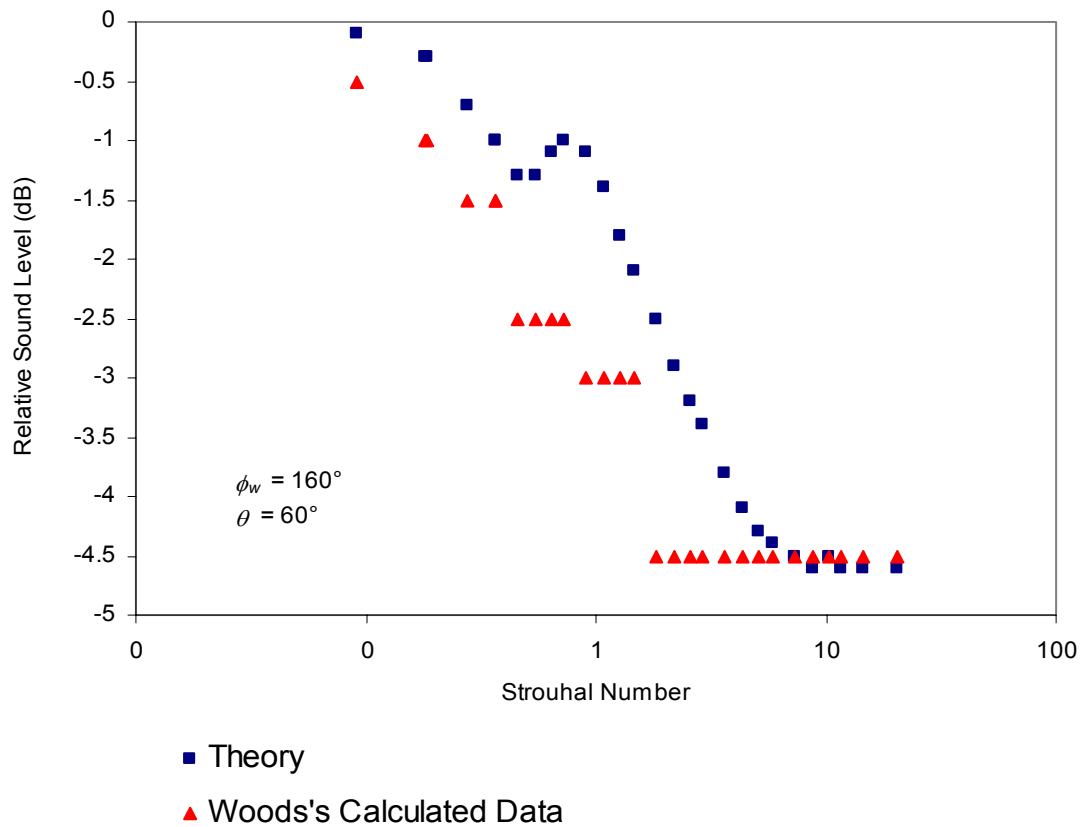


Figure 5.49. Comparison of Woods' calculated data with the theory of section 5.1.1 for the sound level at 60 degrees relative to the sound level at 0 degrees. The theory of section 5.1.1 is used with the weighting function using a weighting angle ϕ_w of 160 degrees.

At Strouhal number 1.8, the difference was as much as 2 dB and at Strouhal number 20.4, the difference between the two models was as little as 0.1 dB.

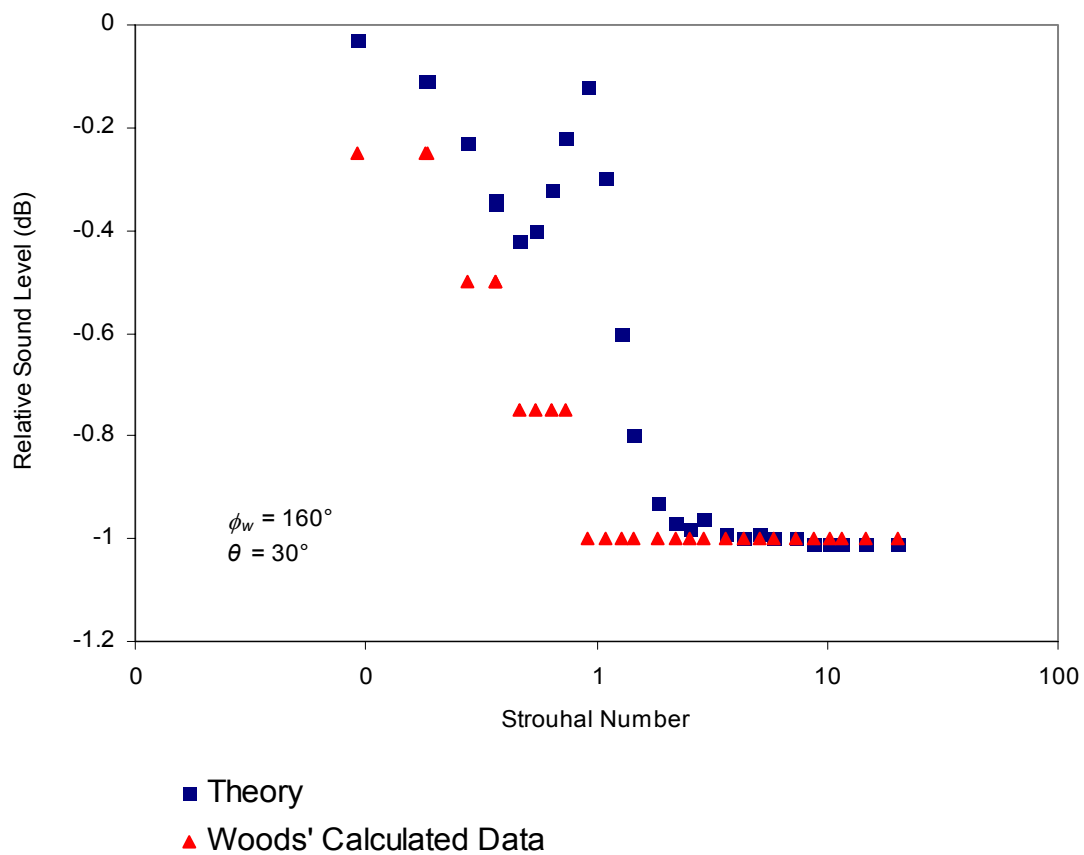


Figure 5.50. Comparison of Woods’ calculated data with the theory of section 5.1.1 for the sound level at 30 degrees relative to the sound level at 0 degrees. The theory of section 5.1.1 is used with the weighting function using a weighting angle ϕ_w of 160 degrees.

The relative sound level curves for 30 degrees were very similar to the relative sound curves for 60 degrees in terms of the shape of the curve. Two models’ prediction curves matched extremely well considering that the biggest difference in directivity for the two models was 0.88 dB at Strouhal number 0.9.

5.1.11 Linear Interpolation

For some of the models that have been investigated during this research there was no indication whether data obtained was measured or calculated. In order to get a better understanding of the directivity curves produced by those particular models, data was interpolated in 5° steps. Linear interpolation of data was calculated using the following relationship:

$$\frac{y - y_1}{x - x_1} = \frac{y_2 - y_1}{x_2 - x_1} \quad (5.33)$$

$$y = \frac{y_2 - y_1}{x_2 - x_1}(x - x_1) + y_1 \quad (5.34)$$

$$= \frac{y_2(x - x_1) - y_1x + y_1x_1 + y_1x_2 - y_1x_1}{x_2 - x_1} \quad (5.35)$$

$$= \frac{y_2(x - x_1) + y_1(x_2 - x)}{x_2 - x_1} \quad (5.36)$$

5.1.11.1 Opening with width of 0.5m

Data of Woods [40], Sharland [39], Levine & Schwinger [41], Bies & Hansen [16] etc., were interpolated and compared. Woods II is the model where Woods' published data was doubled. Sharland II is the model where Sharland's published data was halved. Woods II was introduced into the comparison because it asymptotes to a value of 9 dB at 0 degrees which seems to be the case for the other prediction models. Sharland II was also introduced into the comparison since it was not possible to determine whether the data for Woods II (doubled) and Sharland II (halved) came from the same source.

Figure 5.51 shows relative sound level comparison at 90 degrees for the opening with a width of 0.5 m.

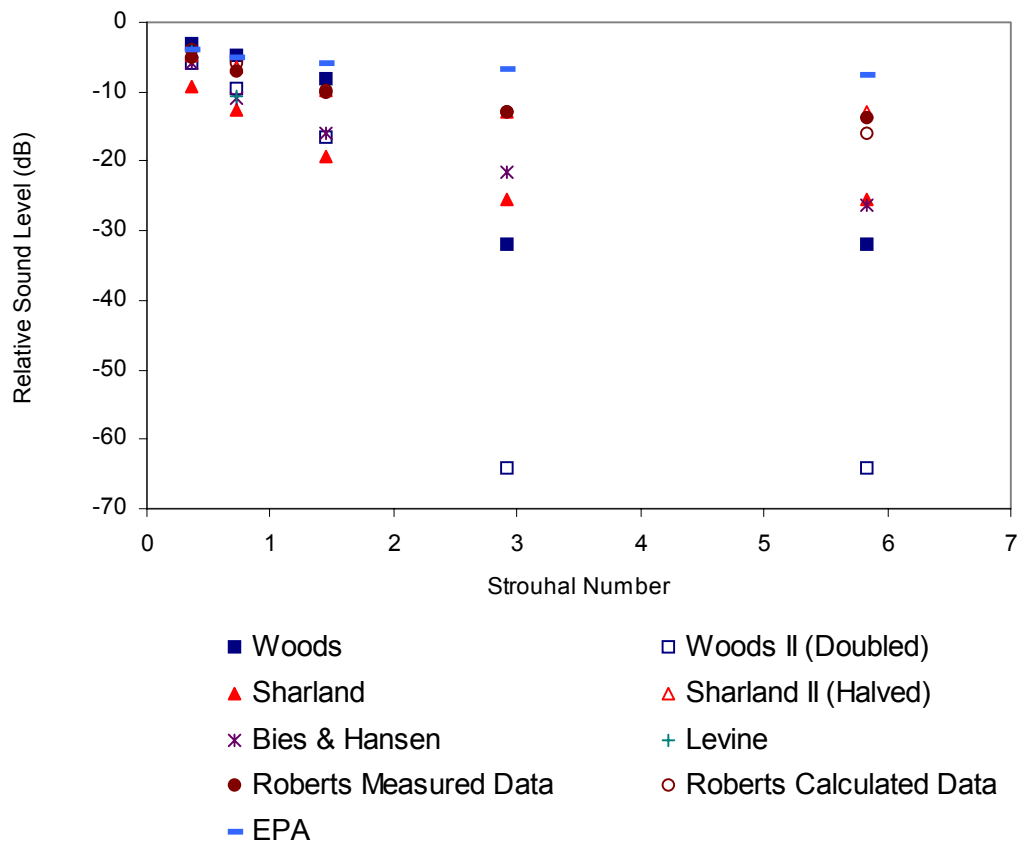


Figure 5.51. Comparison of the relative sound level at 90 degrees for different prediction models for the opening with a width of 0.5 m.

At a low Strouhal number of 0.36 the different models predicted relative sound levels ranging from -3 dB to -9.3 dB. Roberts’ calculated data and the EPA model predicted the same -4 dB relative sound level, while other models predicted relative sound levels within -3 dB, except for Sharland, who predicted a somewhat higher relative sound level of -9.3 dB. At Strouhal number 5.8 there was more variability in the relative sound level prediction between different models. At high Strouhal numbers, agreement between these different models was not as good as for low Strouhal numbers. This shows that there is significant disagreement in the relative sound level loss at 90 degrees at high Strouhal numbers between these models. Woods II at high Strouhal numbers predicted a very high relative sound level decrease, as high as -64 dB.

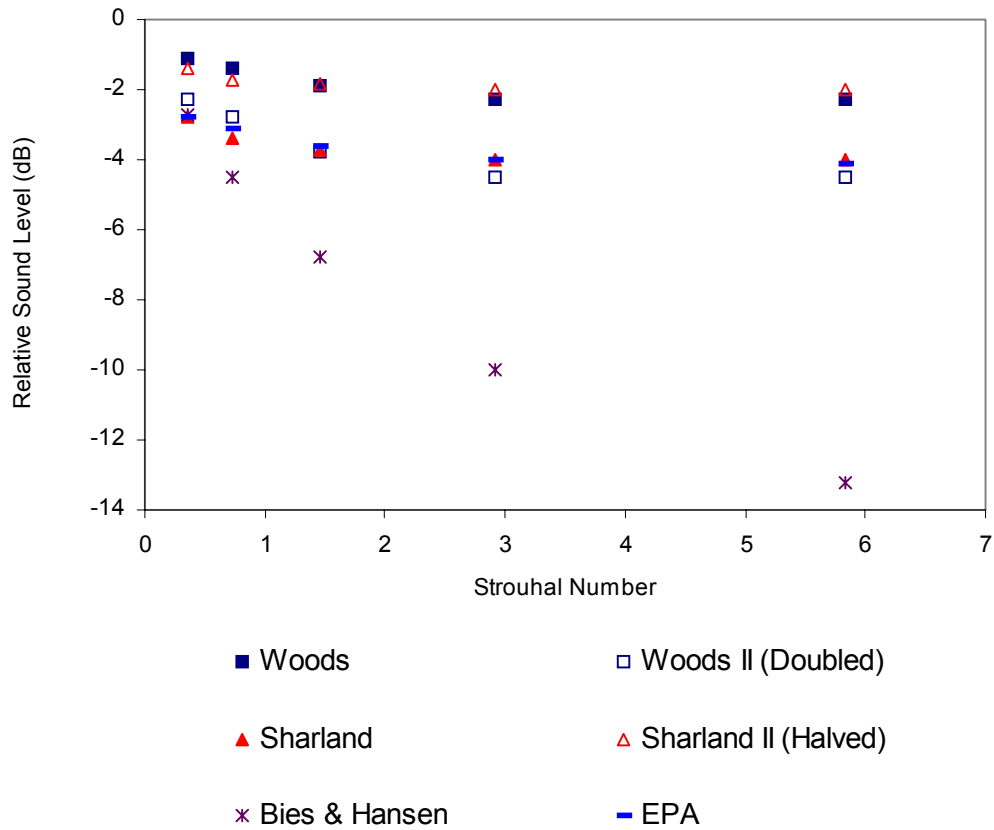


Figure 5.52. Comparison of the relative sound level at 45 degrees for different prediction models for the opening with a width of 0.5 m.

The relative sound level prediction varied between different models. It ranged from -1.1 to -2.8 dB at a Strouhal number of 0.36. At a Strouhal number of 5.8, the relative sound level ranged from -2 to -13.2 dB. At 45°, Bies and Hanson’s model predicts a lower relative sound level than the other models. Bies and Hanson’s model is based on experimental measurements in an anechoic room. The EPA model is based on a limited number of experimental results and the fitting of the model curves to the experimental is now known to be very conservative (Athol Day – personal communication). Bies and Hansen model and the EPA model are for un baffled duct openings while Woods’ model and Sharland’s model are for baffled duct openings. This is believed to be the reason for the difference between these models.

5.1.11.2 *Opening with width of 1.5m*

Interpolation and data comparison were also investigated for the opening with width of 1.5 m.

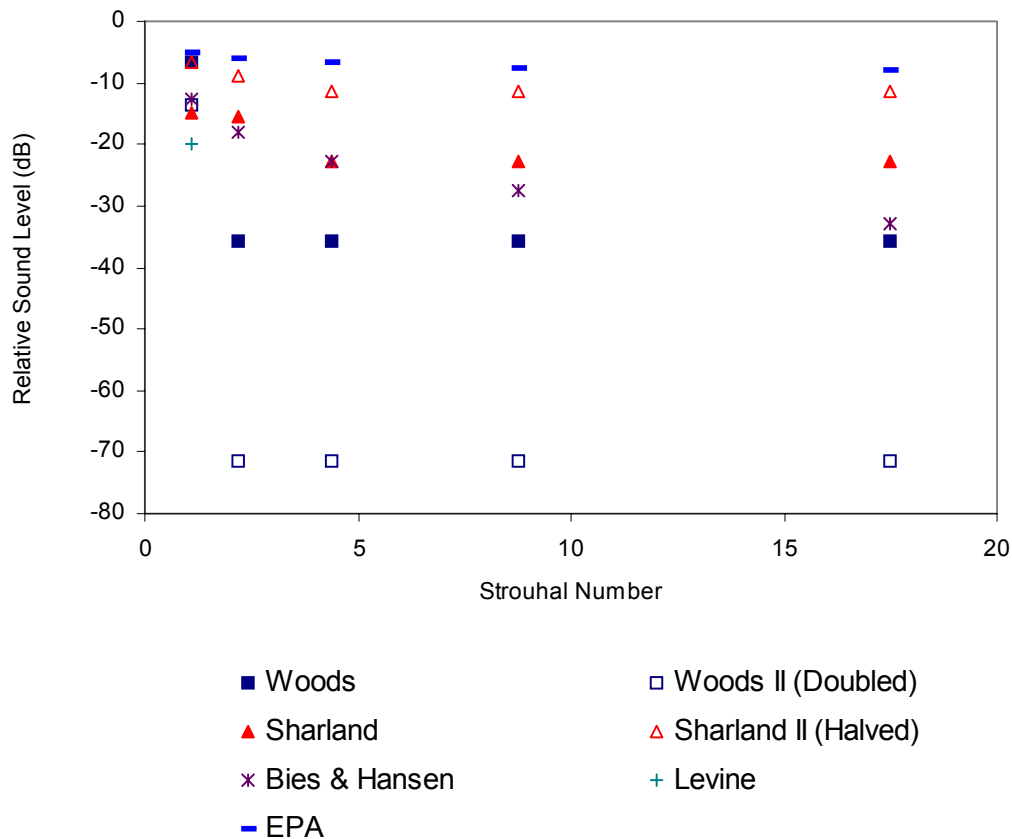


Figure 5.53. Comparison of the relative sound level at 90 degrees for different prediction models for the opening with a width of 1.5 m.

Figure 5.53 showed the relative sound level comparison at 90 degrees for the opening with a width of 1.5 m. At the low Strouhal number of 1.09 different models predicted the relative sound level ranging from -14.8 dB to -5 dB. Woods II at high Strouhal numbers predicted a very high relative sound level decrease, as high as -71.5 dB. An interesting aspect was that Woods', Sharland's and Hansen's data all asymptotes at high Strouhal number, which was not apparent with an opening with width of 0.5m.

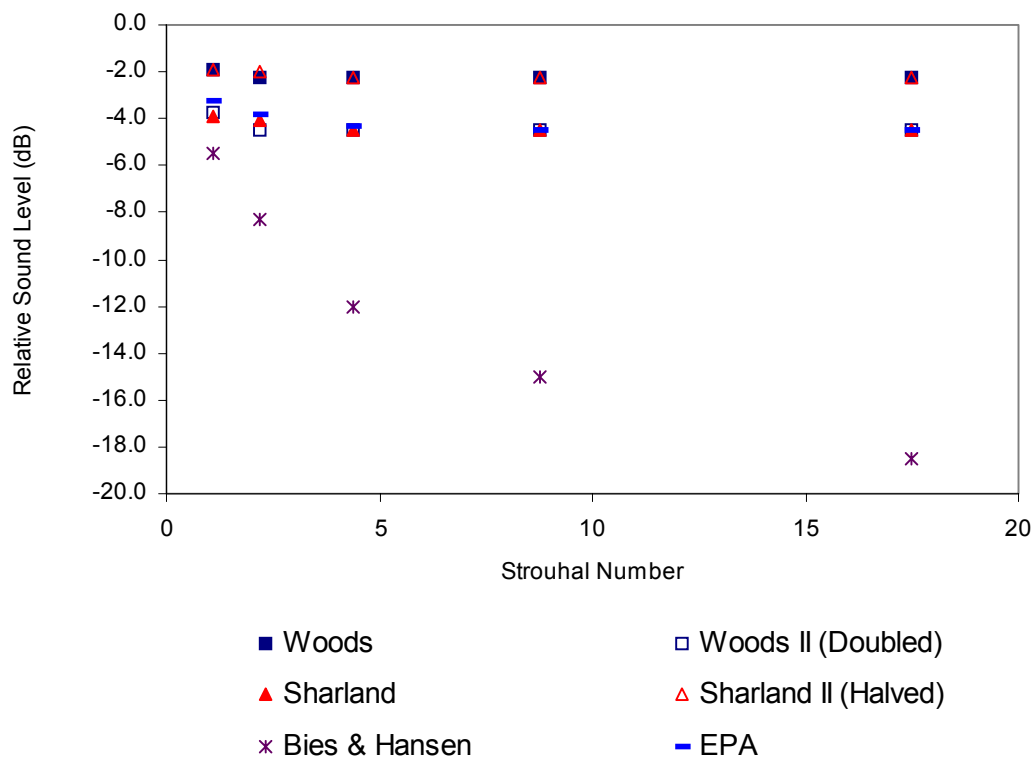


Figure 5.54. Comparison of the relative sound level at 45 degrees for different prediction models for the opening with a width of 1.5 m.

Figure 5.54 shows the relative sound level comparison at 45 degrees for an opening with a width of 1.5 m. At a low Strouhal number of 1.09, different models predicted relative sound levels ranging from -3.8 dB to -1.9 dB. At a Strouhal number of 17.49, the relative sound level ranged from -18.5 to -2.3 dB.

Having investigated and compared different measured and calculated data there appears to be a large degree of variability in relative sound level predictions.

CHAPTER 6

6. Conclusion

The purpose of the present research was to develop the best method for effectively modeling sound radiation from finite size panels and openings at grazing angles relative to that in the normal direction, to examine the contributing factors for the sound propagated to the far-field.

With large flat factory roofs one needs to know the sound radiation at grazing angles. The existing infinite panel theories of sound insulation are not sufficient when the sound radiation is at grazing angles.

Sato has calculated numerical values of radiation efficiency for a finite size square panel. This research presents a simple analytic strip theory which agrees reasonably well with Sato's numerical calculations of the sound radiation efficiency for a square panel. The two dimensional strip model analytic approximation derived in this thesis provides reasonable agreement with three dimensional numerical calculations. This agrees with Ljunggren [5] whose two dimensional numerical calculations agree within ± 0.5 dB of the three dimensional calculations of Sato [4] and Novak [6]. It also agrees with the experimental measurements of Roberts [7], which show that the directivity of the sound radiation from a rectangular opening, which is excited by sound incident on its other side, depends strongly on its length in the direction of measurement but only weakly on its width at right angles to the direction of measurement. Graphs indicated that when the width of the sample at right angles to the direction of observation is changed, it did not make much difference in terms of directivity. However when the width changed in direction of observation, it made big difference in terms of directivity. Thus we can conclude that the radiation efficiency of a forced wave on a panel is mainly determined by the ratio of its length in the direction of observation to the wavelength of the sound in air and the angle of incidence of the forcing wave. This is something that has not been appreciated in terms of directivity and power radiated.

In the sound insulation theory one of the main reasons for a limiting angle above which no incidence of sound occurs is the fact that $\frac{1}{\cos \theta}$ goes to infinity and there is a need to limit it for finite size samples. In the theory of this thesis, the weighting angle controls how quickly the incident sound level decreases as its angle of incidence increases. An infinite weighting angle which imposes uniform weighting on all angles of incidence cannot be assumed. It is important to note that even when the weighting angle was greater than 90 degrees, only angles of incidence between -90 degrees and 90 degrees were included in the calculations. The weighting angle was implemented with a weighting function that controlled the sound energy distribution. Different weighting functions were tested. Triangle weighting was not sufficient because the panel size and the limiting angle are considered when dealing with finite panel sizes. This was the basis of development of the weighting function that was angle dependent, and implemented the weighting angle. In the end a cosine squared weighting function was implemented.

Without making an assumption for the weighting angle, the theory of section 5.1.1 cannot be used to predict sound radiation from finite flat panels. If the theory of section 5.1.1 was used for particular situation there would be a question of what weighting angle would be implemented. The theory of section 5.1.1 was compared with different models using the weighting angle as a varying parameter to produce a curve. A particular distribution was adopted using a \cos^2 type curve with the only variable being weighting angle.

Some guidance for different cases was needed as to what weighting angle will be suitable for a particular situation. Levine considered the situation in which only plane waves propagate in pipe. That being the case, a satisfactory comparison was produced only when weighting angle was set to 1 degree. In the case of Levine, which was definitely the only model using plane waves, the weighting angle of 1 degree was appropriate, whereas with other models higher values for the weighting angle were assumed. A smaller weighting angle was used for Stead's data because the sound absorption coefficient of his room surface was larger than that of Rindel's room surface. The sound, from a source near the centre of the room which reaches the surface of the room close to a grazing angle of incidence, will have had many reflections

at which its sound energy is reduced. None of the models for finite panels showed a great relative sound level decrease as the Strouhal number increased. Instead the models exhibited a relatively flat curve of relative sound level versus Strouhal number, with a peak at the coincidence frequency. This was not case for the finite openings because openings do not have the coincidence effects, but their relative sound levels tended to decrease a lot more at 90 degrees.

The reason for this is that, as shown in section 5.1.1.1, the radiation efficiency appears in the numerator of the expression for the sound pressure. In the denominator the radiation efficiency is multiplied by two times the characteristic impedance of air and added to the panel wave impedance. The modulus squared of this sum is then calculated. For a panel, the panel wave impedance is much larger than the product containing the radiation efficiency. Thus for a panel the radiation efficiency in the denominator has no significant effect and the sound pressure is proportional to the radiation efficiency in the numerator.

For an opening, the panel wave impedance is zero and the squared radiation efficiency in the denominator divides the radiation efficiency in the numerator. Thus for an opening the sound pressure is inversely proportional to the radiation efficiency. The net effect is that the ratio of the sound pressure for an opening to the sound pressure for a panel is inversely proportional to the square of the radiation efficiency.

Below the limiting angle ϕ_l used in the calculation of the radiation efficiency and for panels who dimension are large compared to the wavelength of the sound, the radiation efficiency is inversely proportional the cosine of the angle to the normal of the panel or opening at which the sound is being observed.. Thus the ratio of the sound pressure for an opening to the sound pressure for a panel is proportional to the cosine square of the angle to the normal of the panel or opening at which the sound is being observed.

It is believed that a smaller weighting angle is needed in less reverberant situations as in the case of Stead's model, whereas for comparison with Rindel's model a larger weighting angle was needed, implying that the box Rindel has used in his model was more reverberant. This

has been confirmed by examining the reverberation times. The size of the panel or opening was another significant variable.

The findings indicated that apart from the effect due to coincidence, the panel was non-directional compared to the opening. Rindel confirmed that apart from the coincidence angle for particular frequency, radiation of panel was not very directional. Rindel's results in case of anechoic chamber showed a reasonable relative sound level decrease when close to 90 degrees. For the NSW EPA, at high Strouhal numbers there was a maximum amount of relative sound level decrease. It is important to note that in the theory of section 5.1.1 a modification was introduced when comparing with the NSW EPA model which asymptoted the relative sound level to the maximum decrease.

In an anechoic room if the sound was coming out of the box, at 90 degrees some of that sound will be diffracted into the area for angles greater than 90 degrees. This will start to reduce the sound pressure, as there will be no reflection from the rigid boundary of the half space which the theory of section 5.1.1 assumes. In the case of factory roofs, the radiated sound will diffract and then be reflected by the ground. One could argue that the ground is to some extent, depending on the geometry, like a plane, suggesting that one could expect that the results to be reasonable at 90°. An anechoic room would produce lower values, where in reality in the case of the factory roofs some reflections of the ground coming back up will be produced. The theory of section 5.1.1 does not predict relative sound level for angles greater than 90 degrees. We have not attempted to model the diffraction area or shadow zone. The model that was used really was based on the assumption that there was a source that was radiating on both sides. Using symmetry this implied that the source was radiating on one side and was in an infinite rigid baffle. What the theory of section 5.1.1 is predicting at 90 degrees is probably too high compared to anechoic room without a rigid infinite baffle. Nevertheless, if the ground in case of factory roofs is to some extent like a rigid baffle, one would expect that the results predicted at 90 degrees by the theory of section 5.1.1 to be reasonable.

The understanding gained from this project will assist and provide information to professionals who work with sound radiation reduction. The research report can also be used

as a tool or basis for further research, where sound radiation to the surroundings from structural vibrations will be predicted.

6.1 Recommendation for further study

A subject for future investigations will be a more extensive study of the diffraction area since the theory of section 5.1.1 does not predict relative sound level for angles greater than 90° .

We have not attempted to model the diffraction area or shadow zone.

The present work was an attempt to predict the level of sound radiated from a finite flat panel or finite opening in any particular direction relative to the level of sound radiated in the direction normal to the finite flat panel or finite opening. Although the developed method has given good results for openings and thin single panels, the method is not sufficient for other types of panels such as double panels.

Finally, it is recommended that future research investigate verification of the present work through measurements using real factory roofs.

References

- [1] Cremer, L. and Heckl, M. (1973). *Structure-Borne Sound*. New York: Springer-Verlag Company.
- [2] Beranek, L.L. (1954). *Acoustics*. New York: McGraw-Hill Book Company.
- [3] Gosele K (1953). "Schallabsrahlung von Platten, die zu Biegeschwingungen angeregt sind." *Acustica* **3**(4):243-248.
- [4] Sato, H. (1973). "On the mechanism of outdoor noise transmission through walls and windows - A modification of finite wall theory with respect to radiation of transmitted wave." *Journal of the Acoustical Society of Japan* **29**(9): 509-516.
- [5] Ljunggren, S. (1991). "Airborne sound insulation of thin walls." *Journal of the Acoustical Society of America* **89**(5): 2324-2337.
- [6] Novak, R.A. (1995). "Radiation from partially excited plates." *Acta Acustica* **3**(6): 561-567.
- [7] Roberts, J. (1983). "The prediction of directional sound fields." Transactions of the Institution of Engineers, Australia, Mechanical Engineering, Paper M1153, ME8(1):16-22.
- [8] Alfredson, R.J. (1972). "The propagation of sound in a circular duct of continuously varying cross-sectional area." *Journal of Sound and Vibration* **23**(4): 433-442.
- [9] Beranek, L.L. (ed.) (1971). *Noise and Vibration Control*. New York: MacGraw-Hill Book Company.
- [10] Vér, I. L. and Holmer, C. I. (1971). "Interaction of sound waves with solid structures." *in* [9]: 270-361.
- [11] Maidanik, G. (1962). "Response of ribbed panels to reverberant acoustic fields." *Journal of the Acoustical Society of America* **34**(6): 809-826.
- [12] Wallace, C. E. (1970) "Radiation resistance of a baffled beam." *Journal of the Acoustical Society of America* **51**(3): 936-945.
- [13] Wallace, C. E. (1970) "Radiation resistance of a rectangular panel." *Journal of the Acoustical Society of America* **51**(3): 946-952.
- [14] Heckl, M. (1981). "The tenth Sir Richard Fairey memorial lecture: Sound transmission in buildings." *Journal of Sound and Vibration* **77**(2): 165-189.

- [15] Rayleigh, J.W.S. (1945). *The theory of sound*, 2 volumes. New York: Dover Publications.
- [16] Bies, D.A. and Hansen, C.H (1996). *Engineering Noise Control: Theory and Practice*. London: E & FN Spon.
- [17] Beranek, L.L. and Ver, I.L (1992). *Noise and vibration control engineering*. New York: John Wiley & Sons Inc.
- [18] Davy, J.L. (1991). "Predicting the sound insulation of stud walls." Internoise 91: 251-254.
- [19] Rindel, J.H. (1975). *Transmission of traffic noise through windows. Influence of incident angle sound insulation in theory and experiment*. The Acoustic Laboratory, Technical University of Denmark, Report no. 9.
- [20] Takahashi D. (1995). "Effects of panel boundedness on sound transmission problems". Journal of Acoustical Society of America **98**(1): 2598-2606.
- [21] Stead, M. (2001). *Sound Reduction for Reverberant, Direct and Diffracted Sound through Single Isotropic Glass Panels of Finite Size*. Department of Mechanical Engineering, Monash University.
- [22] Crocker, B.E. and Wells. R.J. (1953). "Sound radiation patterns of gas turbine exhaust stacks." Journal of the Acoustical Society of America **25**(3): 433-437.
- [23] Waters, B.G., Labate, S. and Beranek L.L. (1955). "Acoustical behaviour of some engine test cell structures." Journal of the Acoustical Society of America **27**(3): 449-456.
- [24] Joseph, P. and Morfey, C.L. (1999). "Multimode radiation from an unflanged, semi-infinite circular duct." Journal of the Acoustical Society of America **105**(5): 2590-2600.
- [25] Sutton, M. (1990). *Noise directivity of exhaust stacks* - Final year thesis for the honours degree. Department of Mechanical Engineering, University of Adelaide.
- [26] Croft, G.J. (1979). Final Year Thesis for the Ordinary Degree of Bachelor of Engineering, Department of Mechanical Engineering, University of Adelaide.
- [27] Dewhirst, M. (2002). Final year design project: *Exhaust stack directivity*. Department of Mechanical Engineering, University of Adelaide.

- [28] Sewell, E.C. (1970). "Transmission of reverberant sound through a single-leaf partition surrounded by an infinite rigid baffle." Journal of Sound and Vibration **12**(1): 21-32.
- [29] Fahy, F. (1987). *Sound and Structural Vibration: Radiation, Transmission, and Response*. London: Academic Press.
- [30] Crocker, M.J. and Price A.J. (1969). "Sound transmission using statistical energy analysis." Journal of Sound and Vibration **9**: 469-486.
- [31] Crocker, M.J. and Price A.J. (1970). "Sound transmission through double panels using statistical energy analysis." Journal of the Acoustical Society of America **47**: 683-693.
- [32] Novak, R.A. (1992). "Sound insulation of lightweight double walls." Applied Acoustics **37**(4): 281-303.
- [33] Beranek, L.L. and Work, G.A. (1949). "Sound transmission through multiple structures containing flexible blankets." Journal of the Acoustical Society of America **21**: 419-428.
- [34] Lindblad, S.G. (1973). *Akustik II compendium*. University of Lund.
- [35] Lindblad, S.G. (1985). *Akustik IV*. University of Lund.
- [36] White, P.H. and Powell, A. (1966). "Transmission of random sound and vibration through a rectangular double wall." Journal of the Acoustical Society of America **40**: 821-832.
- [37] Cummings, A., Mulholland, K.A. (1968). "The transmission loss of finite sized double panels in random incidence sound field." Journal of Sound and Vibration **8**: 126-133.
- [38] Mulholland, K.A. and Lyon, R.H. (1973). "Sound insulation at low frequencies." Journal of the Acoustical Society of America **54**: 867-878.
- [39] Sharland, I. (1986). *Woods Practical Guide to Noise Control*. Woods Acoustics, a division of Woods of Colchester Limited.
- [40] Woods, R.I. (1972). *Noise Control in Mechanical Services*. Sound Attenuators Limited and Sound Research Laboratories Limited.
- [41] Levine, H., and Schwinger, J. (1948). "On the radiation of Sound from an Unflanged Circular Pipe." Physical Review **73**(4): 383-406.

- [42] Environmental Protection Authority (EPA), NSW (1995). *Environmental Noise Control Manual*, 207-1.
- [43] Davy, J.L. (2001). *2nd Year Acoustics Lecture Notes*. RMIT University.
- [44] Pain, H.J. (1999). *The Physics of Vibrations and Waves*, London: John Wiley & Sons.
- [45] Gradshteyn I.S. and Ryzhik I.M. (1989). *Table of integrals, series, and products*, Fourth Edition, prepared by Geronimus YuV, Tseytlin MYu, translated from Russian by Scripta Technica Inc., edited by Jeffrey A., New York: Academic Press.
- [46] Russell, D. (2002). "Radiation from a baffled piston (model for a loudspeaker)". Acoustic Animations, Kettering University Applied Physics.
- [47] Russell, D.A., Titlow, J.P., Bemmen, Y.J (1999). "Acoustic monopoles, dipoles, and quadrupoles: An experiment revisited." *American Journal of Physics* **67**(8): 660-664.
- [48] Sparrow V.W, Rochat. J.L., Bard B.A (1996). "The use of colour in the scientific visualisation of acoustical phenomena." *Journal of Computational Acoustics* **4**(2): 202-223.
- [49] Rindell, J.H. (2004). "Modelling the Directional Characteristics of Sound Reflections". Joint Baltic-Nordic Acoustics Meeting 2004.
- [50] Kleiner, M. (1996). "Ojamna vaggar ger battre ljud." *Bygg & Teknik* **88**(1): 22-24.
- [51] Sharp, J.H. (1973). A Study of Techniques to Increase the Sound Insulation of Building Elements. Wylie Laboratories Report WR 73-S. Washington, DC, Report Prepared for Department of Housing and Urban Development.
- [52] Benade, A.H., and Jansson, E.V. (1974). "On plane and spherical waves in horns with nonuniform flare. 1. theory of radiation, resonance frequencies, and mode conversion." *Acustica* **31**: 79-98.
- [53] Stevenson, A.F. (1951). "Exact and approximate equations for wave propagation in acoustic horn." *Journal of Applied Physics* **22**(12): 1461-1463.
- [54] Miles, J.W. (1944). "The reflection of sound due to a change in cross section of a circular tube." *Journal of the Acoustical Society of America* **16**(1): 14-19.
- [55] ISO/FDIS 140-5, P. (1998). Acoustics - Measurement of sound insulation in buildings and building elements - Part 5: Field measurements of airborne insulation of facade elements and facades.
- [56] Bruel & Kjaer Condenser Microphones Data Book.